INVESTIGATION OF TIGHTLY COUPLED ARRAYS FOR WIDEBAND APPLICATIONS

A THESIS SUBMITTED TO
THE GRADUATE SCHOOL OF NATURAL AND APPLIED SCIENCES
OF
MIDDLE EAST TECHNICAL UNIVERSITY

BY

KAAN ARDA

IN PARTIAL FULFILLMENT OF THE REQUIREMENTS
FOR
THE DEGREE OF MASTER OF SCIENCE
IN
ELECTRICAL AND ELECTRONIC ENGINEERING

OCTOBER 2020

Approval of the thesis:

INVESTIGATION OF TIGHTLY COUPLED ARRAYS FOR WIDEBAND APPLICATIONS

submitted by **KAAN ARDA** in partial fulfillment of the requirements for the degree of **Master of Science** i**n Electrical and Electronic Engineering, Middle East Technical University** by,

Prof. Dr. Halil Kalıpçılar

Dean, Graduate School of **Natural and Applied Sciences** _____

Prof. Dr. İlkay Ulusoy

Head of the Department, **Electrical and Electronic Eng.** _____

Prof. Dr. Gülbin Dural

Supervisor, **Electrical and Electronic Engineering, METU** _____

Examining Committee Members:

Prof. Dr. Özlem Aydın Çivi

Electrical and Electronic Engineering, METU _____

Prof. Dr. Gülbin Dural

Electrical and Electronic Engineering, METU _____

Prof. Dr. Birsen Saka

Electrical and Electronic Engineering, Hacettepe University _____

Assoc. Prof. Dr. Lale Alatan

Electrical and Electronic Engineering, METU _____

Assoc. Prof. Dr. Özgür Ergül

Electrical and Electronic Engineering, METU _____

Date: 14.10.2020

I hereby declare that all information in this document has been obtained and presented in accordance with academic rules and ethical conduct. I also declare that, as required by these rules and conduct, I have fully cited and referenced all material and results that are not original to this work.

Name, Last name : Kaan Arda

Signature :

ABSTRACT

INVESTIGATION OF TIGHTLY COUPLED ARRAYS FOR WIDEBAND APPLICATIONS

Arda, Kaan
Master of Science, Electrical and Electronic Engineering
Supervisor: Prof. Dr. Gülbin Dural

October 2020, 136 pages

This thesis aims to provide in depth research on tightly coupled dipole arrays to be used in ultrawideband apertures applications. First, operation principles of tightly coupled dipole arrays are investigated. Starting from the Wheeler's current sheet aperture concept, some calculations on bandwidth and impedance concepts are conducted. B.A. Munk's addition to the concept, use of capacitive elements between adjacent dipoles, are introduced. Array unit cell is modeled using equivalent circuit approach, bandwidth and input impedance calculations are conducted using MATLAB environment. Unit cell designs using two different capacitive coupling mechanisms are given. Optimized final unit cell products that satisfy theoretical bandwidth and pattern requirements are given. Simulations are conducted for determination of number of resistive terminations in tightly coupled arrays. Discussions on number of dummy elements are given. Series of example finite array analyses are conducted. A finite array design that is producible using PCB technology is given. Antenna unit cell is modified in a finite array environment, due to the fact that finite PCB size that restricts maximum number of elements. An ultrawideband aperture that satisfies the theoretical limits is designed using this finite

aperture area. Different array feeding mechanism are given to be used as proposed antenna's feed. Various kinds of feed mechanisms are investigated, only a portion amongst them are determined that they do perform well. Manufacturing process of finite array is given along with the measurement results. Similarity between measurements and simulations are discussed.

Keywords: Wideband Array Antennas, Antenna Miniaturization, Finite Arrays, Tightly Coupled Dipole Arrays, Array Feeding

ÖZ

SIKI ETKİLEŞİMLİ DİZİLERİN GENİŞBANT UYGULAMALAR İÇİN İNCELENMESİ

Arda, Kaan
Yüksek Lisans, Elektrik ve Elektronik Mühendisliği
Tez Yöneticisi: Prof. Dr. Gülbin Dural

Ekim 2020, 136 sayfa

Bu tez, ultra geniş bant açıklık uygulamalarında kullanılacak sıkı etkileşimli diziler hakkında derinlemesine araştırma sağlamayı amaçlamaktadır. Yapılan iş, gerçekleme sürecinden sonra simülasyon ve ölçümlerle desteklenmiştir. İlk olarak, sıkı etkileşimli dipol dizilerin çalışma prensipleri incelenmiştir. Wheeler'ın akım yüzeyi açıklığı konseptinden başlayarak, bant genişliği ve empedans konseptleri üzerine bazı hesaplamalar yapılmıştır. B.A. Munk'ın konsepte katkısı olan bitişik dipoller arasında kapasitif elemanların kullanımından bahsedilmiştir. Dizi birim hücresi eşdeğer devre yaklaşımı kullanılarak modellenmiştir, bant genişliği ve giriş empedans hesaplamaları MATLAB ortamı kullanılarak yapılmıştır. İki farklı kapasitif bağlantı mekanizması kullanan birim hücre tasarımları verilmiştir. Teorik bant genişliği ve model gereksinimlerini karşılayan optimize edilmiş nihai birim hücre ürünleri verilmiştir. Sıkıca bağlanmış dizilerin rezistanslı sonlandırılacak eleman sayılarının tespiti için simülasyonlar yapılmıştır. Uyarılmamış portların sayısı ile ilgili tartışmalar yapılmıştır. Bir dizi örnek sonlu dizi analizi yapılmıştır. PCB teknolojisi kullanılarak üretilebilen sonlu bir dizi tasarımı verilmiştir. Anten birim hücresi, maksimum eleman sayısını kısıtlayan sonlu PCB boyutundan dolayı, sonlu dizi ortamında değiştirilmiştir. Teorik sınırları karşılayan bir ultra geniş bant

açıklığı, bu sonlu açıklık alanı kullanılarak tasarlanmıştır. Önerilen antenin beslemesi olarak kullanılmak üzere farklı dizi besleme mekanizmaları verilmiştir. Çeşitli besleme mekanizmaları araştırılmış, bunların sadece bir kısmının iyi performans gösterdiği tespit edilmiştir. Sonlu dizilerin üretim süreci ölçüm sonuçları ile birlikte verilmiştir. Ölçümler ve simülasyonlar arasındaki benzerlik tartışılmıştır.

Anahtar Kelimeler: Geniş Bant Dizili Antenler, Anten Minyatürleştirme, Sonlu Diziler, Sıkı Etkileşimli Dipol Diziler, Dizi Besleme

To my father, mother, brother and beloved ones

ACKNOWLEDGMENTS

I would like to express my gratitudes to my supervisor Prof. Dr. Gülbin Dural. Her support, motivation and guidance were very helpful to me throught my studies. I will be eternally grateful to her for all the guidance that she has provided.

I would like to express my deepest appreciations to my team leader Dr. Mustafa Kuloğlu. Starting with the proposal of the topic, throught my entire studies, He provided me his invaluable experience both in theoretical and applied areas. Thank you for all the support.

I would like to express my gratitudes to my thesis jury members, Prof Dr. Özlem Aydın Çivi, Prof. Dr. Birsen Saka, Assoc. Prof. Dr. Lale Alatan and Assoc. Prof. Dr. Özgür Ergül for accepting my invitation to the jury.

I would like to thank ASELSAN for supporting me throught my studies and providing use of company sources. I also would like to thank TUBITAK for their supports of this work as a scholarship.

I also would like to thank my family and my beloved ones. Their support was invaluable. At the worst and best of all times, you were the ones that motivated me.

TABLE OF CONTENTS

LIST OF TABLES

TABLES

LIST OF FIGURES

FIGURES

LIST OF ABBREVIATIONS

BOR	Body of Revolution
CSA	Current Sheet Antenna
DC	Direct Current
GND	Ground
PCB	Printed Circuit Board
PD	Power Divider
PEC	Perfect Electric Conductor
PMC	Perfect Magnetic Conductor
RF	Radio Frequency
SMA	SubMiniature version A
TCDA	Tightly Coupled Dipole Array
TEM	Transverse Electromagnetic
UWB	Ultra Wide Band
VSWR	Voltage Standing Wave Ratio
UAV	Unmanned Aerial Vehicle

CHAPTER 1

INTRODUCTION

Electronic warfare applications require bandwidth ratios for a single antenna on the orders of 3:1. Also recent developments such as UWB SAR requires UWB operations that extend up to 1 GHz. To acquire higher quality images at long ranges and high altitudes, operating frequency of the SAR needs to be on the orders of 100 MHz's. Ground penetrating radars is another application that features the UWB technology. To estimate characteristics of the soil, to detect buried various objects, to find humans trapped inside the soil after an earthquake or disaster; ground penetrating radar technology is employed. A similar application, through wall imaging is also another application that requires an UWB operation. At the same time, permissible space for those systems are continuously shrinking. The required antennas for those systems need to be low profile, the aperture depths should be on the orders of $\lambda/10$ at the lowest frequency of operation.

Modern aircraft systems are equipped with multiple antennas for multiple purposes such as tracking, detection, surveillance and various electronic warfare applications. Those functions mostly require UWB operation. For most of the modern aircraft systems, stealth technology is required. Therefore, the antennas to be installed on those aircrafts should not increase the radar target signatures of the platform. For those platforms, low profile antenna installments are desired. Furthermore, antenna platforms that can conform to the shape of the platform are preferred. Conformal installations of the antennas do not increase the radar signature of the aircraft systems and reduces the burden on the aerodynamic design of the aircraft. Also, a ground plane is a must for those antennas to be installed to the aircrafts, because in an aircraft the whole body behaves as a ground plane; one cannot get rid of its effects on the

antenna. Especially for the unmanned aerial vehicles, the permissible space requirements are always reducing. With the recent advances in RF technologies; systems that perform multiple functions and small in size are obtainable. Small in volume, multifunctional UAV's are of greatest interest. The antennas desired for those platforms have to be small in size whereas antenna of small sizes generally perform poorly, as the antenna theory suggests. Therefore, in a general manner, antenna miniaturization is a must for most of the recent systems.

In the light of these recent developments and requirements, antennas that provide UWB operation and are of low profile are required. A ground plane is also a must for these antennas.

Tightly coupled dipole arrays satisfy all those requirements. They are low profile, the aperture depths are on the orders of 0.1λ at their lowest frequency of operation. They provide wide bandwidths; up to 4:1 bandwidth ratios are obtainable under VSWR<2 condition. They also have ground plane below the aperture; as they are applied on several platforms; the antenna performances would not change due to the presence of ground plane. Also, they radiate only one beam towards outer space due to the presence of the ground plane. Tightly coupled dipole arrays have element lengths lower than $\lambda/2$ for all frequencies; therefore, they allow grating lobe free scan at any scan angle for all frequencies.

The bandwidth expectation of an ordinary antenna array is to be narrowband rather than wideband. Most of the time, arrays are comprised of microstrip elements or dipole elements. Microstrip elements themselves are narrowband, hence when placed in an array, the array itself is also narrowband. Dipole elements have bandwidth ratios on the orders of 10% – 20 %, unless they're fed with broadband matching elements. In addition, the mutual coupling between the dipole elements in a dipole array generally disrupts the array's bandwidth performance. However, it is possible to use the mutual coupling between elements for further improving the bandwidth of the array. Traditional array design is based on the design of an isolated element that has broadband operation itself and hope for its to do well in an array

environment. In short, mutual coupling is a principle that has been usually to be dealt with, but it is a beneficial performance factor in tightly coupled arrays. Tightly coupled dipole arrays employ mutual coupling for obtaining higher bandwidths using dipole elements; where they are narrowbanded in an isolated fashion in space. However, in the array, they provide much higher bandwidths.

This thesis aims to suggest some methodologies for designing a tightly coupled dipole array. At the same time, some design requirements were set for the arrays designed. Those requirements are as follows:

- The array aperture size should not be increased beyond the available PCB size. The permissible PCB size is 388 mm by 556 mm.
- The feeding of the array elements should be done by 50 Ω coaxial lines and associated connectors.
- The active S-Parameters for all the excited ports of the arrays should be less than -10 dB referenced to 50 Ω system, in the entire 0.5 – 2.0 GHz frequency band
- Aperture depth of the array and total array depth should be on the orders of λ/10 to λ/20 at the lowest frequency of operation. Total array depth includes the necessary balun and feed networks.

In Chapter 2, a brief literature survey about the topic is provided. Previously done work on wideband arrays and their properties are given and deficiencies of the previously developed wideband arrays are discussed and the motivation for implementing tightly coupled dipole arrays is given. A comparison is provided between the previously designed arrays available in the literature and the antenna presented in the thesis. Operation principles of tightly coupled dipole arrays are given. Starting from the Wheeler's current sheet aperture idea, physical realizations and useful impedance bandwidth are discussed. A MATLAB code that models the tightly coupled dipole unit cell that has lumped capacitance in the dipole tips is written. The code provides input impedance and bandwidth of the unit cell a of tightly coupled dipole array. The code allows one to optimize position of the ground

plane, unit cell lengths, operational frequency band and the desired VSWR in the desired frequency band.

In Chapter 3, the unit cell development phase of the tightly coupled dipole array design is provided. Basics of unit cell approach within the simulation environment is given. A unit cell that incorporates interdigital type capacitance elements between the E-planes of the dipoles is optimized such that it gives active S-Parameters lower than -10 dB from 0.5 GHz to 2.0 GHz. A novel spiral shaped capacitive element is introduced and its effect on the unit cell performance is studied. Finally, this novel unit cell is also optimized and it is observed that it gives active S-Parameters lower than -10 dB in the 0.5 – 2.0 GHz frequency band.

In Chapter 4, previously developed unit cell is tested on finite array environment. Number of elements necessary for convergence of impedance behavior of the finite antenna array elements to the infinite array unit cell analysis impedance behaviour are suggested. The number edge of elements that need to be resistively terminated for proper operation are provided. For applying different excitations schemes to any previously generated finite arrays, a small MATLAB script is written and used.

In Chapter 5, both unit cell designs that were operating properly in 0.5-2.0 GHz frequency band in the infinite array environment are tested in finite array environment. Due to finiteness of available PCB size; these apertures are reoptimized such that they give -10 dB active S-Parameters for their respective excited elements. It is observed that; spiral based capacitance unit cell provides further miniaturization, in comparison to the interdigital capacitance based finite array aperture.

In Chapter 6, several balanced antenna feed methods are applied to the tightly coupled dipole arrays. Only a couple of them perform well for tightly coupled dipole arrays due to the ground plane beneath the aperture. Two different feeding schemes that do not have any further extensions below the ground plane such that they retain low profile property of the array and perform well in finite array environment were suggested. These two feed mechanisms provide good quality patterns such that patterns are not different than the patterns obtained with lumped excitation.

In Chapter 7, the realization process of the antenna designed is given. Necessary measurements are provided, their agreements with the simulations are discussed.

CHAPTER 2

BRIEF INTRODUCTION TO TIGHTLY COUPLED ARRAYS

2.1 Literature Survey

The wideband array designs are generally based on choosing a wideband and narrowbeam element, i.e., the chosen element's radiation beam points mostly towards to the outer space rather than adjacent elements. This is the traditional approach that has been commonly applied in the literature. The examples of this approach are given in [1], [2], [3] and [4] and examples of those arrays are shown in Figure 2.1.

Most of the previously published wideband phased array antennas such as TEM-horn [4], body-of-revolution [1], bunny-ear [2], tapered slot, or Vivaldi [3] relied upon the third dimension of the element (depth), to achieve large bandwidths. As a result, they do not allow for conformal installations. They are also high cost and difficult to fabricate.

In [1], array of BOR elements that provide 3:1 bandwidth, operating from 6 GHz to 18 GHz are presented. The element spacings are 1.9λ at 18 GHz; which prevents the grating lobe free scan at any direction in the space. Therefore, in [1], 45^0 conical scan angle is considered where the scan is grating lobe free.

In [2], array of elements comprised of "bunny-ear" elements in a dual polarization setting, is discussed. Bunny ear term is used for flared dipoles, in this paper it is claimed that it has much shorter elements compared to classic tapered slot antennas. This paper also claims that the new kind of element has lower cutoff frequency compared to the tapered slot arrays. In this array 5:1 bandwidths are provided using those elements, however the aperture depths or lengths were not provided. Also, it is reported that, the array given in [2] requires a 3D mechanical manufacturing process.

In [3], array of vivaldi elements is presented. The array operates from 1 GHz to 5 GHz. At the lowest design frequency, the array has aperture depth of 0.25λ. This depth is the total distance from the aperture to the furthest point of the array.

In [4], array of TEM Horn elements is presented. The array operates in between 1 GHz and 5 GHz. VSWR<3 operation is satisfied in this frequency band. Array element lengths are larger than λ/2 at 5 GHz. Therefore, this array also does not provide grating lobe free scan in the space, at 5 GHz.

Those existing designs have large antenna dimension along z-axis; i.e. antenna's broadside axis. Those arrays have aperture depths on the orders of 0.5λ to the 2λ, where the λ is taken at the lowest design-frequency of the array. Henceforth, those arrays are three dimensional, they require some mechanical production steps unlike printed antennas. Those arrays have array periodicity, that are longer than 0.5λ at some frequencies in their respective frequency bands, hence they have inevitably grating lobes at some directions and at those frequencies.

On the other hand, tightly coupled dipole arrays are very low in aperture depths and also ultrawideband in bandwidth. Without any dielectric slabs in front of the array aperture, TCDA's can have 4.5:1 frequency bandwidth with VSWR ratios lower than 2; at the same time, they have aperture depths on the orders of λ/10 at the lowest design frequency [8]. TCDA's also have ground plane beneath the antenna, they radiate only one beam towards to the outer space. TCDA's have their unit cell element periodicities lower than 0.5λ at all design frequencies. Therefore, at all directions, the arrays scan without any grating lobes. The main beam can be oriented towards any direction above the antenna. While providing those functions, tightly coupled dipole arrays can be manufactured using simple PCB production technologies; they do not require 3D manufacturing techniques. The production costs of TCDA's are low, the production steps are easy.

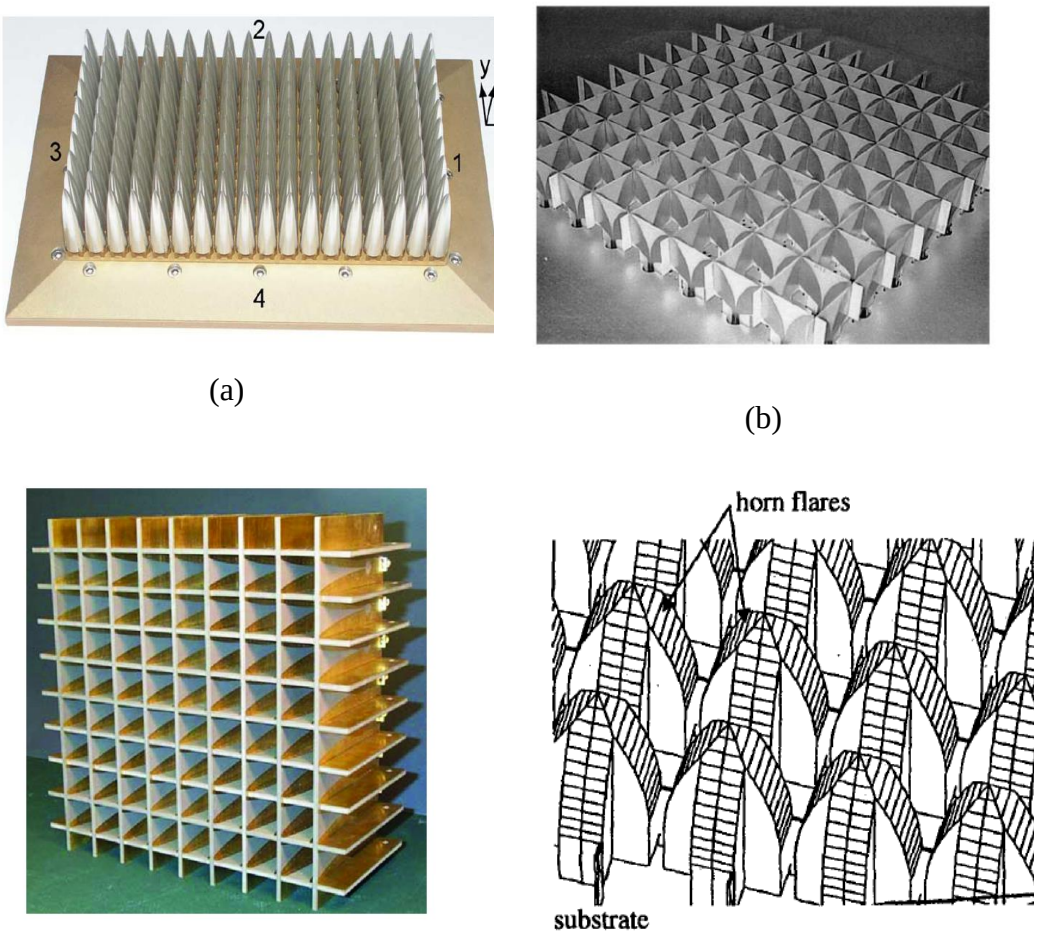

(a) (b)

(c) (d)

Figure 2.1. Examples of Traditional Ultrawideband Arrays; (a) BOR array, (b) "Bunny-ear" Array, (c) Vivaldi Array, (d) TEM-Horn Array

It is well understood that mutual coupling in an array can cause detrimental changes in performance such as element impedance variations, polarization degradation, and undesirable radiation patterns. In fact, mutual coupling is responsible for one of the more challenging aspects of phased array design, that is retaining uniform scan impedance. A fundamentally different design approach was proposed by Munk [8], where mutual coupling is used to lower the operational frequency and increase bandwidth. This approach is similar to designing wideband wide-angle FSS's [9]. Likewise, mutual coupling was shown to lower the operational frequency of a spiral array in [10].

B.A Munk, was the first person to use mutual coupling between array elements to obtain greater bandwidth and reduce the disruptive effect of the ground plane inductance. By placing capacitive elements between ends of colinearly arranged dipole elements to control the mutual coupling and controlling some resonances, he obtained an ultrawideband operation array that is inherently low profile and conformal to the installations of several platforms. That array is simple to produce using printed circuit board technology and has a single beam that can be oriented towards any direction in space, due to the grating lobe free scan. The unit cells of TCDA's are smaller than 0.5λ at all design frequencies. His design was based on Wheeler's "Current Sheet Antenna" concept that was first published in 1965 [5]. Munk applied this current sheet antenna concept in front of a ground plane. His addition was using capacitive coupling elements between dipoles, where he was able to cancel out the imaginary impedance term that comes from the ground plane below the antenna. Actual mission of this capacitance was to control the resonance or the imaginary parts of the array unit cell input impedance.

In [29], Green's function is developed for long slot arrays. By duality principle, the formulations can be used for dipole arrays. It is observed in [29], although isolated dipole is narrowband; in 1D array fashion the bandwidth obtained from the elements of the array is increased. If the array is made 2D, the offered bandwidth is further increased.

In [28], a loop shaped transformer is suggested for obtaining balanced and high impedance output to feed terminals of wideband, wide scan arrays. At the center frequency of such arrays, the input impedance is generally high, on the orders of 377 Ω, intrinsic impedance. In order to avoid common mode resonances that occur while scanning, loop shaped transformer is implemented in the feed network. Although the offered frequency bandwidth is low, 3 GHz to 5 GHz, the provided architecture allowed an impedance transformation from 50 Ω to 350 Ω. The cross polarization levels are reduced due to the proposed transformer network.

In [23] and [24], a similar array to TCDA's, namely PUMA array, is introduced. The introduced array allows modular construction of the array elements. Dual polarization setting is applied in a carefully designed array unit cell element. Coaxial entry is implemented just below the ground plane together with an accompanying matching network on the backside of the GND plane. In the infinite array unit cell approach, 5:1 bandwidth is offered under VSWR<2.1 criteriton; however, WAIM is used above the radiating aperture which increases the total array depth further. In general, the electrical distance between aperture to ground plane is equal to the length of the superstrates above the aperture plane. Multilayer PCB assembly is used for manufacturing of the array, which increases the production costs. In [23], only unit cell approach is given; however, in [24], 16 × 16 realization of the PUMA array is provided. The offered bandwidth is 3:1, from 7 GHz to 21 GHz. The measured finite array VSWR increase beyond 2 towards to the low frequency end, the central element has active VSWR of 2.7 and edge elements exhibit active VSWR of 3 around 8.75 GHz. The total array depth, including the feed and the superstrate, is 8.125 mm, which corresponds to 0.19λ at the lowest operational frequency, 7 GHz. It will be wise to note that solderless, modular assembly of the array is provided in this paper.

In [25], which is a recent paper about TCDA's; the bandwidth offered is 5.5:1 under VSWR<2 criterion, spanning the 0.8 GHz – 4.38 GHz band. WAIM superstrate is used above the aperture of the array. 10 × 10 realization of the developed array is given, the last two rows in the E-plane of the finite array were resistively terminated; i.e., only 6 × 10 center portion is excited. Broadside active VSWR increase beyond 2 both in finite array simulations and measurements. Total array depth including the feed networks and the WAIM superstrate is 52.87 mm, corresponds to 0.141λ at the lowest operational frequency, 0.8 GHz. The distance between ground and aperture is 0.993λ at the same frequency.

In [26], TCDA of 46:1 bandwidth is offered under VSWR<3 criterion, this is the largest bandwidth offered for TCDA's according to the paper's claim. The provided

operational band is between 130 MHz and 6 GHz. By introducing a resistive FSS R-card within the superstrate, the offered bandwidth is significantly improved. The introduced FSS R-card suppresses the periodic GND plane interference that occurs at multiples of 0.5λ across the band. The distance between aperture and ground plane is 3.41λ at 6 GHz, therefore the ground plane interference occurs at several frequencies across the band; the introduced FSS R-card cancels out all of them. However, the efficiencies around the frequencies where ground plane interference occurs are degraded severely, dropping below 0.34 values. At the expense of 1.34 dB loss due to FSS R-card, which results in reduced efficiency across the band; the offered bandwidth is extreme. This provided array also uses superstrate FSS above the aperture.

In [27], a novel electronic circuit approach for modeling TCDA's is developed. The novelty comes from the offered circuit model is able to investigate irregular shaped dipole elements like bowtie dipoles. By employing this ECM approach instead of brute force full wave optimizations, an array is optimized such that it operates between 0.87 GHz and 10.14 GHz at broadside. The feed structure is also included in the circuit approach. Resistive sheet and superstrate are used in this array. Only the central elements' measured active VSWR is given, it is lower than 2 in the entire frequency band.

2.2 Wheeler's Current Sheet Concept

H. A. Wheeler first published a paper on this concept in 1948, [6]. He was basically reporting that, an infinite length current sheet, J or M, radiates to the space with infinite bandwidth. Note that, those currents sheets have 2 beams, one is towards upper hemisphere and the other one is towards lower hemisphere. To direct beam towards any direction, linear phase variation can be applied.

Basically, Wheeler was suggesting that classical flat array of dipoles of λ/2 in length, and array spacings are λ/2, λ/2 in both E-plane and H-plane together with a ground plane which is placed λ/4 below the radiating aperture, has input impedance of 153 Ω. Except for the edge elements, this formulation works for the central elements. The formulation he used was based on infinite periodicity both along the E-plane and the H-plane.

First, a hypothetical waveguide, whose upper and lower walls are PEC boundary condition and the right and left walls are PMC boundary condition is considered as shown in Figure 2.2. The waveguide is filled such that material properties are of the vacuum. The red lines show the electric field distribution along this hypothetical waveguide. The magnetic field distribution is orthogonal to those red lines, starting from left PMC wall and ends at right PMC wall. Perfectly TEM wave, which has a zero cutoff frequency, propagates along $+\hat{a}_z$ direction inside this hypothetical waveguide (or transmission line). PEC walls are of length "a", PMC walls are of length "b".

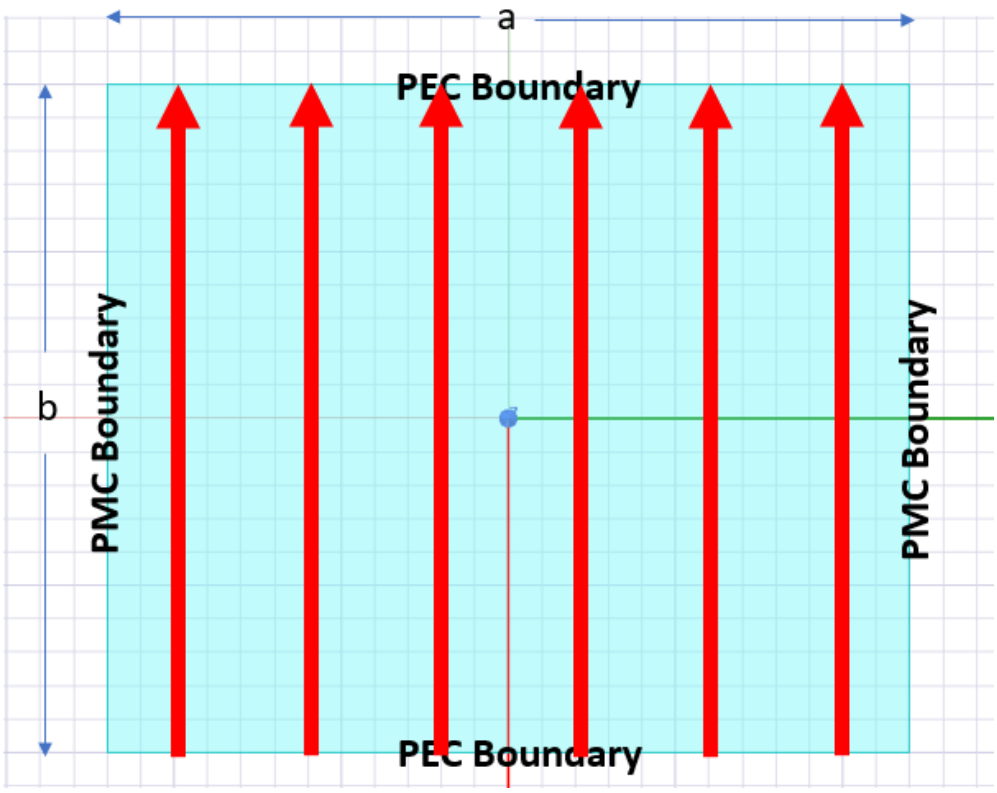

Figure 2.2. Hypothetical Waveguide, Top-Bottom PEC Boundary Condition, Right-Left PMC Boundary Condition

The characteristic impedance of this waveguide is given in (1). Note that characteristic impedance is not equal to the wave impedance. The wave propagating inside this waveguide is perfectly TEM wave, the material filling is air hence the air's intrinsic impedance is the wave impedance of the TEM wave inside this wave.

$$Z_{ch} = \sqrt{\frac{\mu_0}{\varepsilon_0}} \times \frac{b}{a} \quad (1)$$

The following two configurations given in Figure 2.3 use this hypothetical antenna. These are examples of dipole antennas that are placed in this hypothetical waveguide. Wheeler hypothetically considered those dipoles such that they exist inside in this hypothetical waveguide. As long as the waveguide dimensions, "a" and "b", are lower than $\lambda/2$, the only propagating mode is the fundamental TEM mode. In Figure 2.3, the first configuration is a hypothetical waveguide fed by a coaxial

connector. The inner conductor of coaxial line goes up until the top PEC, the outer conductor touches to the bottom PEC. In this configuration, the small inner conductor inside the waveguide behaves like a dipole of very short length, the length is equal to “b”. In Figure 2.3, the second configuration is a dipole antenna whose length is not short, but shorter than the “b”.

These two dipole antennas inside the waveguide excite the fundamental mode of this waveguide, i.e., TEM mode. For dipole antennas, the definition of effective length is easier to visualize. For the first configuration, since the dipole length is small and equal to “b”, the effective length of this dipole, denoted as “h”, equals to “b”. The real physical length of the antenna is denoted as “l”. For very short dipole antennas, their effective length is equal to their actual length. For the second configuration, the effective length is denoted as “h” since the voltage induced on this antenna from the perfectly TEM fields inside this hypothetical waveguide are linearly proportional to its effective length. The reason is due to the electric field distribution is uniform along the “b” dimension. Hypothetically placed dipole’s antenna terminals and hypothetical waveguide from one direction can be thought of a two port system. Assuming that waveguide and the dipole antenna as two ports of a coil transformer, which is also a two port system, the voltage ratio between dipole port and the waveguide port is apparently $\frac{h}{b}$, hence those two ports can be modeled as a transformer having voltage step ratio as $\frac{h}{b}$. One end of the transformer is dipole port, the other end of the transformer is the characteristic impedance of this hypothetical waveguide extending towards infinity. This transformer configuration is given in Figure 2.4.

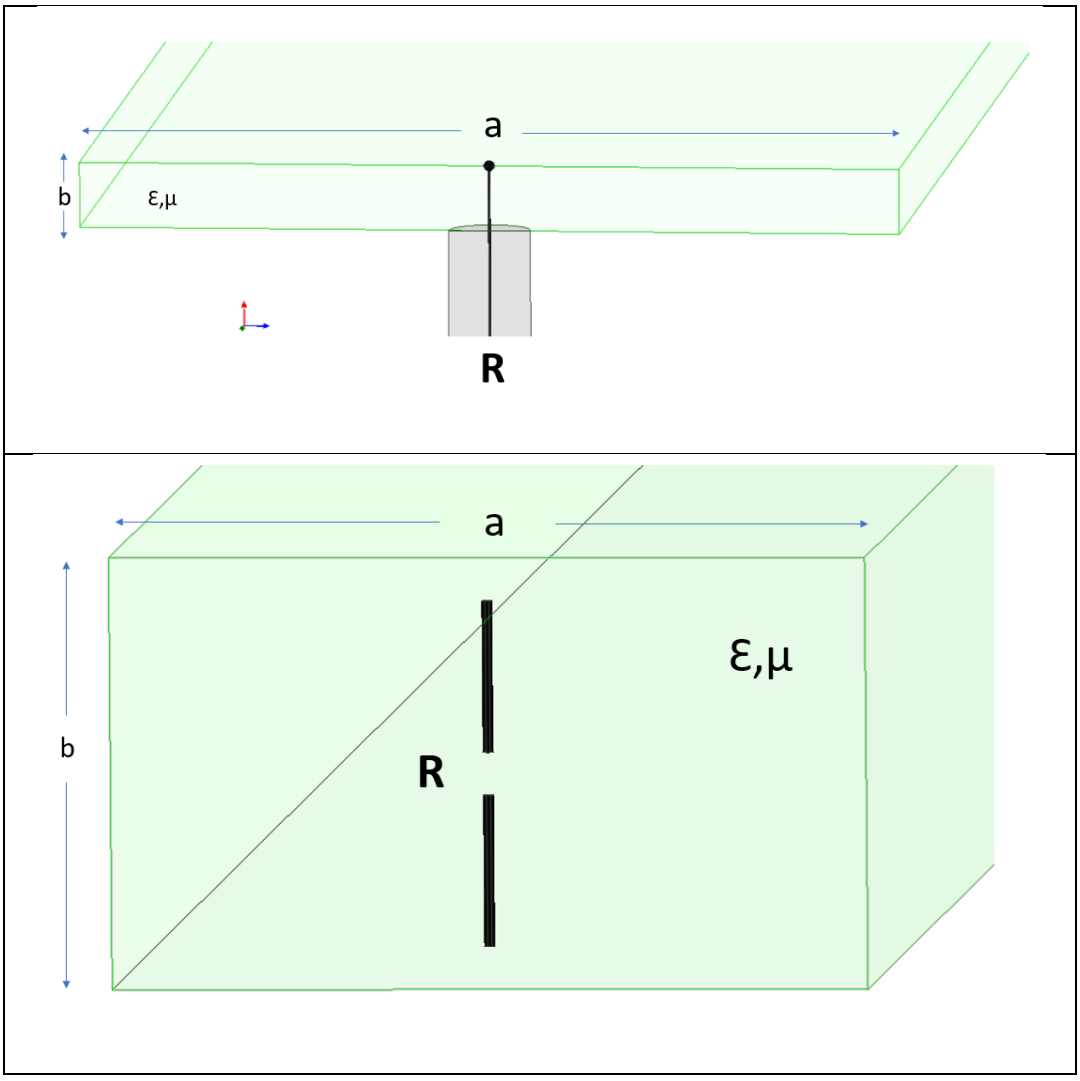

Figure 2.3. Dipole Configurations using Hypothetical Waveguide

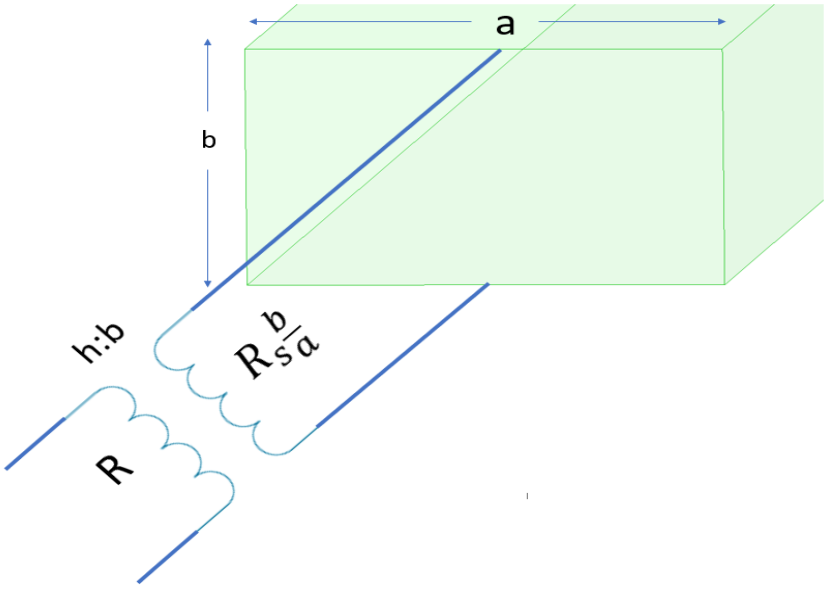

Figure 2.4. Dipole – Waveguide transition as a Voltage Coil Transformer

The characteristic impedance of this waveguide is calculated as $\sqrt{\frac{\mu_0}{\varepsilon_0}} \times \frac{b}{a}$, given in (1). Therefore, using transformer impedance transformation, where the impedance transforming ratio is the square of the voltage transform ratio, that is $\frac{h}{b}$; "R", the dipole terminal impedance is given in (2). It is the characteristic impedance of this hypothetical waveguide seen from the hypothetically placed dipole's terminals inside this hypothetical waveguide.

$$R = \left(\frac{h}{b}\right)^2 \times \sqrt{\frac{\mu_0}{\varepsilon_0}} \times \frac{b}{a} \quad (2)$$

Note that in real world, there exist no PMC boundaries. However, by properly assembling dipoles in an array fashion, one can provide those boundaries. A dipole array that extends to infinity both in E and H planes, radiates only one mode that is

nothing but a perfectly plane wave. Also note that, since dimensions “a” and “b” are smaller than half wavelength; within the unit cell element, there are also only perfect TEM waves with zero cutoff frequency. Considering the unit cell element of this dipole, it can be said that, due to the electromagnetic field distributions, all four boundaries can be thought of PEC and PMC boundaries. In Figure 2.5, this kind of array assembly is given.

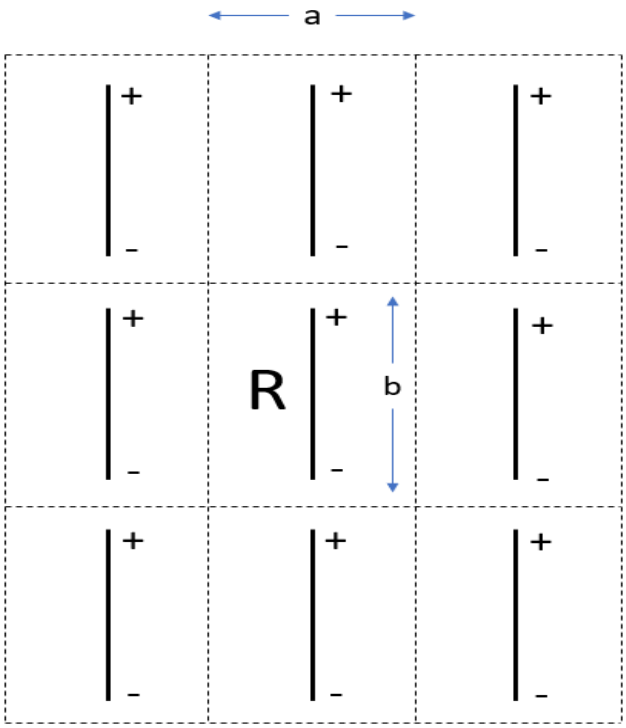

Figure 2.5. Infinitely Long Dipole Array

Along the H-planes, i.e., right and left sides of the unit cell element are PMC boundary condition and the top and bottom sides are PEC boundary condition. The dipole element within one unit cell has radiation resistance given in (2). In (3), it is

given in a simplified form. Intrinsic impedance, $\sqrt{\frac{\mu_0}{\varepsilon_0}}$, is $120\pi\ \Omega$ written directly, rest is simplified in (3).

$$R = 120\pi \times \frac{h^2}{a \times b}\ \Omega \quad (3)$$

A dipole array which has periodicity "a" and "b" equal to λ/2, and dipole effective length "h", lower than "b". As two beams travel outwards, parallel combinations of two R's that were given in (3), generate the radiation resistance of this dipole array's one element is given in (4). Note that still "a" and "b" are small enough such that only permitted mode of propagation is TEM.

$$R_A = 60\pi \times \frac{h^2}{(\lambda/2)^2}\ \Omega \quad (4)$$

Instead of dipole of effective length of "h", a "λ/2" dipole array is a halfwave dipole, "l=b=λ/2", has effective length to actual ratio of 2/π. Using (4), radiation resistance of the unit cell element of this dipole is found to be $\frac{240}{\pi}\ \Omega$, which is 76.4 Ω. Remember that, an isolated λ/2 dipole has radiation resistance equal to 73.13 Ω, at its resonance. Isolated dipole has reactance accompanying this resistance, however our dipole array is completely resistive. This difference can be explained in the following way: isolated dipole has near fields that are responsible for the imaginary reactance; however in an infinitely long array, there are no near fields hence no reactance. The reason for not having near fields is because this array is infinitely long and just above the antenna radiator, there are only plane waves present. On the other hand, plane waves are present only in the far field region of an isolated dipole.

Wheeler also considered this hypothetical array, in front of a ground plane. Different spacings of ground plane and the radiator plane was considered. The most notable ones were the λ/8 and λ/4. In Figure 2.6, the infinitely long arrays with several ground plane spacings can be seen.

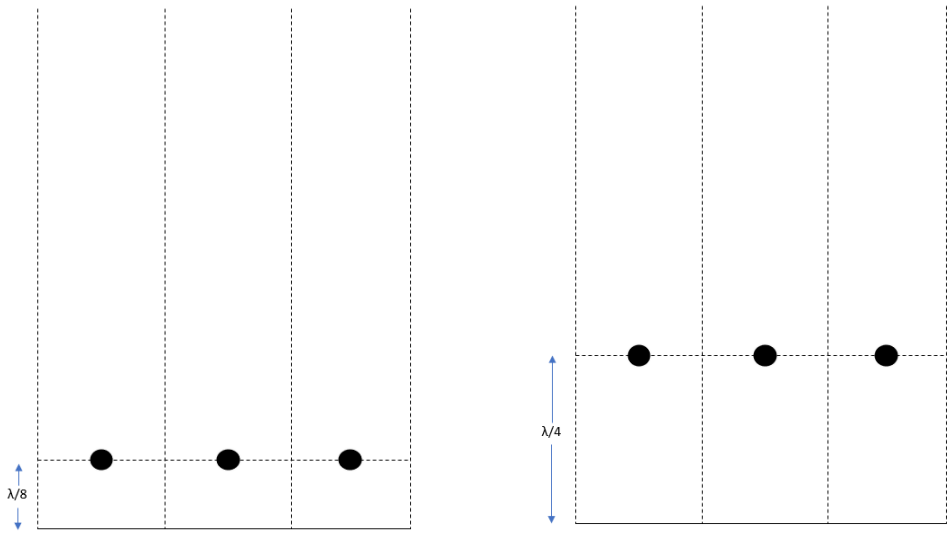

(a) (b)

Figure 2.6. Infinitely Long Array; (a) with λ/8 distance GND plane, (b) with λ/4 distance GND plane

In λ/8 ground plane distance, using (3) and combining several impedance terms; the real part of input impedance of a unit cell element is approximately 73 Ω, that is same with the isolated dipole. Also, the input impedance of unit cell of the array has some reactance accompanying the resistance. However, in this case, the interactions between elements in the array is low. In a real finite array, the edge elements do not mismatch severely due to the small interaction as if it will be in the λ/4 spacing. Mismatch term means the following: for an element of a finite array, it's deviation from the impedance behavior of a central element of this array. However, in terms

of bandwidth and low VSWR, that spacing is narrowband. In the λ/4 ground plane distance, using (3) and combining several impedance terms, the input impedance is completely real, free of reactance. However, the radiation resistance is 152 Ω, higher but also widest possible bandwidth is achieved. But, in this case, in the real finite array, edge elements would experience high levels of mismatch in impedance compared to the central elements; since antenna elements are highly coupled to each other. Except several elements at the edges, most of the excited region of the array obey those input impedance calculations. Additionally, it will be wise to note that; those input impedance calculations are done at the resonance frequency of the array elements. Wheeler, in his paper, did not calculate any frequency except the center frequency but mentioned some comments about the other frequencies that array is not resonant. On the other hand, Munk considered wideband operation rather than single frequency. Wheeler also added that, for wider bandwidths, closely packing up the dipole elements would be better. As the elements grouped closely, their radiation resistance increases. In addition, an array without ground plane, provided that its dimensions are so small that no grating lobes are present, is the one with no reactive input impedance. However, when a ground plane is added beneath the antenna, the antenna has a new reactance in addition to the resistance in the input impedance expression. In addition to the reactance, added ground plane also differs the resistance of the array as well. In [7], array unit cell input resistance and reactance curves are given for a half wave dipole above a quarter wavelength distanced ground plane. In those curves, even for the boresight, nonzero reactance is present.

Bunk's contribution to this problem was to add a Z_L, loading element between the tips of collinear spaced dipole arrays. Specifically, that load impedance was the capacitance physically implemented in various forms. He intensively studied bandpass radomes, hybrid radomes especially in wideband operations. He obtained many formulations, even though most of his studies are for scattering analyses of radomes, but they include finite sized arrays as well. Most analytical formulations about arrays considered in this thesis are valid for unit cell element of the array. Infinite periodicity on both dimensions are assumed. However, in [8], the

formulations and discussions are given for those arrays having finite dimensions along its planes.

2.3 Operation Principles of Tightly Coupled Dipole Arrays

First, a tightly coupled dipole array is a dipole array that consists of dipole elements that are connected along their E-planes via capacitive loads and has a ground plane beneath the array aperture plane. Equivalent circuit approach will be used for the unit cell element of the array.

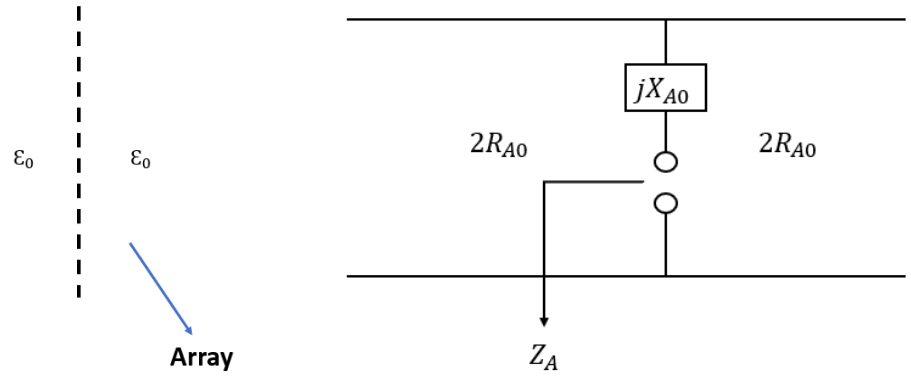

(a) (b)

Figure 2.7. (a) Dipole Array in Free Space, (b) Equivalent Infinite Transmission Line

A dipole array, that is placed in the free space is considered. In Figure 2.7, (a), picture depicting this dipole array can be seen. For the unit cell element in this array, its terminals can be thought as if the array is sandwiched between two dielectrics of air material. The array's unit cell element has input impedance $Z_{A0} = R_{A0} + jX_{A0}$, where "0" subscripts denote that the array is in air. If it was in medium of dielectric

constant ε_1, then its impedance would be $Z_{A1} = R_{A1} + jX_{A1}$. This impedance can be considered as in the form of Figure 2.7, (b). Two semi infinite transmission lines of $2R_{A0}$, extend towards two ends. An infinitely long transmission line sees impedance equals to its characteristic impedance. $2R_{A0}//2R_{A0}$ results in R_{A0}, then a series reactance jX_{A0} added. Antenna input impedance is obtained as $Z_{A0} = R_{A0} + jX_{A0}$.

When building a broadband array, the ideal aperture should be really a continuous current as Wheeler [5] suggested.

Generally, it is stated that radiation impedance of a short dipole is comprised of low resistance and an accompanying high reactance, therefore, to build a broadband array; usage of short dipoles are crisscrossed. The best approximation to such a current sheet is given in Figure 2.8. It is a periodically fed closely spaced wires. This approach would allow a current distribution of sinusoidal type, however with a DC component accompanying this distribution. However, in the case of isolated short dipoles, the current vanishes to zero at the dipole ends. As short wires are associated with inductive elements by their nature, between the adjacent dipoles; series capacitances are added. The added capacitances are parallel with the dipoles' tip to tip capacitances; equivalent capacitance is the summation of those two capacitances. It is beneficial to note that, dipoles' tip to tip capacitances are not too low. However, as it will be explained more clearly, it is not very important that how much of the capacitance comes from tips and added capacitance. The net result denoted by C_0 is important. The inductance associated with the dipole arms is denoted by L_0.

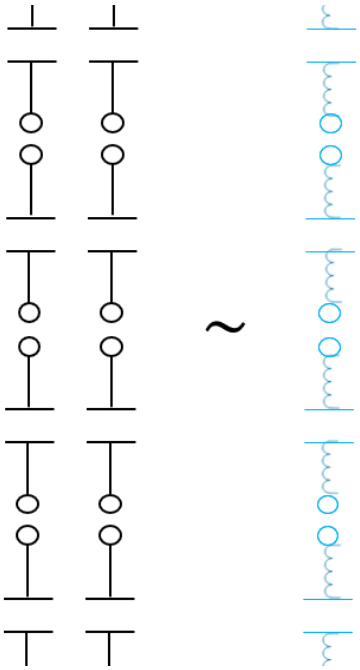

Figure 2.8. Practical Implementation of Current Sheet and its Equivalent

In Figure 2.9, (a), a λ/2 dipole array layout and its equivalent circuit is given. The array resonates around f_0. In Figure 2.9, (b), it is scaled down by a ratio. For the array; its longitudinal length, periodicity along E and H planes, thickness' and the associated tip capacitances are scaled by that ratio. Essentially, for the array everything remains constant, but the resonance frequency scales up by the ratio of down scaling. In [8], this scaling amounts are given for 2/3 scaling ratio. In this thesis, this scaling effect will be given for our design objectives, for a more realistic situation; where in [8], it is solely given for explaining the scaling concept. Input impedance of the unit cell of the infinitely periodic array of dipoles without ground plane is given by (5). Note that (5) is valid only for arrays of periodicities smaller than 0.5 λ, because only those arrays do not have any grating lobes independent of the scan angle. The more general version of (5), with resistance and reactance part of the Z_A, can be found in [9].

$$R_A = \frac{Z_0}{2 \times D_x \times D_z} \times \frac{1}{r_y} \times \left[P_{\perp} \times P_{\perp}^t + P_{\parallel} \times P_{\parallel}^t \right] \quad (5)$$

In (5), Z_0 is the intrinsic impedance of the medium that array is placed, which is 120π Ω. D_x, D_z are the periodicities along the x and z dimensions respectively; r_y is the cosine angle of the beam directed with respect to the boresight axis. $P_{\perp}, P_{\perp}^t, P_{\parallel}, P_{\parallel}^t$ are the orthogonal and parallel pattern components under receiving and transmitting conditions, respectively. $P_{\perp}, P_{\perp}^t, P_{\parallel}, P_{\parallel}^t$ are nothing but a different definition of the effective length, which is generally used for wire type of antennas. For further reference on $P_{\perp}, P_{\perp}^t, P_{\parallel}, P_{\parallel}^t$ and their definitions, consult [9]. (5) is very similar to (4), where (4) was one of the outputs of the Wheeler's old paper [6].

Finally, in [9], it is stated that; when an array is scaled, everything remains in (5) same but the D_x, D_z are decreased by the scaling amount. This scaling results in an increase of terminal impedance, hence more bandwidth is obtained for smaller element array spacings. For closely spaced arrays, that resistance can easily go high up until several hundred ohms.

In the application presented in this thesis the TCDA array is desired to be in the frequency band of 0.5 GHz to 2.0 GHz while the center frequency, f_0, is set to 1.25 GHz. $\lambda_{1.25GHz}$ is 240 mm; hence a half wave closely spaced dipole array and its periodicity is 120 mm. The dipoles are closely spaced; hence dipole lengths are also λ/2. In the desired frequency band, in order not to have a grating lobe independent of the scan angle, the unit cell dimensions of the array should be smaller than 75 mm, that is nothing but the half wavelength of the 2.0 GHz. The half wave dipole array should be scaled down to 75 mm from 120 mm, in both two dimensions. In Figure 2.9, (b); the scaled array and its equivalent circuit are given. When the array is scaled, instead of f_0 resonance frequency, which is nothing but $f_0 = \frac{1}{2\pi \times \sqrt{L_0 C_0}}$, now it starts to resonate at $(\frac{120}{75}) f_0$. As the array is scaled, the inductances associated with the wire

lengths are scaled to $(\frac{75}{120})L_0$, the tip capacitances associated with the thicknesses of the dipoles are scaled down to $(\frac{75}{120})C_0$. That scaling operation results in a resonance frequency that is $1.6f_0$. However, by increasing the tip capacitances, it is possible for new scaled array to resonate at the same initial f_0. If the total tip capacitance somehow made $C'' = (\frac{120}{75})C_0$, when multiplied with the new $L' = (\frac{75}{120})C_0$; the resultant resonance frequency would still be f_0, even though the array dimensions are scaled. If somehow by loading extra capacitive elements to the dipole tips, it has been possible to resonate the scaled array at the same frequency as the half wave dipole.

Furthermore, as the array is scaled; in (5), everything remains the same but not the periodicities. The array's terminal impedance would be squared by the scaling amounts. Applying (5) to this half wave dipole array, for boresight operation, the terminal resistance would be the same resistance calculated via (3); happens to be $\frac{480}{\pi}$ Ω, that is 152.8 Ω. This terminal resistance is valid for 120 mm lengths of dipole array. As the array is scaled down by 1.6; this resistance increases to 391.2 Ω, which is $1.6^2 \times 152.8\ \Omega$. In Figure 2.10, the equivalent circuit for an array with a ground plane backing is given. In Figure 2.10, two dots indicate dipole terminals. The dashed termination to the right corresponds to the ground plane. Two impedances labeled as, Z_1^+ and Z_1^-, correspond to the impedances seen when looking towards right and left, respectively.

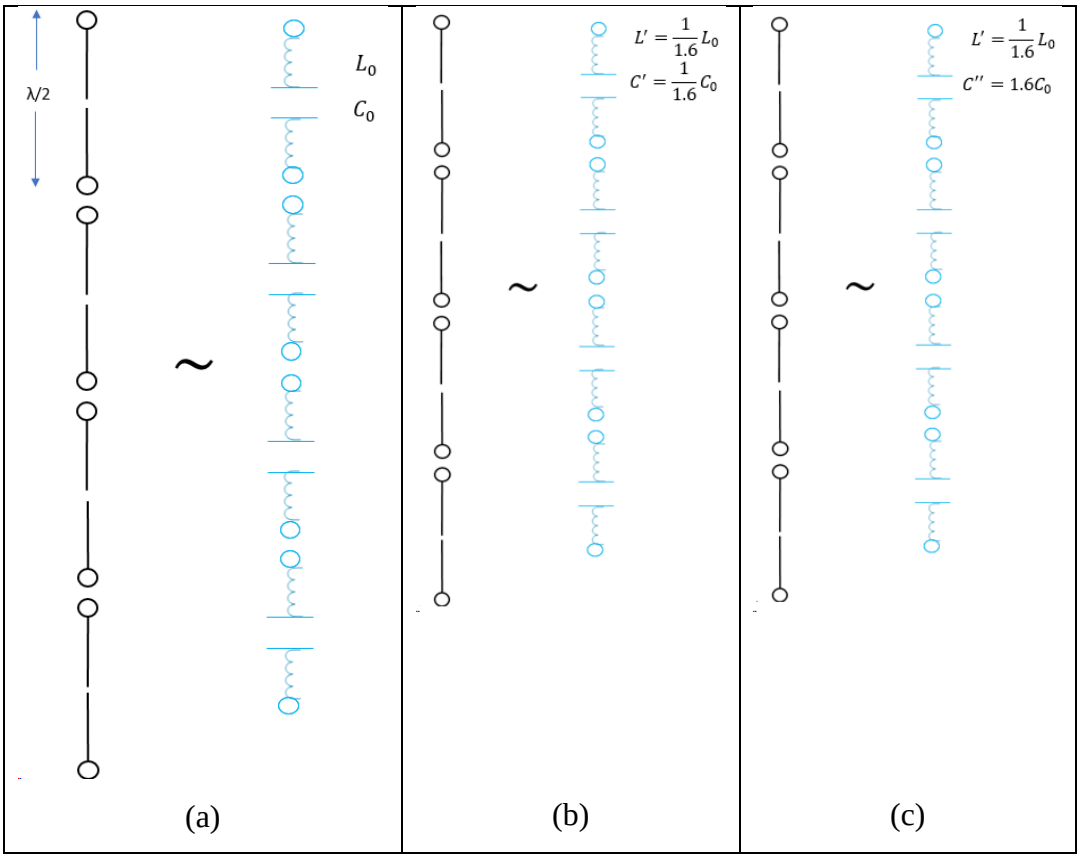

Figure 2.9. (a) λ/2 Resonant Dipole Array and Equivalent Circuit, (b) The Scaled Array Equivalent Circuit, (c) The Scaled Array Equivalent Circuit with Tip Capacitance Increased

The antenna's input impedance in the air without ground plane is $Z_{A0} = R_{A0} + jX_{A0}$; the resistive part is distributed as two parallel connections of infinitely long transmission lines, as explained before. This time, right transmission line is terminated with a short circuit. The length between the antenna terminals and the ground plane is denoted as "z_{GND}". z_{GND} should not be very low, because as it gets shorter, antenna gets shorted, input impedance would become very hard to match; due to the fact that actual currents of the aperture cancel out with the image currents generated by the infinite ground plane. Horizontal line type of currents above a

horizontal ground does not radiate and gets shorted by the image of itself. If "z_{GND}" increase much, beyond 0.5λ at any frequency; then the antenna's fields that are originating from itself and the ones that are reflected from the ground plane would add up out of phase resulting in a beam cancellation. In the light of these facts, the ground plane distance should be chosen in between those two constraints.

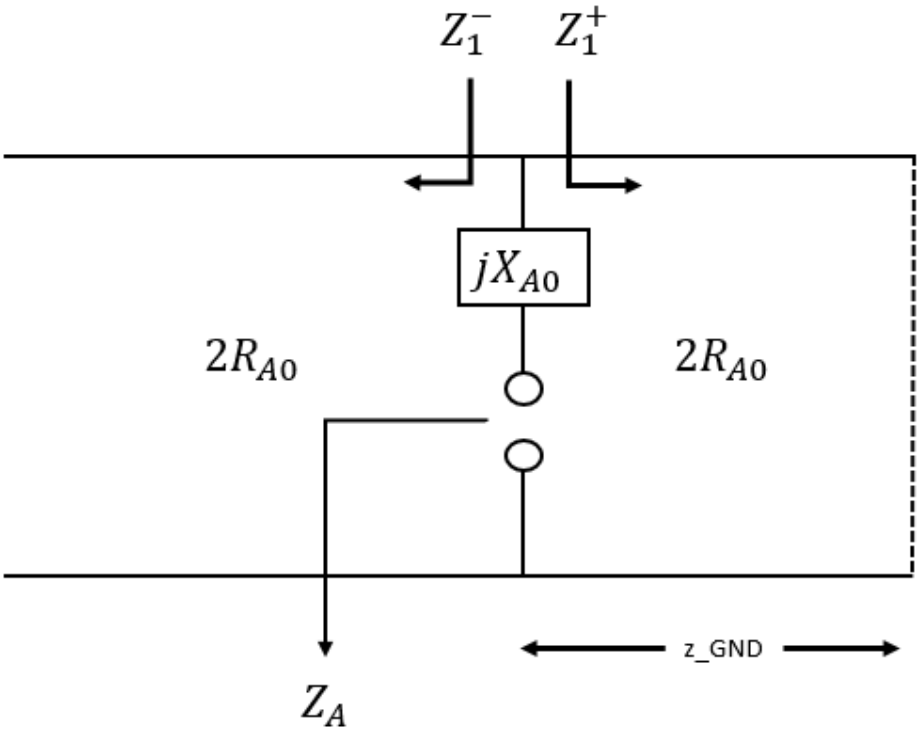

Figure 2.10. Equivalent Circuit of the TCDA with a Ground Plane

Z_1^+, is an impedance curve of transmissison line terminated with a short circuit and of z_{GND} length. In (6), Z_1^+ is given as an expression, where $2R_{A0}$ is 391.1Ω. For ground plane spacing, at the lowest design frequency 0.1λ appears to be a good choice. In the highest design frequency, for a 1:4 BW, that length corresponds to

0.4λ. Taking the z_{GND} to be 60 mm would be an appropriate choice for the desired frequency band of this thesis.

$$Z_1^+ = 1j \times 2R_{A0} \times \tan\left(\frac{2\pi}{\lambda} \times z_{GND}\right) (6)$$

The center frequency would be the one that makes Z_1^+ infinity, that is open circuit. When the z_{GND} becomes λ/4, Z_1^+ becomes open circuit. As z_{GND} is 60 mm, the center frequency corresponds to 1.25 GHz frequency of a band of 0.5-2.0 GHz. 1:4 bandwidth ratio occurs in this band. In Figure 2.11, the plot of Z_1^+ is given on the Smith Chart, whose reference impedance is $2R_{A0}$, that is 391.1 Ω. Z_1^+ is inductive at lower frequencies and it is capacitive at higher frequencies.

Then, according to the equivalent circuit given in Figure 10, Z_1^+ is parallel connected with Z_1^-; the obtained impedance is given in Figure 2.121. Note that Z_1^- is an open-ended transmission line of $2R_{A0}$. The resultant impedance curve is given in Figure 2.11.

Finally, jX_A is added to the parallel combination of Z_1^+ and Z_1^-. jX_A is capacitive at lower frequencies and inductive at higher frequencies. jX_A can be thought as if it consists of inductance L_0, representing the dipole arms and in series with a capacitance C_0, representing the total tip capacitance. Discussion on C_0 was given previously, an equivalent circuit for representing jX_A is given. in Figure 2.12.

For obtaining antenna's final input impedance jX_A is added in series with the $Z_1^+ // Z_1^-$. Final input impedance of the array is obtained. Here, L_0 and C_0 are picked such that at the lowest and the highest design frequency, the final antenna impedance has no reactive parts. Two equations exist for the two unknowns, L_0 and C_0. L_0 and C_0 were found to be 19.73 nH and 1.283 pF, respectively. Plot of X_A vs frequency is given Figure 2.13.

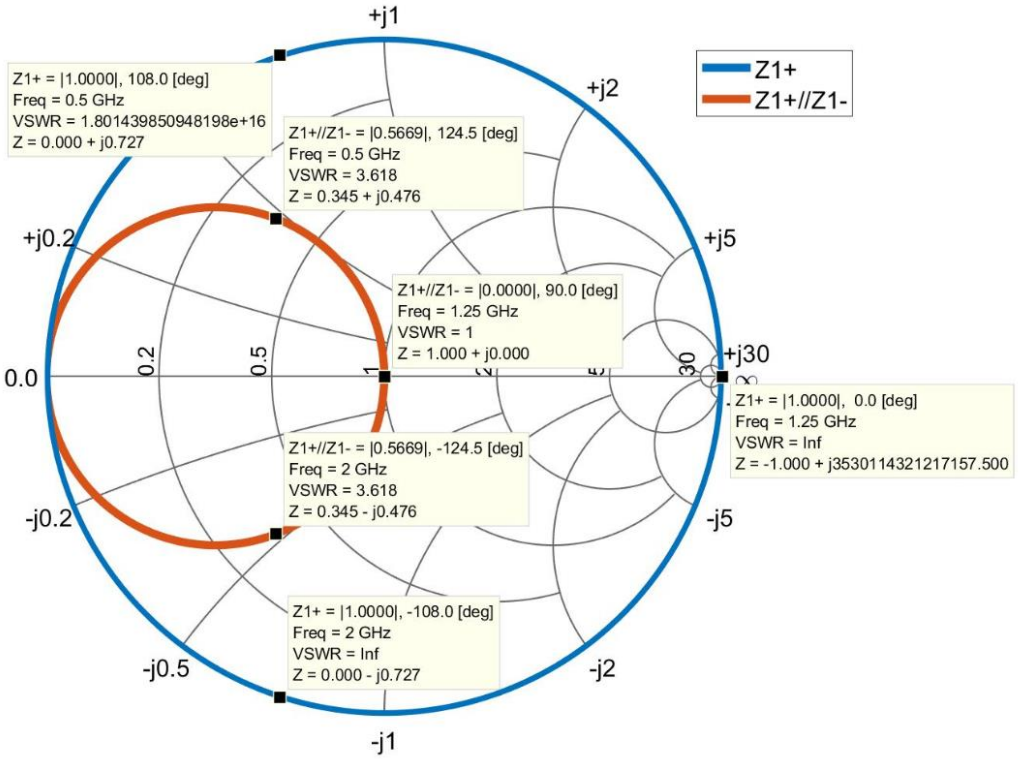

Figure 2.11. Plot of Z_1^+ and $Z_1^+ // Z_1^-$ vs Frequency on a Smith Chart, in 0.1 GHz to 4.0 GHz Frequency Band, 391.1 Ω Reference Impedance

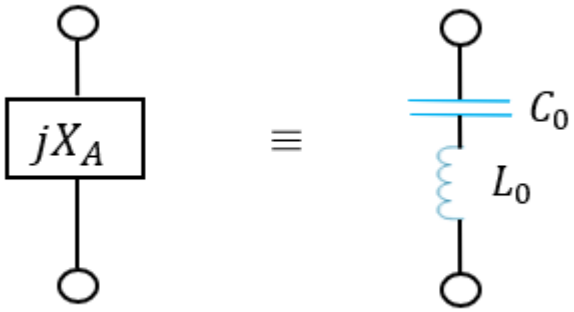

Figure 2.12. Equivalent Circuit Representing jX_A

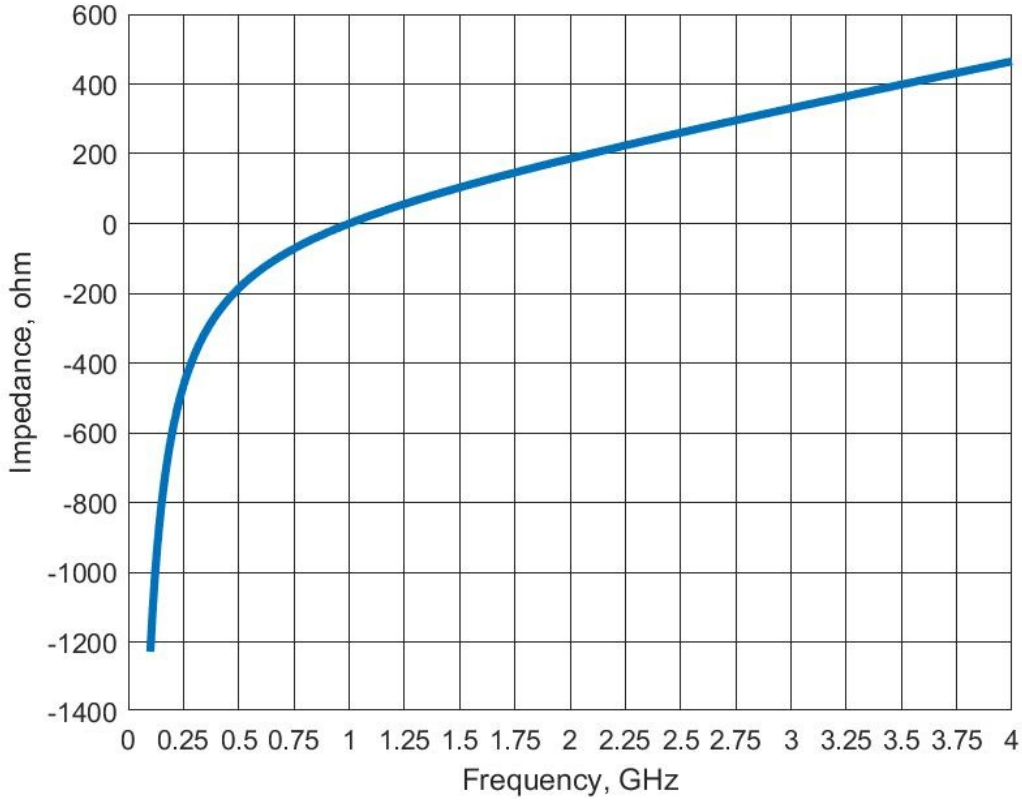

Figure 2.13. Plot of X_A vs Frequency, in 0.1 GHz to 4.0 GHz Frequency Band

The discussion and calculations on jX_A are idealized. In a more realistic scenario, one is able to tune out C_0 by changing the capacitance between adjacent dipoles; L_0 can be controlled by the width of the dipole wires, since periodicities are fixed in the calculations. Actually, the tip capacitance between the dipoles in the calculations are solely for the tuning properties of the jX_A, such that a current sheet is implemented at the array aperture. The resonance frequency of the jX_A resonator is 1 GHz, different from the antenna's center frequency that was 1.25 GHz. By examining Figure 2.13, it is observed that jX_A obtains its zero value at 1 GHz. This difference results in a higher VSWR around the center frequency of the desired frequency band.

Final input impedance of the array unit cell is calculated and it is given in Figure 2.14. For clarity, it is given in a Smith Chart that has reference impedance same with

the other Smith Chart's given before in this chapter. As it can be seen in the Figure 2.14, the final impedance curve is clustered for the desired frequency band of this thesis, if one can cluster this impedance around the right impedance, then one can obtain a wideband array.

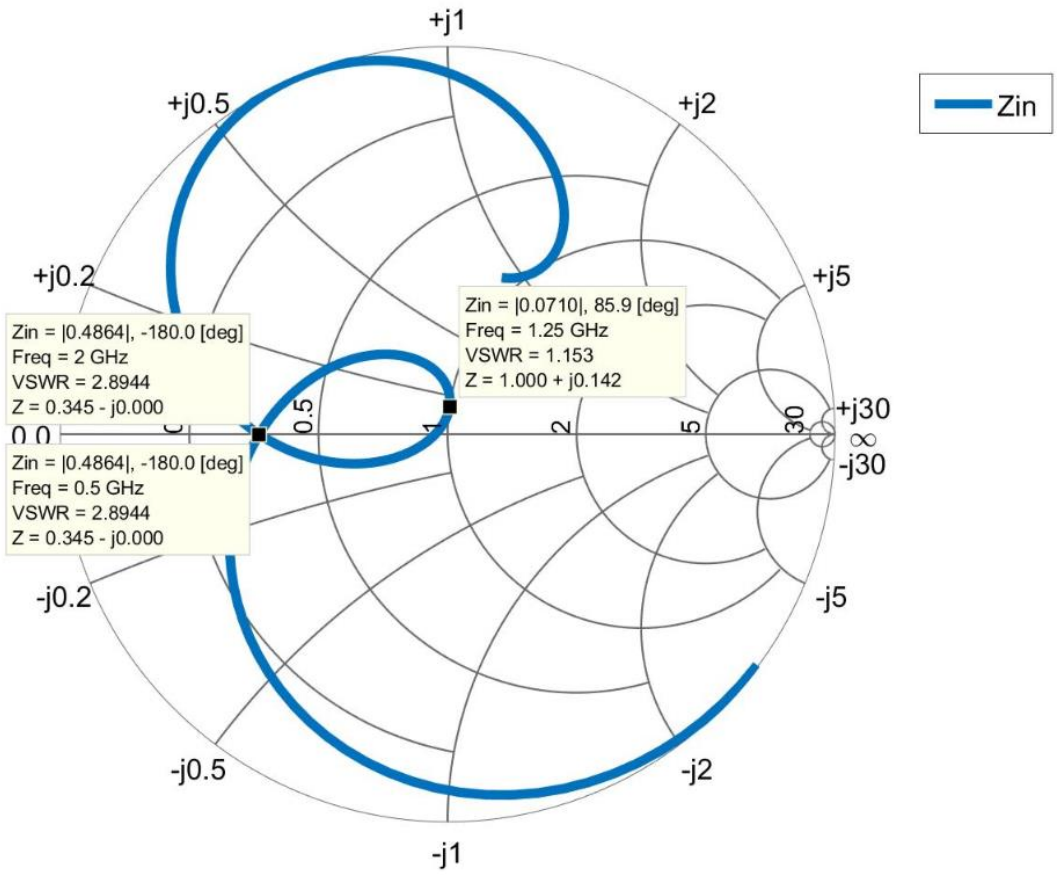

Figure 2.14. Final Input Impedance of the Array Unit Cell, on Smith Chart, in 0.1 GHz to 4.0 GHz Frequency Band, 391.1 Ω Reference Impedance

By examining Figure 2.14, it is observed that 200 Ω is an impedance that centers the final resultant impedance curve cluster. Furthermore, the input impedance of the array unit cell obtained is somewhat idealized; L_0 and C_0 are picked such that they completely cancel out the imaginary parts. $2R_{A0}$ will vary with frequency as well.

$2R_{A0}$ is a resistance that will also change due to the addition of ground plane as well as X_{A0}, reactance part of the Z_{A0}. Addition of a ground plane alters both of these quantities and makes them frequency dependent [7]. jX_A is not only associated with the wire inductances and tip capacitance; however, the calculations assumed that they're not effected by the addition of ground plane. In practice, jX_A gets effected by the addition of the ground plane.

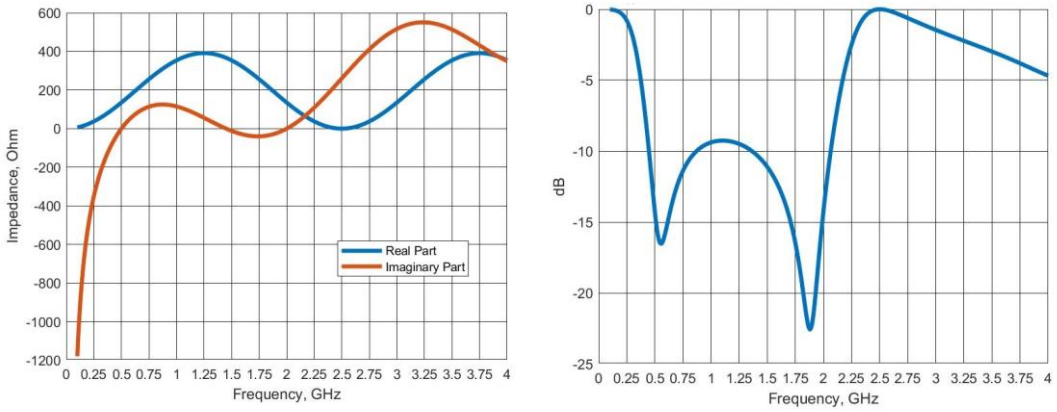

(a) (b)

Figure 2.15. (a) Input Impedance of the Array Unit Cell, Real and Imaginary Parts, (b) Input Return Loss of the Array, 200 Ω Reference, dB Scale, in 0.1 GHz to 4.0 GHz Frequency Band

In Figure 2.15, the real and imaginary parts of input impedance of the array unit cell and input return loss of the array unit cell in dB scale with respect to the 200 Ω reference impedance is given. Referring to Figure 2.15; at the center frequency of the array, i.e. at 1.25 GHz, antenna unit cell input impedance has non-zero reactance; resulting in that region's VSWR to increase beyond 2. For reference, VSWR of 2 corresponds to an input return loss of 9.54 dB. Theoretically, a TCDA can operate on a 4:1 frequency band with VSWR<2, as indicated in [8]. It is beneficial to mark the fact that, jX_A resonates at 1 GHz, as provided in Figure 2.13. The curve for antenna unit cell input impedance given in Figure 2.15, providing 4.56:1 frequency

bandwidth, under VSWR~2 criterion. The highest return loss of 9.26 dB occurs at 1.11 GHz. Furthermore, the antenna unit cell input impedance in dB scale attains zero value at two locations: first one is towards 0.1 GHz frequency; at such low frequencies impedance curve gets affected severely from the presence of ground plane. Dipole currents get shorted with their images, horizontal currents above a horizontal infinite ground plane does not radiate. The second one is at 2.5 GHz, this is the frequency where distance between antenna aperture and infinite ground plane is exactly λ/2. That condition is equivalent to aperture to infinite ground plane distance being zero.

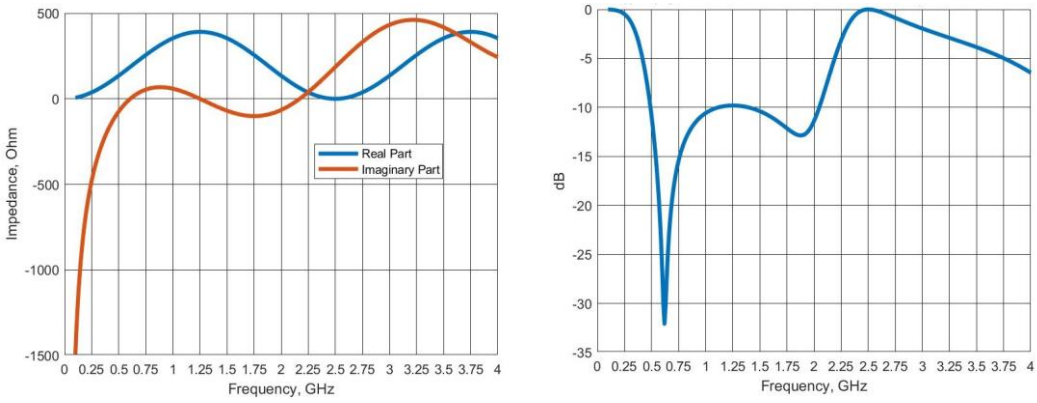

(a) (b)

Figure 2.16. (a) Final Input Impedance of the Array Unit Cell, L_0 and C_0 are compensated, Real and Imaginary Parts, (b) Final Input Impedance of the Array Unit Cell, L_0 and C_0 are compensated, 200 Ω Reference, dB Scale, in 0.1 GHz to 4.0 GHz Frequency Band

Furthermore, by scaling the L_0 and C_0 by 0.8; such that jX_A's resonance frequency is shifted to 1.25 GHz rather than 1 GHz; VSWR<2 is obtained in the entire desired frequency. Scaling L_0 by 0.8 physically corresponds to increasing the dipole arm widths. Scaling C_0 by 0.8 physically corresponds to reducing the dipoles' tip

capacitances. In Figure 2.16, the resultant new impedance curves and their dB equivalents are given. Note that, at the center frequency, 1.25 GHz; this time input impedance of the array unit cell, has no reactance, it is composed of pure resistance at 1.25 GHz. The resultant impedance curve gives 4.26:1 frequency bandwidth under VSWR<2 criterion in the desired frequency band. The input return loss attains its highest value of 9.8 dB at 1.25 GHz. Note that, at the expense of reducing the maximum VSWR inside the band; the bandwidth offered is reduced. Actually, the author suggests that L_0 and C_0 must be determined by applying formal optimization techniques for the required return loss and bandwidth. In this thesis, as stated previously, L_0 and C_0 were initially calculated so that, the antenna unit cell input impedance has no reactance terms at 0.5 GHz and 2.0 GHz, as given in Figure 2.15.

CHAPTER 3

UNIT CELL ANALYSIS OF TCDA

In this chapter results of the simulations which are carried out in the HFSS environment are presented to demonstrate the concept. First, a previously published paper on TCDA is taken and it is implemented by scaling its frequencies to the design frequencies. At the same time, dual linear orthogonal polarization is implemented while the original paper has single linear polarization. Then, new spiral shaped capacitance elements are used for the unit cell of TCDA. Finally, two TCDA unit cells using those structures are optimized for design frequencies.

3.1 Implementation of a TCDA Antenna for Dual Linear Orthogonal Polarization

Initially, in order to prove the concept, the author thought that it would be appropriate to take an existing TCDA antenna with given dimensions and simulate it by using HFSS. There are several existing papers that incorporate TCDA concept [10]–[13]. There is a given TCDA antenna unit cell with dimensions in [13]. Although proposed antenna of [13] is for 8.0 – 12.5 GHz, it is still considered to be a good place to start. First, the antenna is drawn with all the dimensions scaled down to the desired frequency band of 0.5 – 2.0 GHz. Appropriately, all the dimensions given in [13] are multiplied. Furthermore, any dielectric layers between the radiator and the ground plane were not considered; only the antenna radiator and the ground plane were present. Since the goal is to obtain a TCDA antenna of dual linear polarization operating in 0.5-2.0 GHz, another dipole arm and associated coupling capacitor are drawn. In Figure 3.1, the top view of the antenna unit cell is given. Unit cell was 69 mm × 69 mm and distance between antenna and the ground plane was 48 mm.

The red portions in Figure 3.1 indicate the dual linear feeds, the yellow portions indicate the antenna metallization. Port impedance is taken as 200 Ω for the entire of the studies if not stated otherwise.

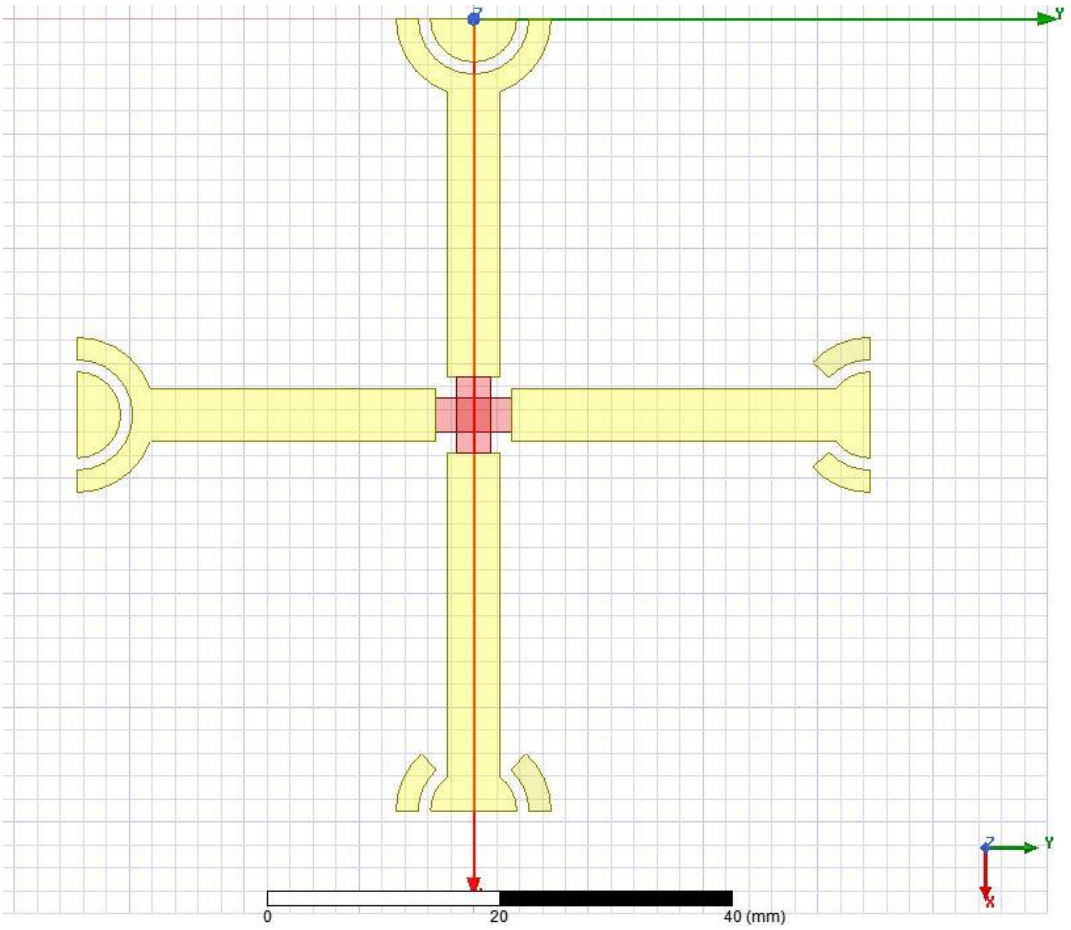

Figure 3.1. Dual Orthogonal Linearly Polarized TCDA

In Figure 3.2, one set of master-slave boundaries is given as a reference configuration. The master boundary, its corresponding slave boundary and their excitation vectors are given. Boresight excitation is simulated; i.e. no progressive phase shift is given between master and slave boundaries. The results for the proposed HFSS analysis are given in Figure 3.3. Both polarizations are excited.

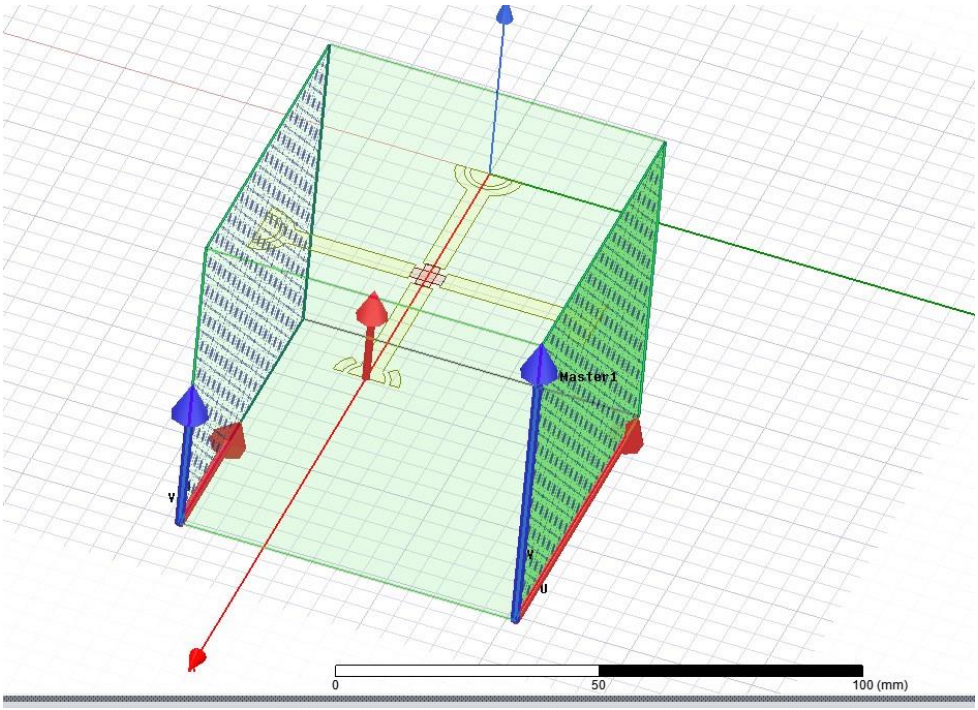

Figure 3.2. Dual Orthogonal Linearly Polarized TCDA, Master and Slave Boundaries for HFSS Infinite Array Unit Cell Analysis

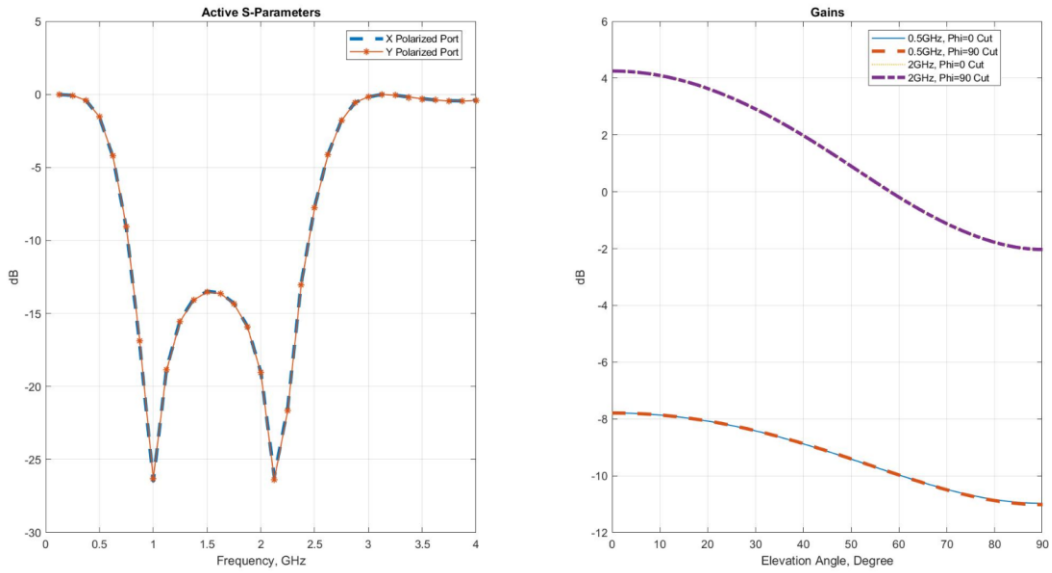

Figure 3.3. Active S-parameters and Gains for 0.5 GHz and 2.0 GHz

From this analysis, we conclude that the TCDA concept presented here works properly. A TCDA antenna unit cell can have good impedance matching to a specified impedance that is generally 188 or 200 Ω without any dielectrics or superstrates.

The provided gain for the unit cells is the pattern of one element in an infinite array. It does not contain the input return loss. To obtain total array gain, that gain is multiplied with the isotropic array factor.

3.2 A TCDA Unit Cell Element Utilizing Interdigital Type Capacitances

In order to optimize faster, the antenna is simulated as a single polarized antenna, having only one set of dipole arms along $\hat{y}$ direction. Therefore, there is only one set of S-parameter vs frequency data. The motivation behind this method lies in the following fact: the other polarization is orthogonal to the current one and the author expects minimal coupling between two modes, in theory zero coupling ($-\infty$ dB), using Rumsey's reactance definition [16].

In Figure 3.4, the unit cell structure of the TCDA using interdigital capacitors and its input return loss performance is given. It clearly gives VSWR<2 in the band of 0.5-2.0 GHz frequency and the unit cell is around 65 mm in length. Also note that, in the unit cell's active S-parameter results, at 2.5 GHz, active S-parameter attain a 0 dB value, means that all the incident power has returned to the source. This is due to the fact that at that frequency, the infinite ground plane below the antenna aperture and aperture have distance of $\lambda/2$. The short circuit impedance of ground plane has revolved an exact full tour at that frequency, active input resistance of the unit cell becomes zero.

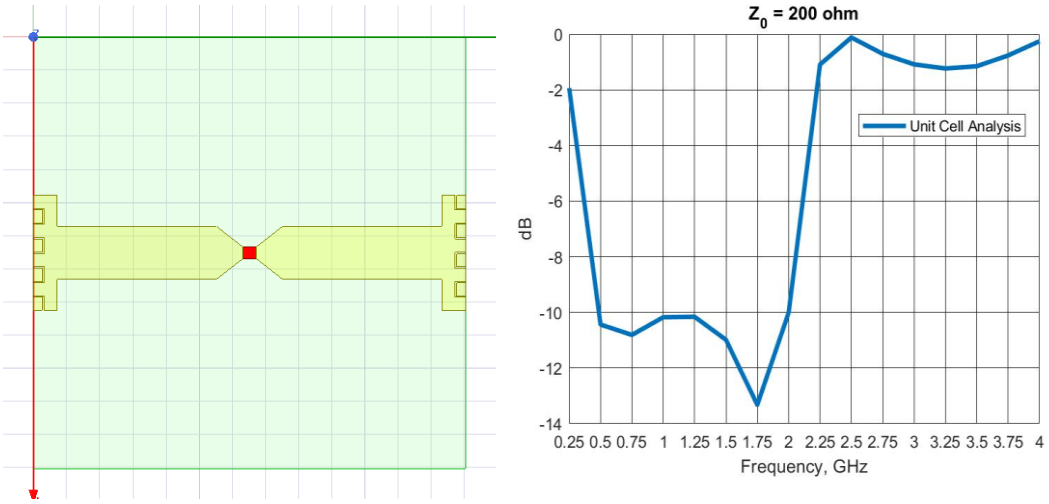

(a) (b)

Figure 3.4. (a) Top View of the Interdigital Capacitance Unit Cell, (b) Active S-Parameter of the Interdigital Capacitance Unit Cell

In Figure 3.5, the patterns for this tightly coupled dipole array unit cell are given. The unit cell patterns are good, they show no sign of grating lobes as expected, due to the fact that dimensions of the unit cell are lower than $\lambda/2$ for all frequencies in the 0.5-2.0 GHz frequency band. Also note that, $\Phi=0^0$ degree cut patterns have exact nulls towards endfire direction. The reason is due to the existence of infinite ground plane. The actual currents on the dipole terminals and their images created by the infinite ground plane completely cancels out each other along those directions. Therefore, true nulls occur along those directions at $\Phi=0^0$ cuts. $\Phi=0^0$ is the H-plane of the antenna.

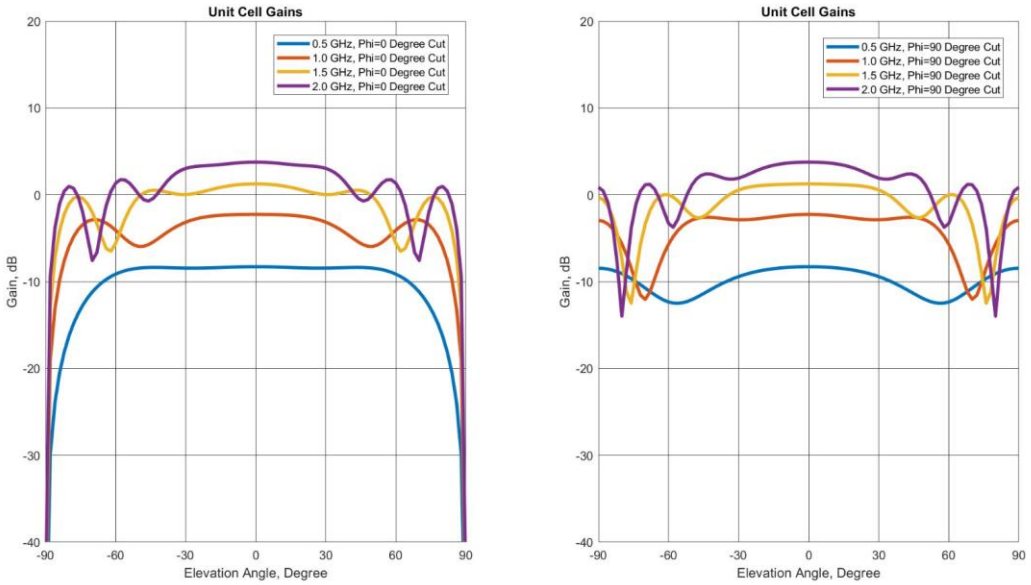

Figure 3.5. (a) For the optimized antenna unit cell, $\phi = 0^0$ cut Gains of 0.5-2.0 GHz, (b) For the optimized antenna unit cell, $\phi = 90^0$ cut Gains of 0.5-2.0 GHz

3.3 Implementation of Coupling Capacitors of Spiral Like Shape

Existing capacitance shapes of TCDA antennas are generally patented by several patents that are usually linked to each other. One is a US Patent given in [14]. In [14], under it is claims the author specifically stated that fingered capacitive coupling structure is under patent's rights. In [15], multi-layer implementation of the capacitance element is claimed though. Some papers using different shapes have been published, one is [13]. In order to not to use the shape given in existing literature a new kind of spiral based capacitance structure proposed that is the original contribution of this thesis work. This new capacitance shape that allow capacitive coupling between adjacent elements of TCDA antenna, can be seen in Figure 3.6.

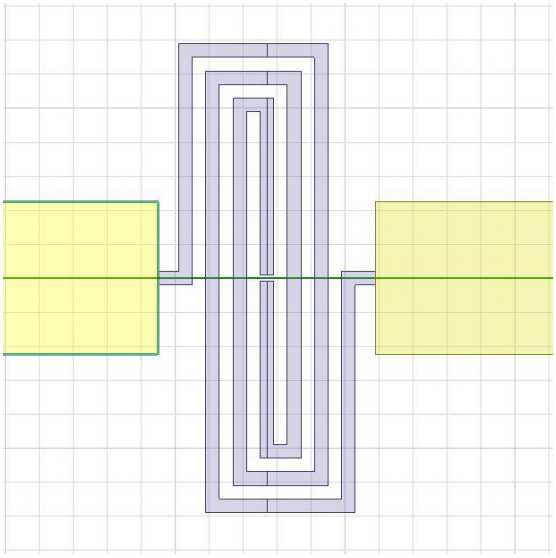

Figure 3.6. New Spiral shaped Capacitive coupling scheme for TCDA

In order to justify that the aforementioned structure can be used, the author needed some optimization work to be done. To lower the antenna's lowest frequency of operation, capacitance between them shall be increased. Spiral arms were made a little thicker and their widths were increased at the dipole ends. After several electromagnetic simulation attempts, the author could have been able to achieve input active S-Parameters almost below -10 dB for all 0.5-2.0 GHz bandwidth, and element Gains are uniform. By uniformity the author means that the following: element pattern has no sign of any sidelobes, at highest frequency there is no gain dropout and for all frequencies, the gain patterns are similar. In Figure 3.7, active S-parameter in dB scale and gains in dB scale for both $\phi = 0^0, 90^0$ cuts can be seen. Note that, $\phi = 0^0$ cuts, i.e. along the H-plane of the dipole; patterns have nulls at +/-90^0 elevation angles. The reason of this effect is due to the original antenna currents and their images generated by the infinite ground plane cancel out each other. A perfect null occurs along those directions due to the cancellation with the image currents. However, at E-plane; such an effect does not occur. There are not any pattern nulls along those directions. Also note that, the active S_{11} of this

nonoptimized unit cell attains its zero dB value at 2.3 GHz as it can be seen in the Figure 3.7. The distance between aperture and infinite ground plane for this unit cell was 65 mm. At 2.3 GHz, that distance corresponds to λ/2.

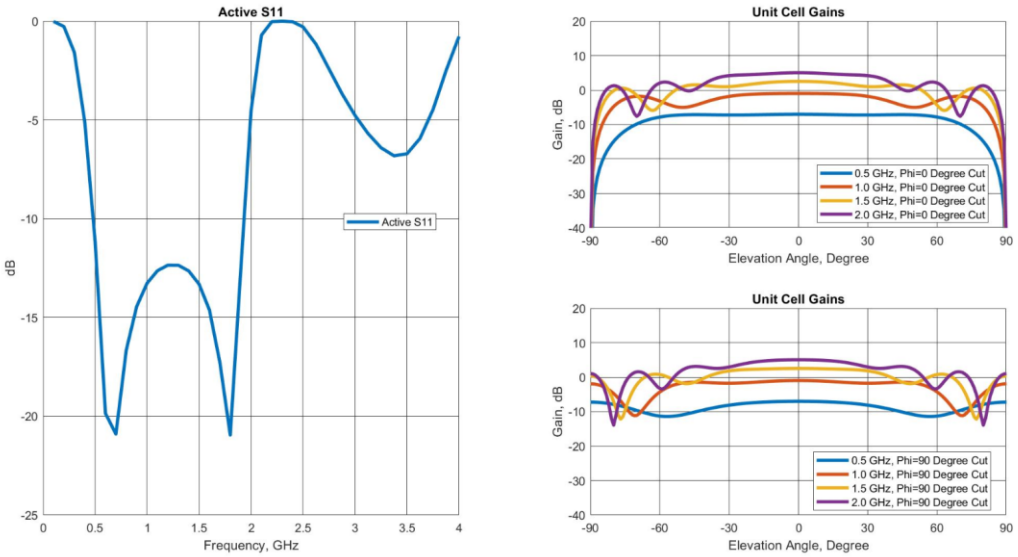

Figure 3.7. Active S-Parameter and Gains of TCDA of Spiral Shaped Capacitor, for $\phi = 0^0, 90^0$ Cuts

3.4 Optimization of Spiral Shaped Capacitance Structure and Dipole Array Element

It is stated that in [8] that TCDA of having one dielectric layer achieve 4:1 bandwidth under VSWR<2 criterion. VSWR=2 corresponds to reflection coefficient of -9.54 dB, in dB scale. In this thesis, 0.5 - 2.0 GHz frequency band is set for design goals, including impedance matching and Gain pattern quality as well as -10 dB input active S_{11} for all ports or if any corporate network input. As a dielectric layer, RO3003 substrate ($\varepsilon_r = 3.0, thickness\ 1.524\ mm$) is picked, which is available to the author in the facility where he is working for. Beneath the dielectric substrate, a

foam material of having $\varepsilon_r = 1.07$ is put, all the way down the GND plane beneath the dielectric card. The distance between the GND plane and the antenna should not exceed λ/2 in all frequencies. Then, the limiting frequency is 2.0 GHz. $\lambda_{2GHz} = 150\,mm$; therefore, ground plane spacing shall not exceed 75 mm, which is half wavelength at 2.0 GHz. This limit lies in the following fact: antenna metallization above the dielectric card radiates basically 2 beams, one is towards $+\hat{z}$ direction, i.e. towards air. The other beam is towards $-\hat{z}$ direction; i.e. towards GND plane. When the GND plane spacing is λ/2 in any frequency, the 2 main beams cancel each other resulting in a gainless antenna. Because in the vicinity of half wave spacing, even though the two beams do not cancel each other exactly; it is wise to stay away from the λ/2 resonance. However, one cannot pick extremely small ground plane spacing beneath the antenna. The reason behind the latter limit is due to the following fact: If the antenna radiator is too close to the GND plane, GND plane creates an image of the currents under the GND plane, cancelling out the actual antenna currents; namely shorting the antenna. For the latter limit for the GND spacing, the limiting frequency is 0.5 GHz. $\lambda_{0.5GHz} = 600\,mm$, GND plane spacing in terms of wavelengths is smallest for the 0.5 GHz. In the light of these limitation, 60 mm for the GND plane spacing is picked, which is 0.1λ in the lowest design frequency.

After GND plane spacing is fixed, to achieve desired design, some optimizations on unit cell of the TCDA have been made and the new type of spiral shaped capacitance element. For a grating lobe free array at any scan frequency, the antenna unit cell has to be smaller than λ/2 [7]. If that criteria met, antenna array will not have any grating lobe within $\theta = [0^0, 90^0]$ scan angle. Note that, θ larger than 90^0, corresponds to the space below the GND plane, where the author expects to have no field propagating towards that direction. So, optimization should consider the fact that antenna unit cell to not to exceed 75 mm, where $\lambda_{2GHz} = 150\,mm$.

In the limitations stated above, dipole radiator's arm length, width as well as spiral capacitance were used in this optimization. Spiral capacitance was tuned by changing 3 parameters, namely they are width between spiral arms, lengths of arms and widths

of arms. Furthermore, dipole is constructed as a bowtie element in order to obtain additional bandwidth contribution. Thickness of the bowtie type dipole is varied to get 10 dB return loss bandwidth. In Figure 3.8, infinite array active S-parameters results can be seen together with the antenna shape obtained after the optimization. In addition, one should note that unit cell analysis is such fast that it allowed author to optimize easily using a personal use laptop, the whole frequency band was possible to be solved within 1 minute. Note that 60 mm ground plane to aperture distance, results in zero dB active S_{11} if air would be present between those two planes. Now, there is a foam material of $\varepsilon_r = 1.07$, electrically increasing that distance. Therefore, instead of observing 0 dB exactly at 2.5 GHz; it is observed between 2.25 GHz and 2.3 GHz.

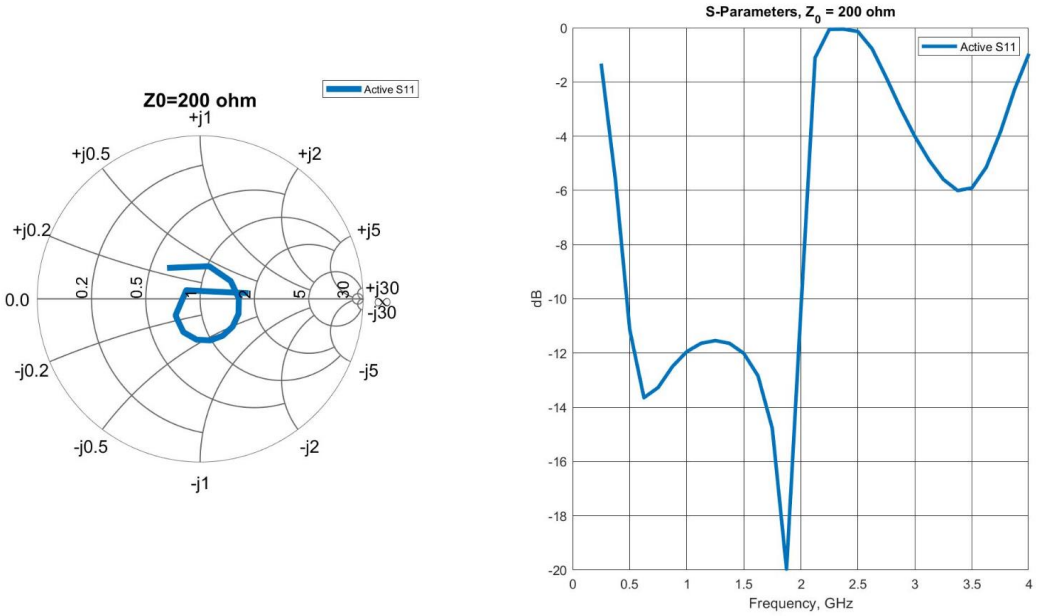

Figure 3.8. Active S-Parameter of the optimized antenna plotted on a 200 Ω referenced Smith Chart, in 0.5 – 2.0 GHz frequency band and S11, dB of the optimized antenna, in 0.25 – 4.0 GHz frequency band

The shape of the optimized antenna is shown in Figure 3.9. The infinite ground plane is also visible in Figure 3.9.

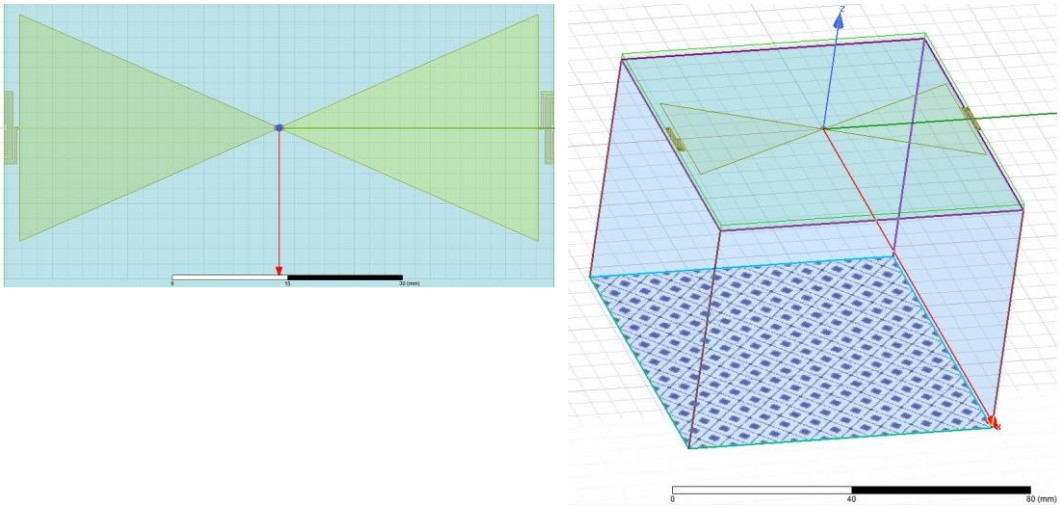

Figure 3.9. (a) The optimized antenna unit cell, Top View, (b) The optimized antenna unit cell together with the infinite GND plane

The patterns of the unit cell analysis are given in Figure 3.10, for both 0° and 90° Cuts, as a function of the azimuth angle θ. As expected, the patterns are uniform and there are no signs of grating lobes at any frequency. $\Phi=0^{0}$ cuts have perfect nulls along $\theta = +/-90^{0}$ directions again here, due to the existence of infinite ground plane below the aperture.

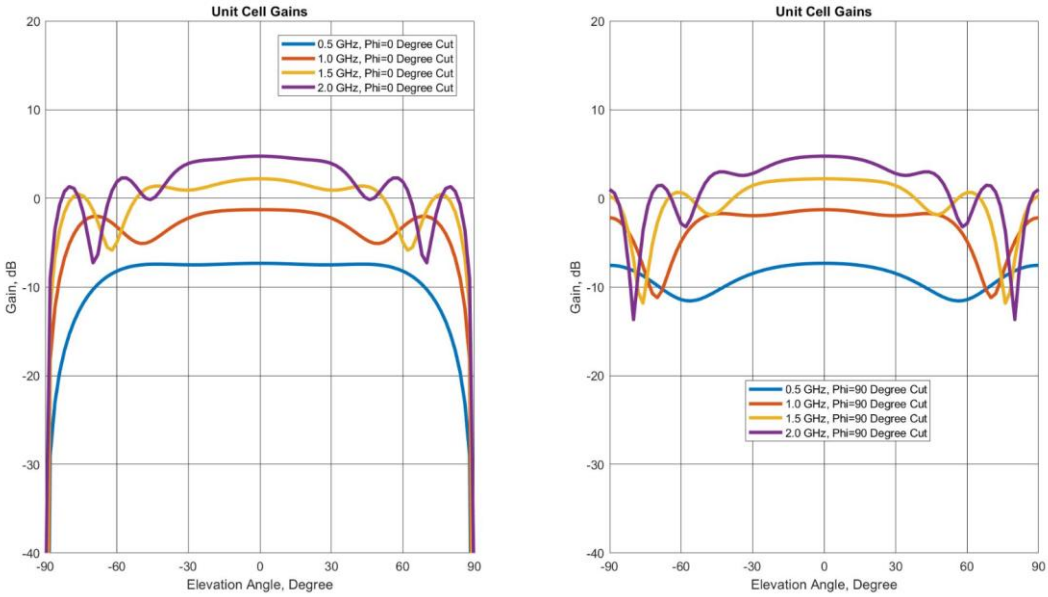

Figure 3.10. (a) For the optimized antenna unit cell, $\phi = 0^0$ cut Gains of 0.5-2.0 GHz, (b) For the optimized antenna unit cell, $\phi = 90^0$ cut Gains of 0.5-2.0 GHz

CHAPTER 4

FINITE ARRAY STUDIES

Using the experience gained in the unit cell analysis, the next work is the analysis of finite antenna arrays. The problematic conditions emerged when analyzing finite size arrays, especially at the low frequency end of the desired frequency band. Therefore, the simulations provided in this chapter are focusing to the lower frequency end of the desired frequency band of this thesis.

First, a single polarized tightly coupled dipole antenna array of 4×4 elements is designed and constructed as shown in Figure 4.1.

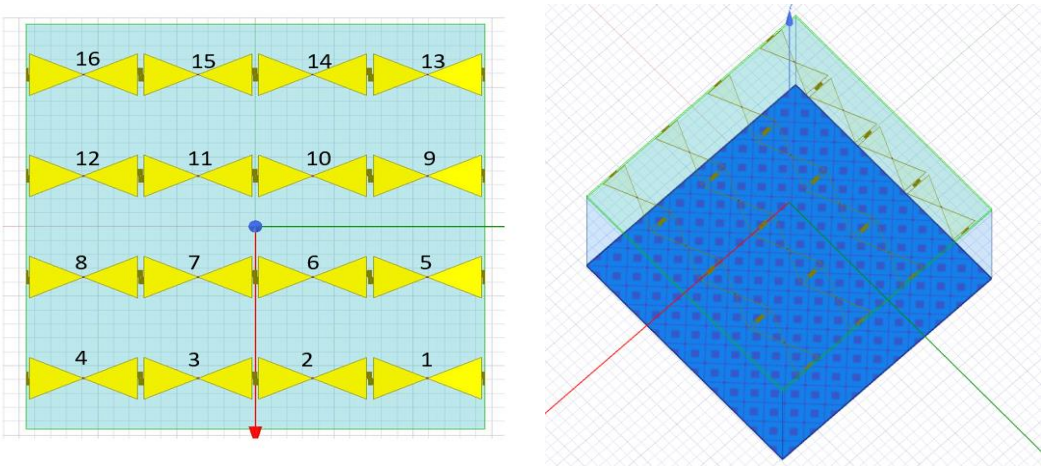

(a) (b)

Figure 4.1. (a) 4x4 Prototype Tightly Coupled Dipole Array, Top View, (b) 4x4 Prototype Tightly Coupled Dipole Array, 3D View

In the prototype array, 4 rows of tightly coupled dipole elements exist, where each row has 4 elements. In order to reduce the simulation complexity, foam and dielectric card is made up from a box whose widths and lengths are 4 unit cell length. The dipole arms and lumped element feed are duplicated along x and y directions so that the array is 4×4 resulting in 16 lumped ports. In Figure 4.1, (a); the port numberings are shown in Figure 4.1, (a). One element is 68.6 mm in both width and length, hence the array spacing in both directions is taken of the same length. Unit cell is 0.115λ in 0.5 GHz and 0.46λ in 2 GHz. The finite array makes approximately 0.5λ and 2.0λ in lowest and highest design frequencies, respectively. As the TCDA concept miniaturizes the distance between GND plane and the antenna radiators, the aperture is not taken too large as well. Additionally, as the initial aim were to check the proof of concept, the array constructed is not so large so that the results can be seen in a quick way.

In Figure 4.2, one can see the active S-parameters of individual elements, in (a) they are on the Smith Chart, in (b) they are shown in dB scale. For the reference, the active S-Parameters of the unit cell element that was considered previously is also given. Even though the design frequency band of the antenna is 0.5-2.0 GHz, in Figure 4.2 the reflection coefficients are given for 0.25-2.0 GHz, since the lowest design frequency is important in UWB antennas. Frequencies higher than 2.0 GHz are not provided in this chapter since the problematic part of the band is around lower frequencies. Solving for frequencies below the lowest design frequency is a method that is applied for the rest of the analyses as well. For checking behavioral similarity between the unit cell analysis and the finite array analyzes, the data is given as such.

One would expect that the peripheral elements in the finite array would be mismatched. By using mismatch word, it is said that an element on the edges do not have similar impedance behavior in comparison to the central elements over the frequency band considered. By using impedance mismatch, it is concluded that active impedances in complex plane diverge from 200 Ω; which was the input impedance of the unit cells considered. As peripheral elements are on the edges,

they do not exhibit the infinite array behavior. Furthermore, in tightly coupled dipole array, those elements' outer side capacitance is not coupled to any adjacent element. This makes another reasoning for those elements' impedance behaviors to become mismatched. In Figure 4.2, this effect can be seen. However, in Figure 4.2, there is something more important. Even the most central 4 elements, that are ports 6, 7, 10, 11; have active S-Parameters far from the unit cell element's simulated active S-Parameters. In Figure 4.2, for the representation of central elements; namely, ports 6, 7, 10, 11; the data is given only for the port 6. Since the ports 6, 7, 10, 11 are reciprocal in the array environment; such an action is viable. Even those central elements have active S-Parameters higher than -10 dB almost all of the band. In [12], this issue was addressed as well, when such an array is fully excited without any terminations at the edges, it is reported that even though the central elements mismatch significantly. In [12], along with resistive termination, open and short circuit terminations of the edge elements are considered. The latter ones are better from the antenna efficiency point, however the former one is best for lowest active VSWR and henceforth widest bandwidth. As a solution, it was suggested that two rows of elements on each side in an 7×7 finite array, are terminated with resistive loads so that only three rows of arrays are excited; hence the lowest active VSWR's across the whole band is obtained.

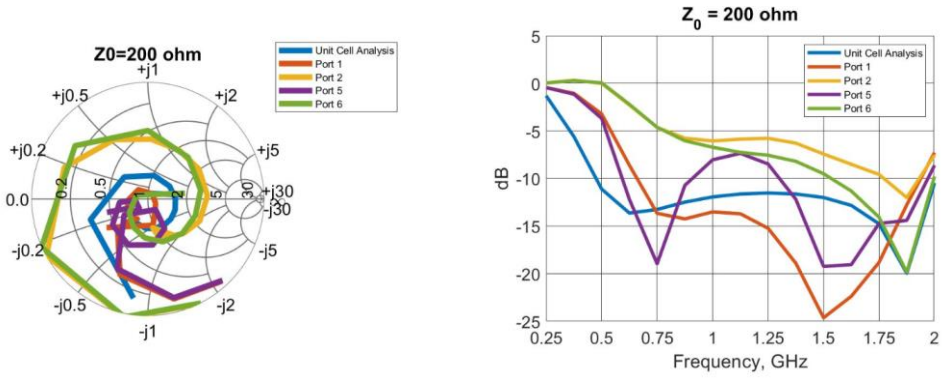

Figure 4.2. Active S-Paramaters of Individual Elements, 200 Ω Reference, Linear and dB scale, in 0.25 – 2.0 GHz Frequency Band

To solve that issue, all the peripheral elements are excited with zero energy, based on the definition of S-parameters. When a port is excited with zero energy; it is terminated with the system Z_0. As a side note, this concept is checked in HFSS environment and has been verified in the simulation environment as well. Therefore, for any element that is being terminated with a resistor, it is appropriate that resistance value equal to the system Z_0, that is 200 Ω, can be placed to its port. In Figure 4.3; active S-Parameters of the port 6; i.e. central elements' representation, while the elements around the edges of the finite array are terminated with matched loads, are given. For comparison, active S-Parameters of those ports under fully array excitation and the active S-Parameters of the unit cell analyses are included.

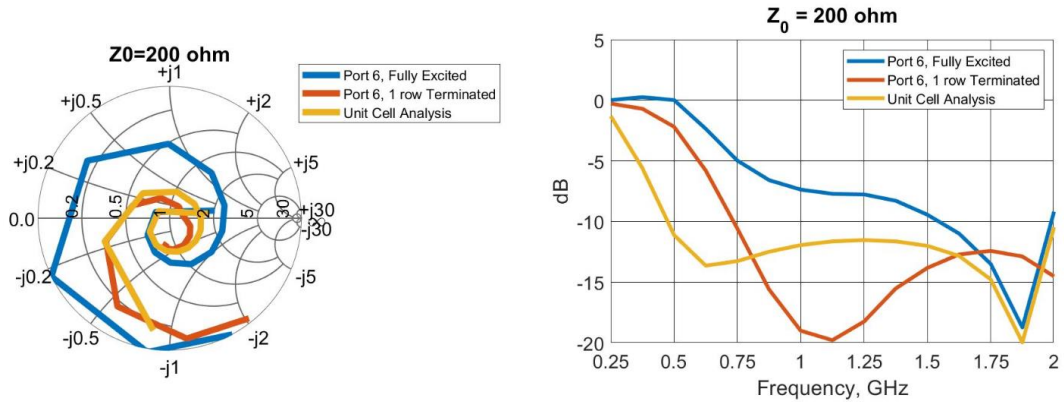

Figure 4.3. Active S-Parameters of Port 6, 200 Ω Reference, in 0.25 – 2.0 GHz Frequency Band

As it can be seen in Figure 4.3, after terminating the outer elements with the resistive 200 Ω loads; active S-parameters of the central elements are improved. Almost the whole band have active S-parameters lower than -10 dB; however, in the low frequency end, especially below 0.75 GHz, a significant impedance mismatch does still exist. At the lowest design frequency, the central ports have active S-parameter values worse than -2.5dB.

4.1 Determination of Number of Excited Elements In Finite Arrays Using Stick Arrays

To investigate impedance mismatch issue at low frequencies; arrays that have more than 4 elements have been constructed and analyzed. The aim is to find out how many elements are required for a finite array to mimic the unit cell impedance behavior. Firstly, "stick arrays" have been constructed for this investigation. The "stick array" definition comes from [8]. In Figure 4.4, an example of stick array of 1 × 5 elements can be seen.

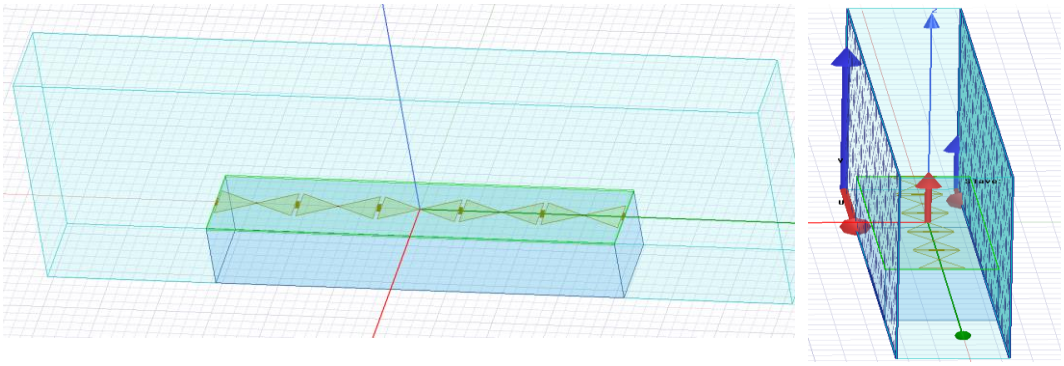

Figure 4.4. An example Stick Array of 1 × 5

In a stick array, array behaves like infinite along the normal of the master and slave boundaries, however finite along the arraying direction. Master and slave boundaries are applied along H-plane. In Figure 4.4, master and slave boundaries are given. By increasing number of elements in the stick array, infinite array impedance properties were obtained. Several simulations of stick arrays have been conducted. The first one is 1 × 5 stick array. In Figure 4.5, active S-parameter of the center element of the stick 1 × 5 array and the infinite array unit cell element's active S-parameter are

given on the same charts. Note that, all the elements in the stick array were excited, none of the elements were resistively terminated.

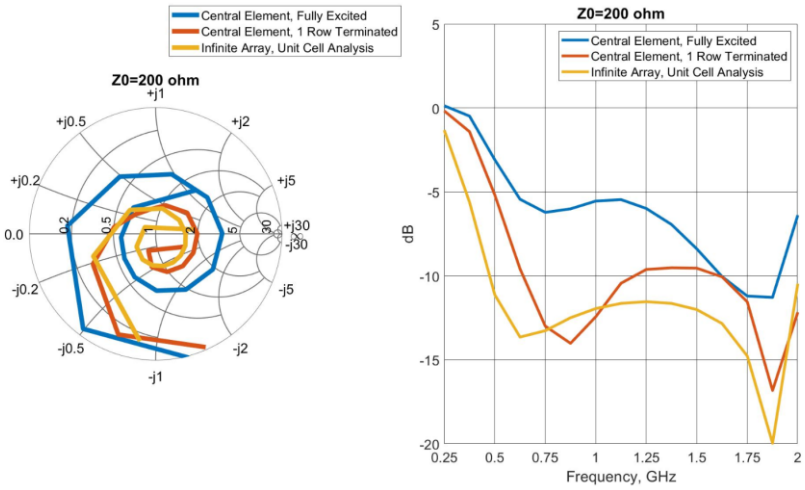

Figure 4.5. Active S-Parameter of Central Element Under Full Array Excitation Along with Infinite Array, Unit Cell Analysis, 200 Ω Reference, in 0.25 – 2.0 GHz Frequency Band

As indicated in Figure 4.5, the central element's active S-parameter under complete excitation of all elements of stick array is similar to the infinite array unit cell analysis. However, the impedance curve of the central stick elements has been enlarged for some amount. Especially at the low frequency end of the frequency band, the real part of the active impedance of the stick array's central elements is very low, almost short circuit. Here one thing to remind that design is in between 0.5-2.0 GHz, in order to understand the behavior of the array, especially at the low frequency end, the impedance curves are given from 0.25 GHz.

With the similar intentions, the number of elements in the stick array is increased further. In [17], the necessary finite antenna lengths are given. In [17], arrays of element lengths as low as 0.1λ are investigated. Note that our element is approximately 0.1λ at the lowest design frequency. It is concluded that, at any

frequency, such an array should have size at least 5λ × 5λ. It is stated that, in classical 0.5λ element narrowband arrays, 10 × 10 element model is often suggested, however for arrays having bandwidth ratios such as 5:1 or more, 25 times more elements are needed. In the paper, it is stated that central elements impedance response in comparison to the infinite array unit cell analysis, depends on frequency. In the higher end of the band may behave well according to the unit cell analysis, however the lower frequency part degrades more severely. Therefore, in the investigations that follow, the lower frequency of the band is given more importance. Stick arrays of 7 elements, 9 elements up until 17 elements are analyzed while all the elements in the arrays are excited. In Figure 4.6, active S-Parameters of those stick arrays together with the infinite array unit cell analysis are given both in Smith Chart and in dB scale.

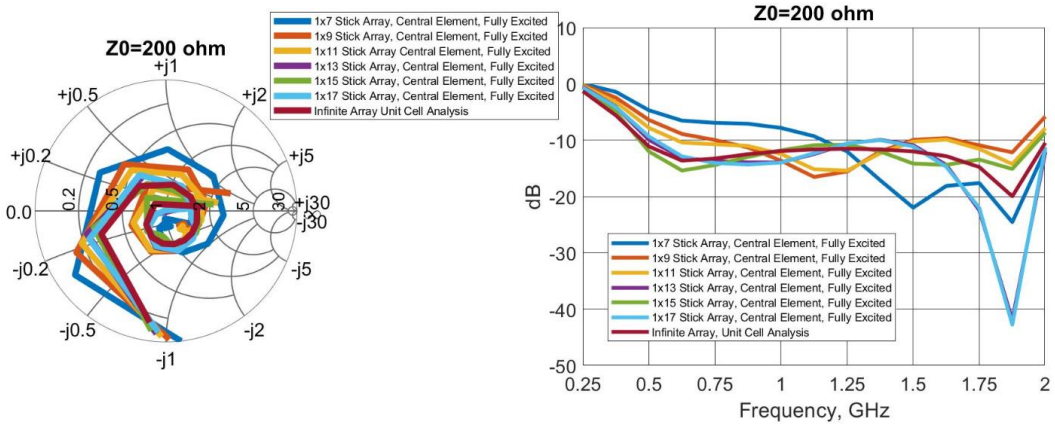

Figure 4.6. Active S-Parameters of Central Elements of Stick Arrays Under Full Array Excitation, Along with Infinite Array Unit Cell Analysis, 200 Ω Reference, in 0.25 – 2.0 GHz Frequency Band

As it is seen in Figure 4.6, as the number of elements increase in the stick array, the active S-parameter approaches to the infinite array unit cell analysis. The active S-parameter of the central element becomes lower than -10 dB only after the number

of elements in the stick array reaches 15. In 1 × 13 stick array, it is almost in all band below -10 dB except the 2 GHz frequency point. In 1 × 15 stick array, the central element has the active S-parameter lower than -10 dB in whole band as if it is in the infinite array unit cell analysis. As expected, in 1 × 17 stick array, the central element has the same property as well.

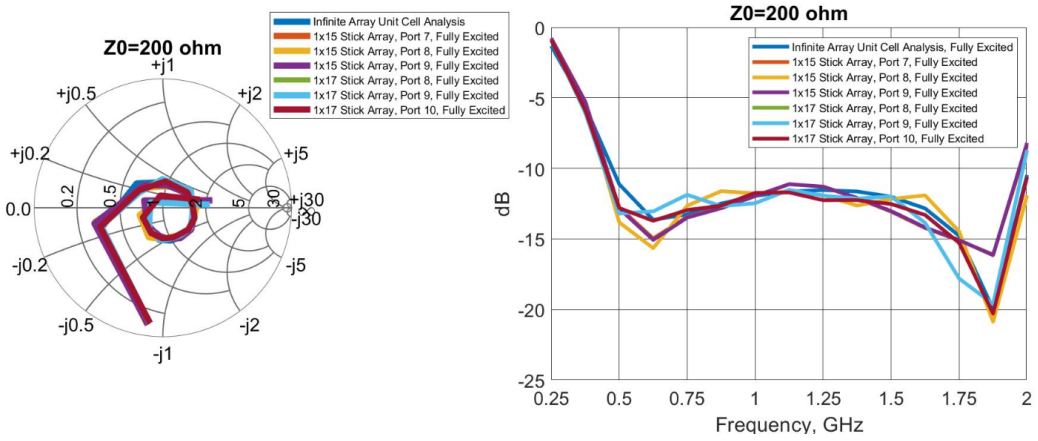

Figure 4.7. Active S-Parameters of Three Central Elements of Stick Arrays Under Full Array Excitation, Along with Infinite Array Unit Cell Analysis, 200 Ω Reference, in 0.25 – 2.0 GHz Frequency Band

Even though 15 elements may seem to be enough for the finite array to represent the infinite array unit cell analysis, that is not the case exactly. The reason for such an array configuration is as follows: not just only the central element but remaining elements are also fed. Therefore, an evaluation just by considering the central elements would be an erroneous approach. One may take under consideration the 2 elements that are adjacent to the most central element. In a 1 × 5 stick array, the central element has active S-Parameters below -10 dB for the whole band but the adjacent 2 elements to that have not. The adjacent elements are slightly mismatched in terms of active S-Parameters, around -8.5 dB at 2 GHz. However, in a 1 × 17 stick array, the two adjacent elements also have their active S-Parameters below -10 dB

in the whole frequency band. In Figure 4.7, active S-Parameters of the most central three elements, under full array excitation along with infinite array unit cell analysis is given.

In finite antenna arrays, usually some central region of the array is excited while the rest is terminated with resistive loads, due to reason that peripheral elements usually get mismatched, i.e. their active impedance behaviour degrades compared to the central elements. The determination of excited and nonexcited area can be represented in stick array concept as well. To determine the number of resistively terminated elements, i.e. elements that are parasitically excited, the following strategy is followed: after how many elements are resistively terminated, the worst active S-parameter among the remaining fed elements is what. 1×17 stick arrays have been considered for such an investigation. In Figure 4.8, active S-parameters of stick arrays under different excitation schemes are provided. For reference, only the active S-parameters of elements that are on one end of the array and the central element are given. First, stick array is under full excitation i.e.; all the excitation coefficients are 1W. Then, one outermost row on each side are terminated with resistive loads, then the two outermost rows terminated with resistive loads until a substantial active S-parameter is obtained. When the stick array is excited fully, i.e.; no rows terminated with resistive loads, the central elements do well, their performance is similar to the infinite array unit cell analysis. However, the outermost element has active S-parameter about -5.93 dB at 0.5 GHz, which is acceptable but far from the infinite array unit cell analysis. It is known that elements that are on the ends of the array have active impedance behavior degraded due to primarily two reasons. First, as they are on the edges, they exhibit less mutual coupling since they do not have any adjacent element on their one side. In addition, in finite active arrays; surface waves do exist even at the low frequencies. Those surface waves are not the surface waves that show up when the frequency goes up but they rather show themselves below the resonance frequency, approximately 20-30% below the resonance and if the interelement spacing is less than 0.5λ in the center frequency. Element of consideration here satisfies those properties. In [8] detailed discussions

about those surface waves are given. In [8], it is stated that those surface waves should not to be confused with the surface waves that are existent on the stratified mediums, when the frequency is high enough. Detailed discussions are given in [8].

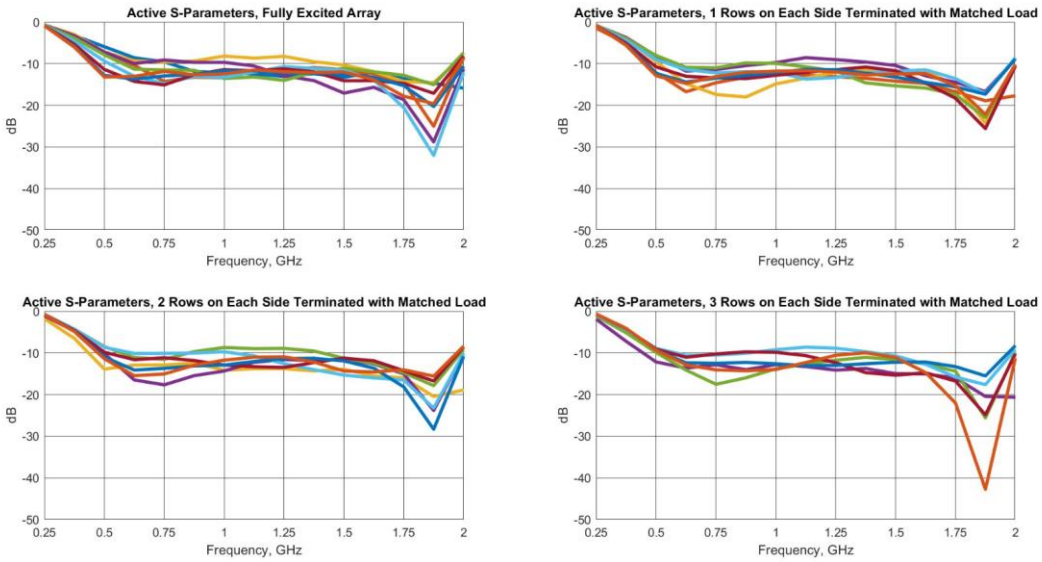

Figure 4.8. Active S-Parameters of Elements of Stick Arrays Under Different Excitation Schemes, dB Scale, in 0.25 – 2.0 GHz Frequency Band

To solve out this mismatch problem, one row on each side of the stick array is terminated with the matched load. In this case, it is observed that worst element has -8 dB active S-Parameters at the 0.5 GHz frequency; which is a substantial improvement compared to the infinite array case.

Next, two rows on each side are terminated with the matched load and the worst element had attained -8.50 dB at the 0.5 GHz frequency. Then 3 rows on each side are terminated with the resistive loads and the worst element has become -9.00 dB at the 0.5 GHz frequency. Almost all elements had -8.5 dB active S-Parameters in the whole band, whereas the previous one had worse in band behavior. There still has been an improvement, but the improvement is not much substantial. From those

observations, it can be stated that two rows resistive termination is enough for determination of number of excited elements for finite tightly coupled dipole arrays, however if the array is too large, three rows resistive termination could be good if superior performance is of interest.

4.2 Determination of Number of Excited Elements in Finite Arrays Using Double Periodic Arrays

For determining number of excited elements in a finite array, similar analyses are repeated for double periodic arrays. The array is finite periodic in both directions. Initially, 4×4 array has been constructed and the results were given at the beginning of this chapter. For investigation purposes, arrays of 5×5, 7×7, 9×9 and 11×11 elements are considered at first. In order to determine number of elements that are terminated resistively, those arrays are investigated. All the arrays are investigated under full excitation and some of the rows from two sides are terminated with resistive loads. In Figure 4.9, the active S-Parameters of the central elements of the finite arrays under investigation are given.

7×7, 9×9 and 11×11 arrays are terminated with resistive loads up to two rows on each side, however 5×5 array is terminated with resistive load only in one row from each side. The reason behind this choice is that, in a 5×5 array; if two rows from each side are terminated with resistive loads, it means that only the central element is excited with non-zero power where all the remaining elements are excited with zero power. Furthermore, that kind of excitation is by definition against to the infinite array unit cell analysis. In the infinite array unit cell analysis, a unit element and port corresponding to that element is surrounded by master and slave boundaries. Hence, port in the unit cell element thinks as if along its E-plane direction and H-plane direction there are adjacent ports to itself. However, in the 5×5 array, two rows in each side are terminated with resistive loads; that kind of excitation is by definition against to the infinite array unit cell analysis. In addition, it should be noted that, for different kinds of excitation schemes in different sized arrays, a MATLAB script is

written such that an excitation file that depicts the complex powers as inputs to the HFSS. It is very possible that one can make mistakes while providing different excitation schemes to the HFSS, especially if the number of elements in the array grows larger. At the same time, this written code enabled easiness.

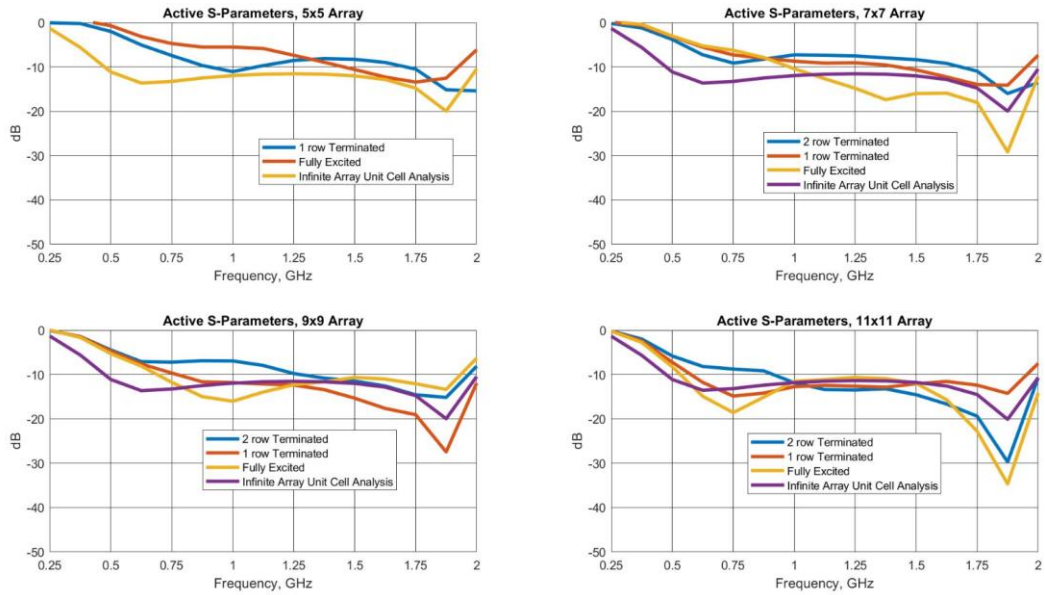

Figure 4.9. Active S-Parameters of Central Element of Double Periodic Arrays Under Different Excitation Schemes, dB Scale, in 0.25 – 2.0 GHz Frequency Band

In 5 × 5 array, in terms of central elements' active S-Parameters, fully excited case is the worst, it has active S-Parameter of -0.7 dB at 0.5 GHz. When 1 row from each side are terminated with resistive load, an improvement occurs, it becomes -2 dB. When the element number is increased to 7, things got better. In the 7 × 7 array, when the array is fully excited, central element has -3 dB active S-Parameter. When it is terminated with resistive loads from each side, it becomes slightly better. However when the array is two rows from each side resistively terminated, the active S-Parameter becomes -3.8 dB, which is a better improvement.

In the 7 × 7 and 9 × 9 arrays, in terms of the central elements' active S-Parameters, the situation changes a little bit. First, as it can be seen from the overview of Figure 4.9, the central active S-Parameters under different excitation schemes are similar. Furthermore, the arrays attain their best active S-Parameter value for their central element when the array is fully excited. 7 × 7 array, have -5 dB active S-Parameter at 5 GHz, when fully excited. But the 11 × 11 array gets –8 dB active S-Parameter, when it is fully excited. 11 × 11 array can be commented that it is almost under VSWR criteria value lower than 2, where VSWR ratio of 2 can be accepted to be a good match. The 11 × 11 array has its worst active S-Parameter at 0.5 GHz frequency, which is slightly worse than infinite array unit cell analysis.

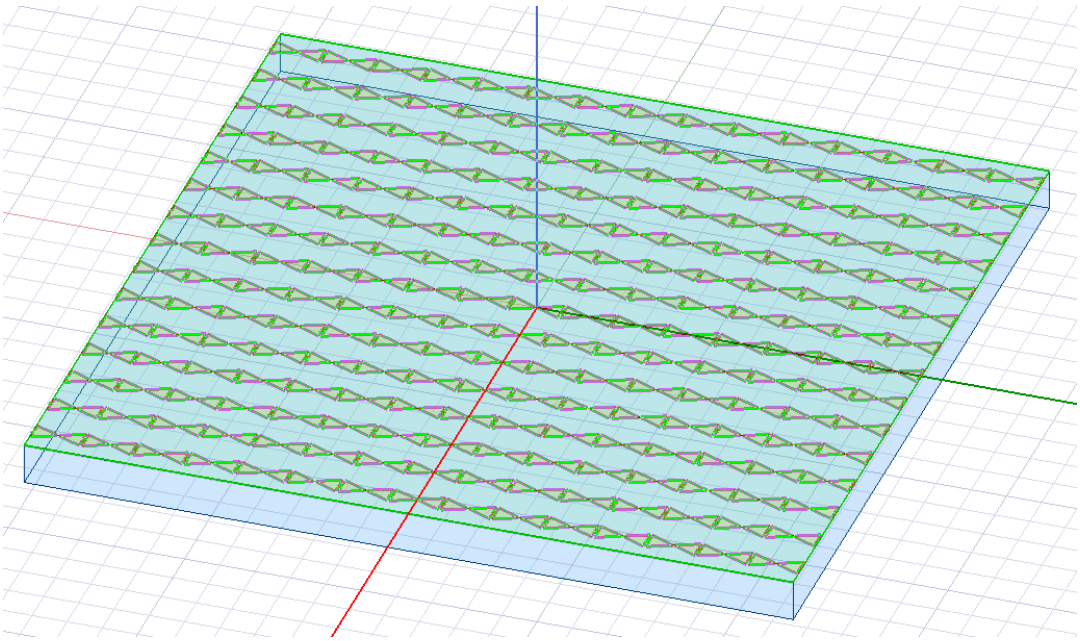

Figure 4.10. Double Periodic Array of 15 × 15 Elements, 3D View

For further investigation of the subject, and from the stick array's results, the array size is further increased. Double periodic array of 15 × 15 elements is constructed and analyzed. In Figure 4.10, 3D view of the constructed 15 × 15 array is given. The

array has aperture size 1091 mm × 1091 mm, while the distance between the GND plane and the radiating aperture is 60 mm. From the stick array analyses, it is known that tightly coupled dipole arrays converge to the infinite array unit cell analysis after number of elements exceeds a value like 15 or 17. That result has been validated in the case of double periodic arrays as well. In Figure 4.11, active S-parameter of the central element in the 15 × 15 array is given. In terms of active S-parameter, it can be stated again that 15 elements are enough for convergence to the unit cell analysis.

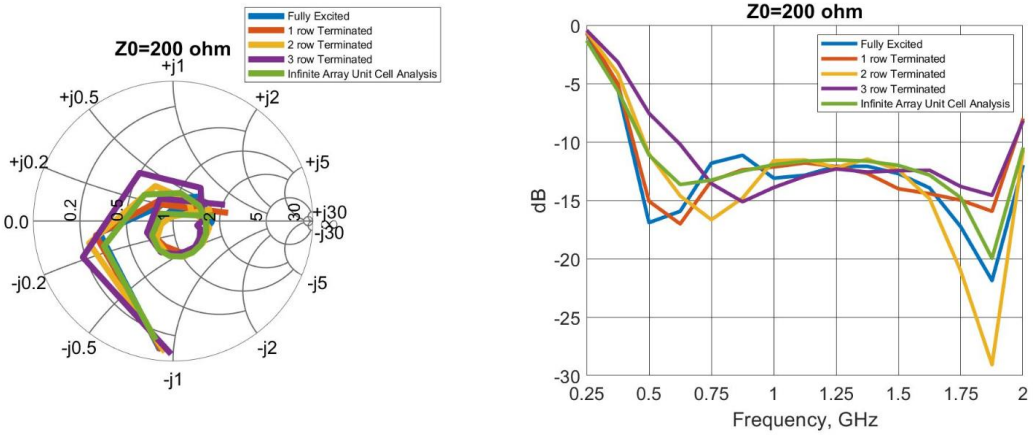

Figure 4.11. Active S-parameter of Central Element Under Different Excitation Schemes, Along with Infinite Array Unit Cell Analysis, 200 Ω Reference, in 0.25 – 2.0 GHz Frequency Band

To be sure about the convergence to the infinite array unit cell analysis, both real and imaginary parts are given in Figure 4.11, (a), on the Smith Chart. Both the real parts and the imaginary parts of the active S-parameters are converged.

In 15 × 15 array, one row, two rows and three rows from each side of the array are resistively terminated. When three rows are resistively terminated, the central element active S-Parameter diverged from the unit cell analysis. Among the fully excitation, one and two rows resistively terminations; 2 rows resistively termination provides the best results. When the arrays are terminated with resistive loads from

the two ends, the active S-parameter of the central element remains lower than -10 dB in the whole frequency band as if it is in the infinite array unit cell analysis. As it can be seen in the Figure 4.11, on the Smith Chart, in terms of impedances' both real and imaginary parts, that kind of termination schema provides the nearest results to the infinite array analysis.

Furthermore, for this 15 × 15 array, rather than central elements, the other elements' active S-parameters shall be investigated additionally. In a finite array, the non-central elements are also fed, they have additions to the corporate feed network VSWR. For the corporate feed network's VSWR to be small, those elements that are located towards to the edges shall be considered. In 15 × 15 array, when the array is fully excited, none of the rows are terminated with resistive loads, it is expected that the element whose active S-parameter is the poorest, would be around the peripherals, especially at the corners of the array. To be more rigorous, the investigation here is continued with elements of rows rather than single elements and their corresponding ports. In Figure 4.12, for this 15 × 15 array, port numberings of the first quadrant along with the central two rows that are on the boundaries of the first quadrant are given. Investigation of the first quadrant is equivalent to the investigation of the whole array since the antenna's terminals, i.e. ports are reciprocal in between each other. For example, an element that is n_x element adjacent to the central element along the E-plane of the array and it is n_y adjacent to the central element along the H-plane. Then for another element whose distances to the central element are $-n_x$ and n_y. Those two elements must have the same active S-parameters. Note that for any port, there are three more reciprocal of that port in the finite array. For our example, the reciprocal of our elements are located ($-n_x$, n_y), (n_x,$-n_y$) and ($-n_x$, n_y) adjacent to the central element, respectively. This concept has been verified for several elements in the 15x15 array. Therefore, investigation of first quadrant's rows along with the central rows are adequate.

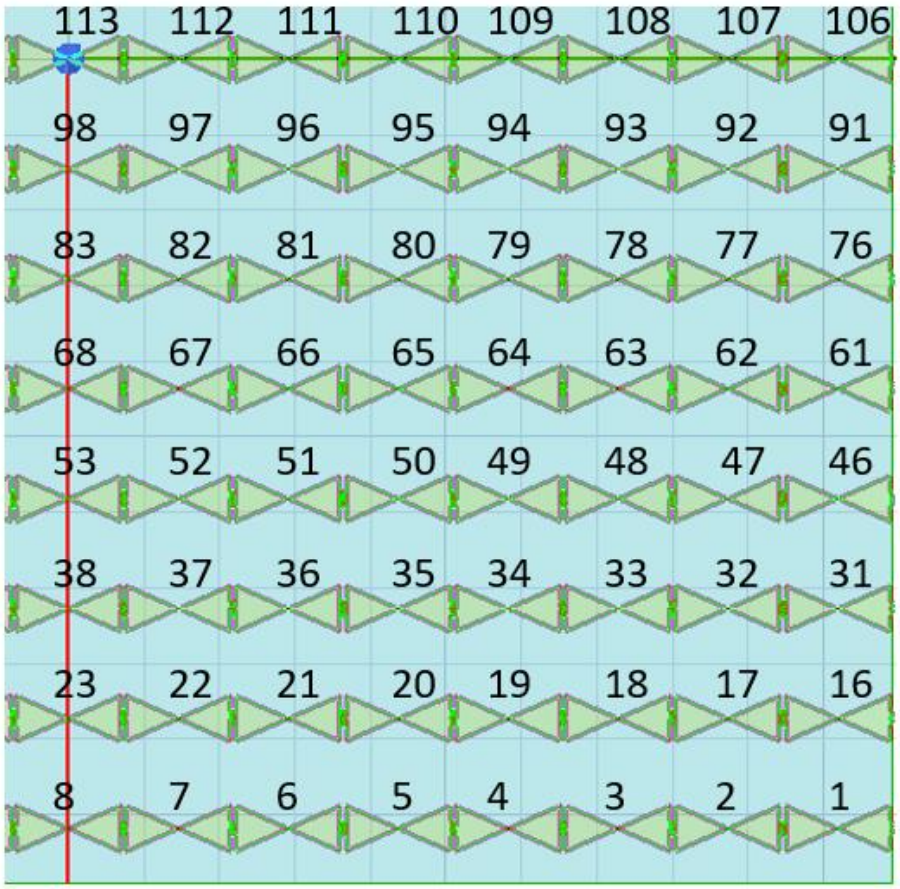

Figure 4.12. First Quadrant of Double Periodic Array of 15 × 15 Elements, 3D View

Under full array excitation, the first row of the array is considered. The active S-Parameters of the ports 1:8 given in Figure 4.13. The strategy is again the worst active S-Parameters of the array is what. The worst active S-Parameter performance observed element is the port 3, it has active S-Parameter around -3.5 dB at the 0.5 GHz frequency. Also note that, Port 8 has almost below -10 dB active S-Parameter for most of the desired band. Its active S-Parameter rises above -10 dB around 0.5 GHz frequency. Port 8 is the center element of this row, hence it is the best performing element among this row.

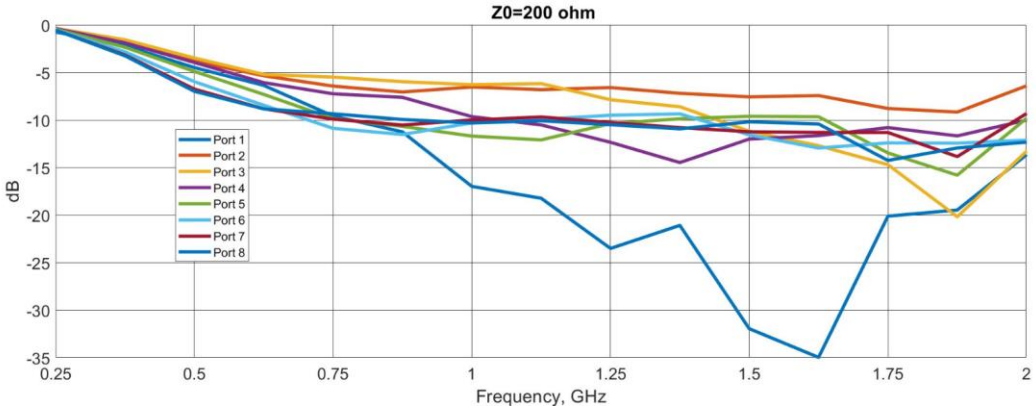

Figure 4.13. Active S-Parameters of the First Row, Ports 1:8, dB Scale, in 0.25 – 2.0 GHz Frequency Band

Next, one row from all sides are terminated with resistive loads. Note that this time, there are 7 active S-parameters instead of 8 as if it was in the fully excited case. As one row is resistively terminated, Port 16 is terminated in this row too. In this case, the worst performing port's active S-parameter got better compared to the previous case. The active S-parameters of the ports 17:23 are given in Figure 4.14. Note that, the worst performing element has -4.5 dB active S-parameter at the 0.5 GHz frequency. Furthermore, the ports' active S-parameters in dB scale got closer. In fully excited case, they were more scattered around a value; however, in this excitation scheme they are less scattered around a value that is between -5 dB and -10 dB.

Then, two rows from all sides are terminated with resistive loads. In this case, in the worst performing row, all the ports have active S-Parameters lower than -5 dB. The active S-Parameters are contracted further. The worst performing element had attained its worst value at 0.5 GHz frequency, it is -5 dB. For most of the band, all the ports have active S-Parameters around -7 dB, which is a significant improvement. In Figure 4.15, the worst performing rows active S-Parameters can be seen. Note that, in this case there are six ports displayed, since two rows are terminated resistively in this row.

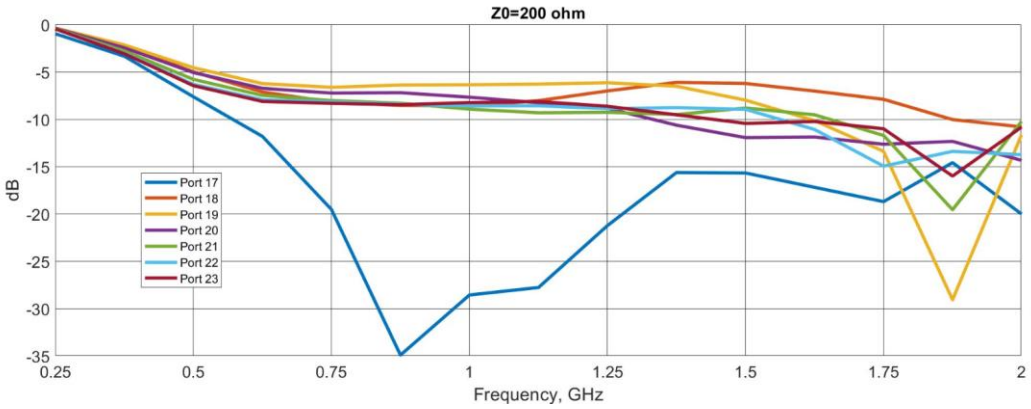

Figure 4.14. Active S-Parameters of the Second Row, Ports 17:23, dB Scale, in 0.25 – 2.0 GHz Frequency Band

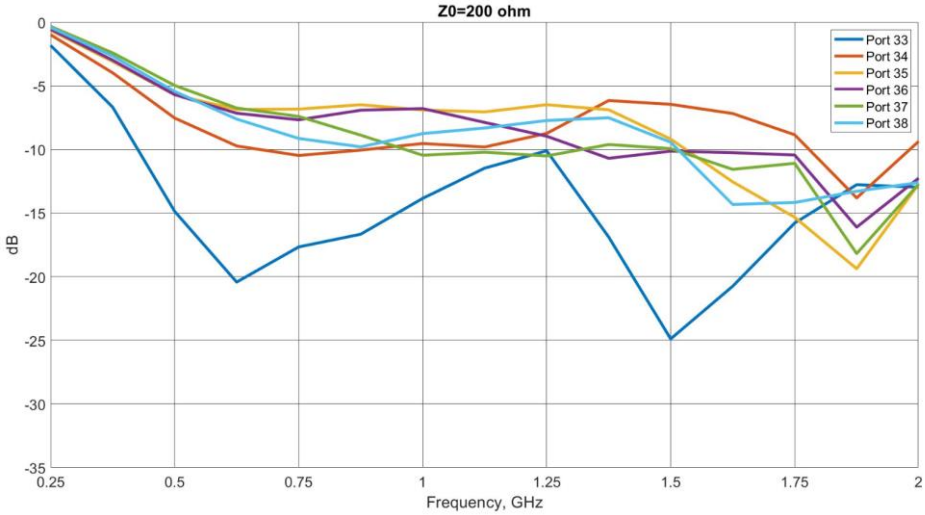

Figure 4.15. Active S-Parameters of the Third Row, Ports 33:38, dB Scale, in 0.25 – 2.0 GHz Frequency Band

Then, three rows from all sides of the 15 × 15 array are resistively terminated. For the worst performing row, the results did not improve this time. The worst performing element had attained -4.39 dB active S-Parameter at 0.5 GHz frequency.

In Figure 4.16, the active S-Parameters of the worst performing row are given. Note that in this case there are five ports including the central element of this row. Therefore, it is best to terminate two rows resistively from all sides in a finite array. Region with real excited elements should start 2 rows after from the most adjacent elements. Those elements that are on the edges shall be terminated with resistive loads, i.e. 200 Ω. Resistors of 200 Ω values can be soldered in between arms of those elements.

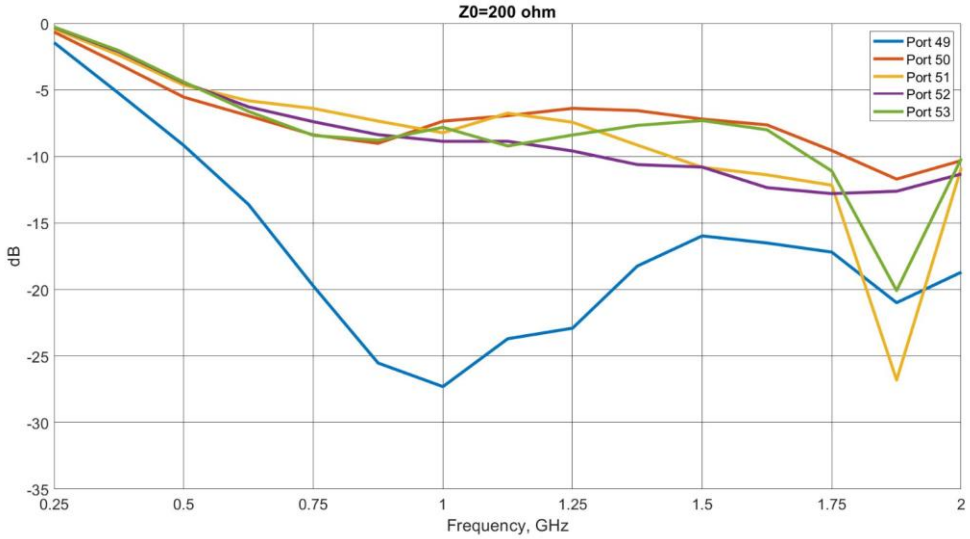

Figure 4.16. Active S-Parameters of the Fourth Row, Ports 49:53, dB Scale, in 0.25 – 2.0 GHz Frequency Band

Furthermore, the remaining rows of the 15 × 15 array under real excitation while two rows from all sides resistively terminated, are investigated. In Figure 4.15, Ports from 38:53 are given to represent the worst performing row in this excitation scheme. In Figure 4.17, the rows active S-Parameters', starting with 48 until to the central row that starts with port 108 are given.

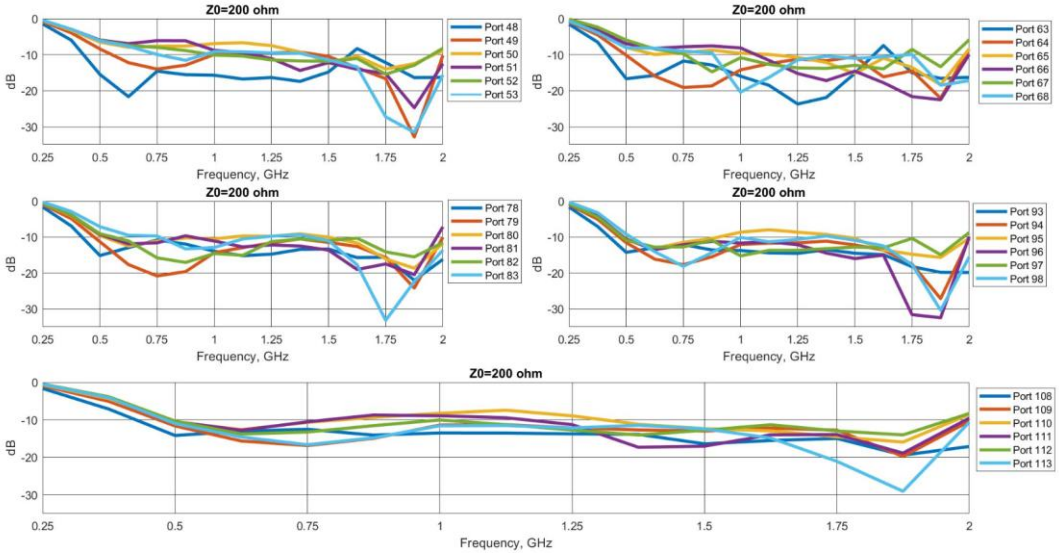

Figure 4.17. Active S-Parameters of the Fourth Row, Ports 48:113, dB Scale, in 0.25 – 2.0 GHz Frequency Band

By examining Figure 4.17, it is observed that as the row gets closer to the array's central row, the active S-Parameters get better. They also clamp up around some value as well. In this excitation scheme, almost all ports in the rows have active S-Parameters around -10 dB, only the worst performing row that is at the edge of excited region has its elements' active S-Parameters around -7 dB. The best active S-Parameter is obtained for the most central row and the one below that row, having approximately -10 dB active S-Parameters for all elements in them.

4.3 Comparison of Memory Consumption Amounts of the Finite Arrays Considered

Before concluding this chapter, there are some marks about the simulations given in here shall be considered. Infinite array, unit cell analysis is the least source consuming simulation for the TCDA's. It is good for fast prototyping, especially

after obtaining some values such as distance to the GND plane from the radiator aperture and element length hence periodicity along 2 directions etc. For matching the antenna to the specified band and tuning the capacitance in between elements, it is accurate enough. However, for finite arrays, some elements get their impedance behavior worsened, especially the peripheral ones. Therefore some kind of resistive terminations should be applied as in the other UWB arrays. Stick array, as explained previously, is capable of determining such region terminations. However, one should be aware of the fact that stick arrays are infinitely periodic along their H-planes, hence they are not as accurate as 15 × 15 Array. 15 × 15 array is the most source consuming; however, it is the most accurate model for TCDA's. After the unit cell is designed in the desired frequency band and using stick arrays, the number of excited and nonexcited elements are determined, for a one time, the array should be simulated under double periodic array to check everything is valid with the predictions. In the following Table 1, the source usage amounts of three different simulations are given. Note that 15 × 15 did not converge at 2 GHz because the available RAM was only 360 GB. To solve this problem, the same simulation setup was solved with 1 GHz and frequency sweep is done using that solution and its mesh.

Table 4.1 Source Usage Amounts of 3 Kinds of Setups

	Infinite Array Unit Cell Analysis	1 × 15 Stick Array	15 × 15 Double Periodic array (1 GHz Solution)
Number of Used Tetrahedras	11,518	198,611	4,829,090
Memory Used	482 MB	7.53 GB	267 GB

CHAPTER 5

DESIGN OF A FINITE ARRAY

In this chapter TCDA studies are extended to the design of a finite array. To construct a finite sized antenna, rather than working with the spiral coupled elements, interdigital type of capacitances were used. The main reason behind this choice was the number of agents to tune out the antenna is less in interdigital structure compared to the spiral structure. Lengths of fingers and their widths are the main tuning parameters.

The unit cell of the TCDA were allowed to be maxiumum of $\lambda_{high}/2$, 75 mm in both dimensions, actually that is the case both in this work and the other existing works in the literature, that was the limit for non grating lobe operation. The maximum available PCB size is 388 mm × 556 mm. Therefore, maximum available element that we can use is 4, since our unit cell size is maximum 75 mm. Based on those facts, an array of 4 × 4 elements is designed. As the number of elements are low to observe the infinite array unit cell behavior, this antenna should be modified in finite array environment.

In Figure 5.1, the unit cell structure of the TCDA using interdigital capacitors and its input return loss performance is given. It clearly gives VSWR<2 in the band of 0.5-2.0 GHz frequency and the unit cell is around 65 mm in length. Also note that, in the unit cell's active S-parameter results, at 2.5 GHz, active S-parameter attain a 0 dB value, means that all the incident power have returned to the source. This is due to the fact that at this frequency, the infinite ground plane below the antenna aperture and aperture have distance of $\lambda/2$. The short circuit impedance of ground plane has revolved an exact full tour at that frequency, active input resistance of the unit cell becomes zero.

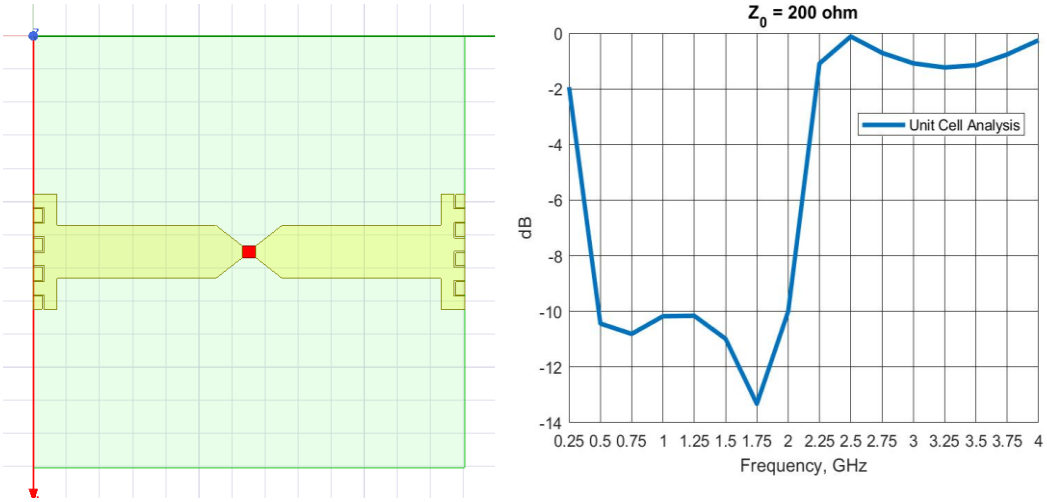

(a) (b)

Figure 5.1. (a) Top View of the InterDigital Capacitance Unit Cell, (b) Active S-Parameter of the InterDigital Capacitance Unit Cell

5.1 Finite 4 × 4 Array

Using this unit cell, an array of 4 × 4 elements are constructed. Only the 4 ports that reside in the center of this 4 × 4 array are excited, the rest is terminated with resistive loads. The frequency response results of this 4 × 4 structure are given in Figure 5.2, only one port of the central excited ports' active S parameter is provided for clarity. Note that, at 2.5 GHz frequency, the active S-parameter of the central element is close to 0 dB but not exactly zero. This is due to the fact that, as the antenna aperture is finite and the ground plane is of the same size as well. Therefore, the finite ground plane is not an infinite ground plane as it was in the Chapter 2 and Chapter 3. In Chapter 2, the unit cell was modeled using MATLAB, assuming an infinite ground plane below the antenna aperture. In Chapter 3, all of the provided results were also for the unit cell of the antenna, hence they also included an infinite ground plane. All of the active S-parameters provided in those two chapters have a 0 dB value at

exactly 2.5 GHz; however around that frequency all the finite antennas approach to zero but never attain that value. The reason is due to the finiteness of the ground plane.

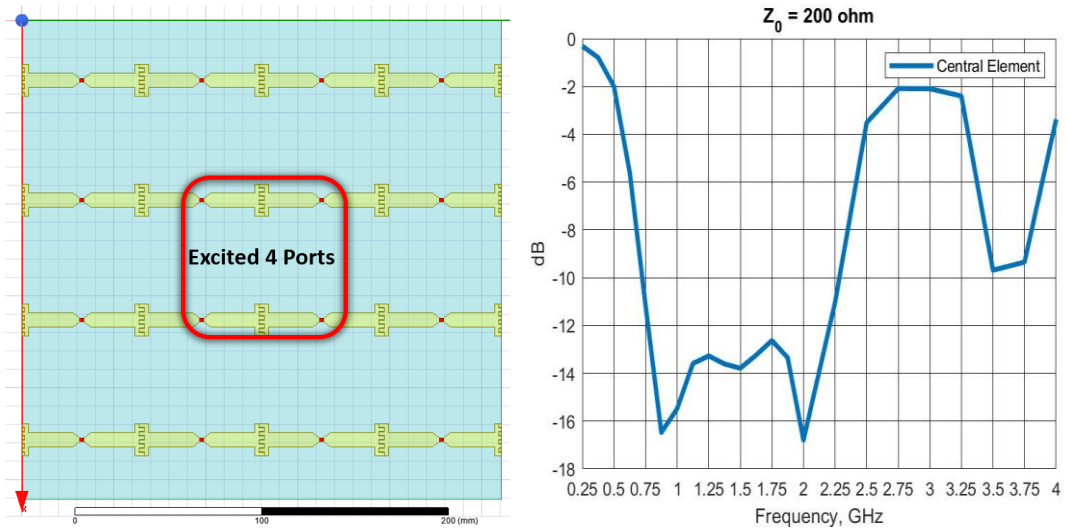

(a) (b)

Figure 5.2. (a) Finite 4 × 4 Array Using Unit Cell, (b) Active S-Parameter of the Finite 4 × 4 Array Using Unit Cell

As it can be seen in Figure 5.2, using only four elements is not sufficient for achieving unit cell active impedance performance; especially for the low frequency end of the antenna. At 0.5 GHz, the antenna has active S-Parameter of -2 dB. Therefore, some post processing operations shall be made in the finite 4 × 4 array. This structure will be a baseline design for the optimizations done. For reference the Gain vs frequency plots of both E-plane and H-plane are given in Figure 5.3. $\phi = 0^o$ corresponds to the H-plane and $\phi = 90^o$ corresponds to the E-plane in Figure 5.3. The provided gains do not include loss due to the input reflection coefficient.

Moreover, in Chapter 3, a unit cell of TCDA using spiral shaped capacitance elements were designed and optimized for VSWR<2 operation in the band 0.5-2.0 GHz. Prior to the determination of number of resistively terminated elements for a typical TCDA array, using this unit cell a finite antenna of 4 × 4 elements was constructed and the results were analyzed. Here in Figure 5.2, a very similar performance is obtained, the mid band and high end of the band are good, matching with the unit cell behavior. However, the low frequency end performance is far from the unit cell predictions, input return loss is about -2 dB in both finite arrays of two different unit cell structures. To ensure that reason of the present mismatch between those finite 4 × 4 arrays and the unit cell are not due to the spiral shaped capacitance element, the studies continued with the interdigital type capacitance element instead of spiral shaped capacitance element. Interdigital shaped capacitance element is one of the most popularly used capacitance shape used in TCDA's, however the former is not.

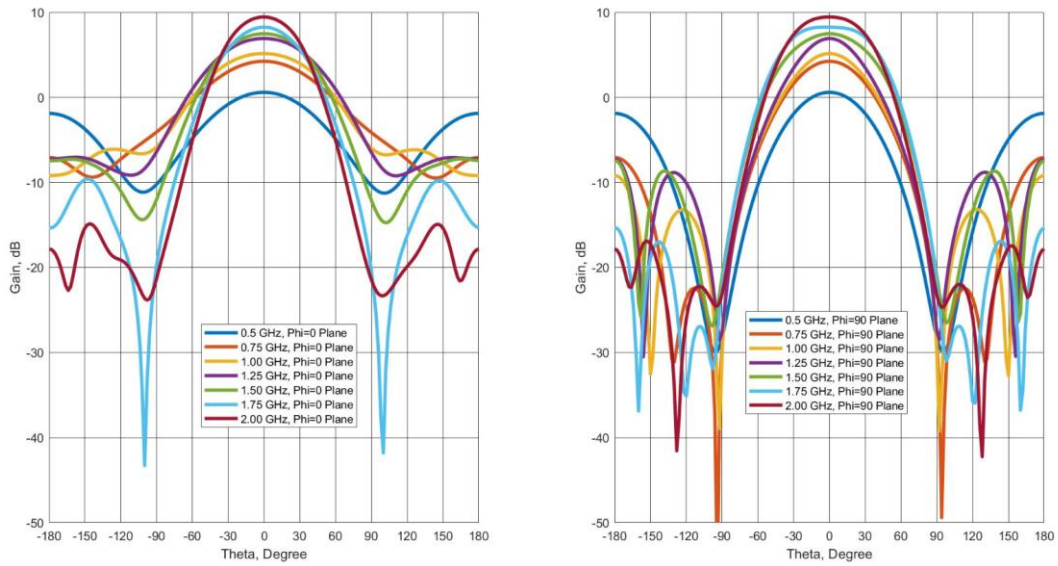

Figure 5.3. E-plane and H-plane, Gain vs Frequency Plots of 4 × 4 Antenna Using Unit Cell

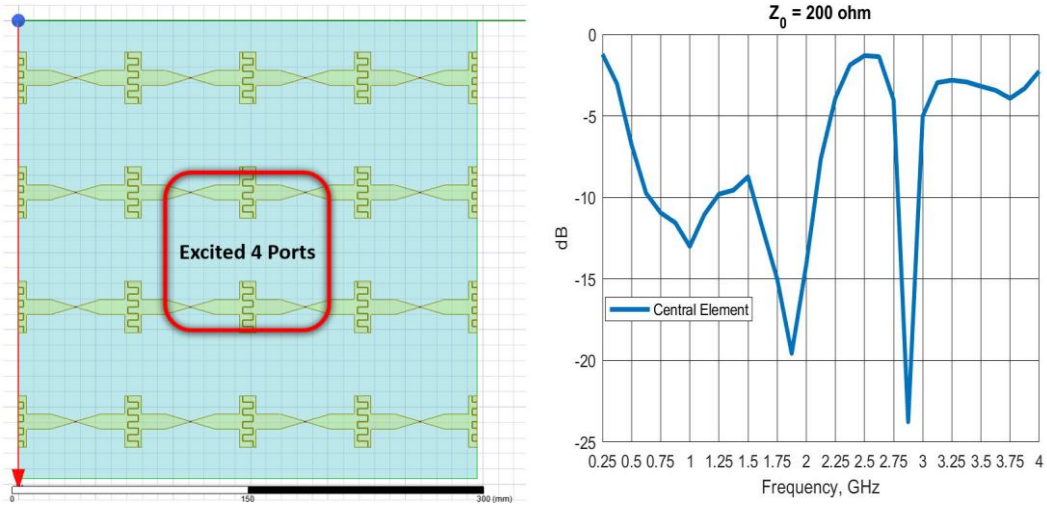

(a) (b)

Figure 5.4. (a) Finite 4 × 4 Array, After Finite Array Optimizations, (b) Active S-Parameter of the Finite 4 × 4 Array, After Finite Array Optimizations

To improve matching at low frequencies, the first idea was to increase the length of the unit cell such that the finite array structure becomes longer. Initial unit cell was between 60 mm and 70 mm. By increasing the finger lengths of the interdigital capacitors and increasing dipole lengths, the unit cell length was made around 75 mm. The limiting factor is around 90 mm since the size of the PCB available is 388 mm × 556 mm. At the limit, for boresight operation, neglecting array scanning at other angles, the antenna unit cell length is still lower than 1λ at all frequencies; hence antenna still has grating lobe free operation.

Some parametric studies are conducted; hence antenna is made into the shape given in Figure 5.4. Active S-Parameter of the antenna's central element is also given in Figure 5.4. The thicknesses of the dipole arms are increased, coupling capacitors are enlarged; whereas feed length and width are miniaturized. The antenna unit cell became 74.12 mm, which still has grating lobe free operation. The 0.5 GHz active S-Parameter is reduced down to -6.76 dB, while the remaining band is fully lower

than -8 dB. For most of the band, the antenna still has active VSWR<2, that is -9.54 dB, except the low frequency end.

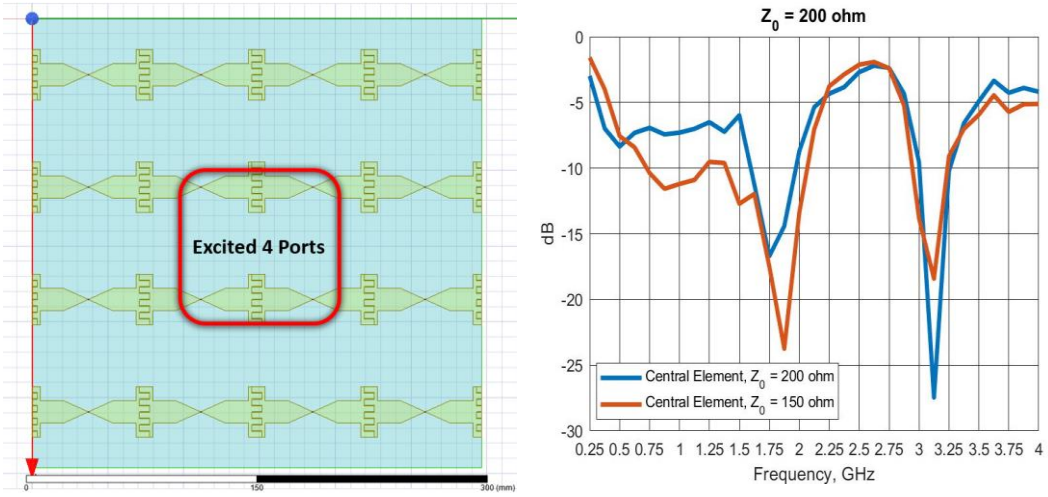

(a) (b)

Figure 5.5. (a) Finite 4 × 4 Array, After Finite Array Optimizations, (b) Active S-Parameter of the Finite 4 × 4 Array, After Finite Array Optimizations

Dipole arm thicknesses were further increased while the unit cell length still remaining around 75 mm to ensure grating lobe free operation at any frequency and scan angle. By doing so, 0.5 GHz active S-Parameter has been able to reduce down below to the -8 dB, that became -8.36 dB. However, the cost was the rest of the band's active S-Parameter performance worsened, compared to the previous case. Now not much of the band is around -10 dB. Even though that is the case, when the antenna input impedance was matched to a 150 Ω port rather than 200 Ω port, a better wideband performance is obtainable. 0.5 GHz active S-Parameter became -7.56 dB, but that operation brought much of the band to the -10 dB levels. Remember that, the finite 4 × 4 array that consists of original unit cells, that was the baseline finite array, had similar frequency response: the almost whole band's active S-Parameter was lower than -10 dB except the frequencies lower than 0.75 GHz.

However, that baseline had its 0.5 GHz active S-Parameter of being -2 dB; while this newly achieved one has -7.56 dB. In Figure 5.5, the antenna and its active S-Parameter performance is given. Eventually, dipole terminal impedance becomes 150 Ω, which is crucial due to the feed network that will be considered in the next chapter. Rather than designing the feed network that ends with 200 Ω, 150 Ω is better. The transforming ratio for the common 50 Ω system will eventually be 1:3 instead of 1:4 ratio.

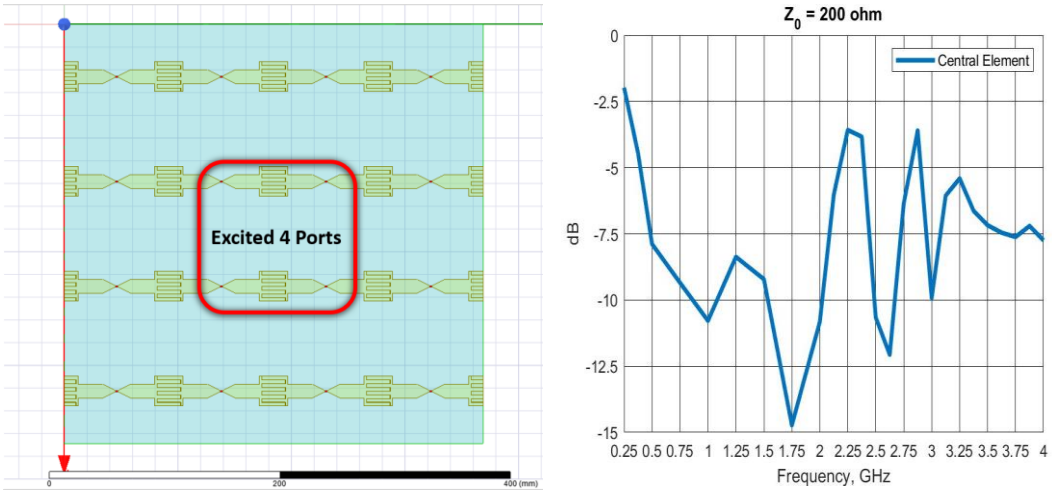

(a) (b)

Figure 5.6. (a) Finite 4 × 4 Array, After Finite Array Optimizations, (b) Active S-Parameter of the Finite 4 × 4 Array, After Finite Array Optimizations

Then, dipole arm thickness is reduced to 12 mm, while dipole arms and fingers of the interdigital capacitors are increased further. Therefore, length of the finite antenna is increased, the antenna is further miniaturized. The widths of the fingers of the interdigital capacitors are decreased since larger the area of the capacitance would be the cause of unwanted resonances in the active S-Parameters. In Figure 5.6, the antenna and its active S-Parameter performance are given. This time, the

whole band has active S-Parameters lower than -8 dB and the antenna input impedance is backed to 200 Ω as well. However, the antenna unit cell is no longer below λ/2, it is 92 mm. However, it is still below 1λ for all frequencies, allowing grating lobe free operation at boresight for all frequencies.

5.2 Evolution to the Finite 4 × 6 Array

The physical structure of the antenna array is modified. Instead of using 4 × 4 finite array, it was decided to add a row of dummy elements to the both edges on the E-plane of the antenna. Therefore, the antenna becomes a 4 × 6 array of most central 4 ports are excited. Instead of one row terminated with matched loads, 2 rows are terminated with matched loads; along the E-plane. The highest coupling between array elements are along their E-planes. In the H-plane, there are still four elements, only two of them are excited, rest is resistively terminated. Note that the available PCB size is 388 mm × 556 mm, therefore having a non square array as explained is possible, provided that unit cell sizes are on the orders of 60 mm to 90 mm's.

In the previous 4 × 4 array, the couplings and the dipole widths etc. were increased in order to reduce active S-Parameter of the antenna. In the new physical structure of 4 × 6 array; to see the effect of physics change; the couplings are reduced, dipole widths are decreased. The unit cell was around 91.2 mm. In Figure 5.7, top view of this 4 × 6 array and its active S-Parameter performance are given. As it can be seen in Figure 5.7, the hope for achieving VSWR<2 in the band of 0.5-2.0 GHz is clear.

Then, the antenna is optimized for this new geometry. Dipole widths are increased as well as coupling elements between dipole elements. Dipole arm thickness again became 12 mm. The final optimized antenna unit cell became 66.1 mm, which is suitable for grating lobe free operation at any frequency and any scan angle. In Figure 5.8, the results of this optimizaiton process is given. Obtaining active VSWR<2 in the 0.5-2.0 GHz frequency band required less effort compared to the optimizations

done in the 4 × 4 array case. The inital unit cell element in the 4 × 6 array had already -10 dB active S-Parameter in the 0.5 GHz and it had -8 dB in the whole frequency band. As it can be seen in Figure 5.8, the array has active S-Parameter lower than -10 dB in full band.

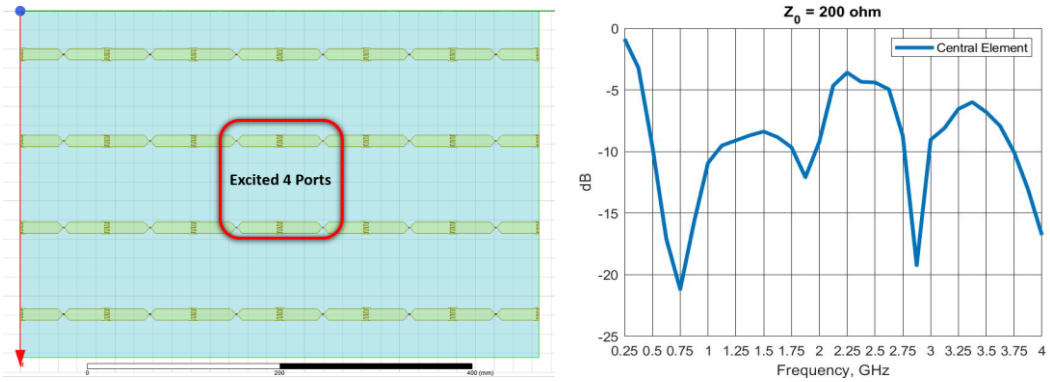

(a) (b)

Figure 5.7. (a) Finite 4 × 6 Array, (b) Active S-Parameter of the Finite 4 × 6 Array

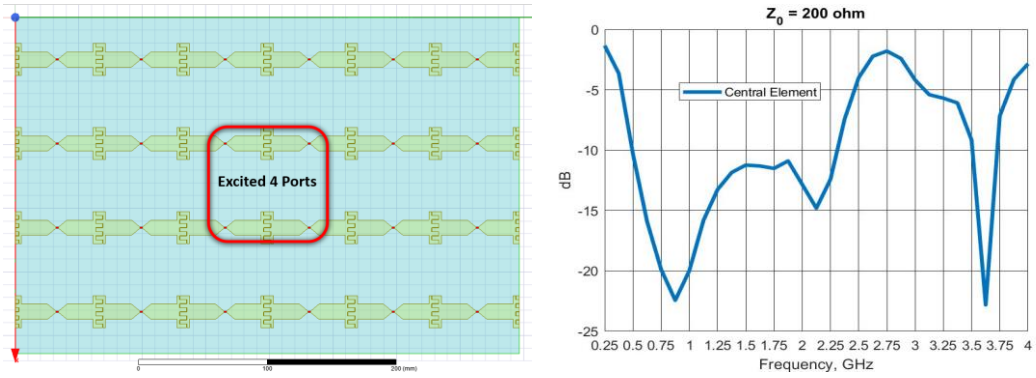

(a) (b)

Figure 5.8. (a) Finite 4 × 6 Array, After Finite Array Optimizations, (b) Active S-Parameter of the Finite 4×6 Array, After Finite Array Optimizations

In the previous design, the antenna had feed section of 1 mm by 1 mm squares, modeling for the lumped ports that excite those four elements. However, in a real life scenario; that feed lengths can be idealistic. For the placing of resistors to the non-excited, resistively terminated, i.e. parasitically excited peripheral elements as well as realistic feeds using center portion of the antenna; the feed length shall be increased. Therefore, the length of the feed section is made 2 mm, while the width of the feed section remains the same, 1 mm. However, the effect of changing the feed section was on the active S-Parameters. They were distrupted by a small amount. To compensate that affection, the lengths of the dipole arms are increased, resulting in a unit cell element of 75.1 mm. The antenna shape and the resultant active S-Parameters are given in Figure 5.9. The antenna still satisfies the requirements of the grating lobe free operation.

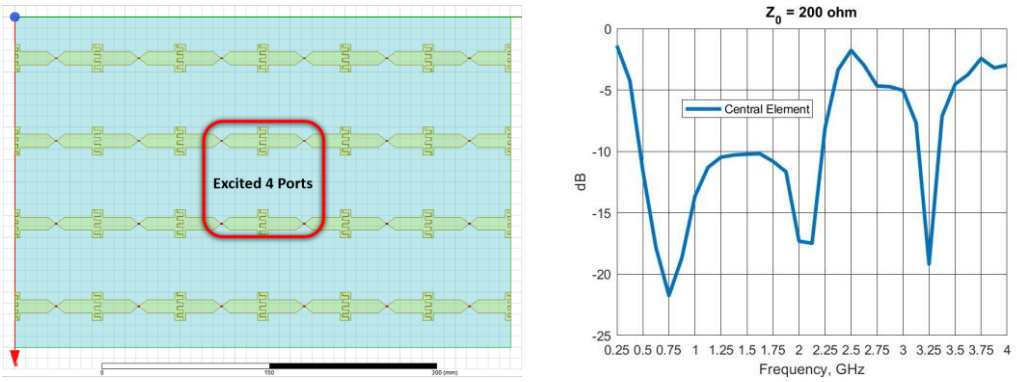

(a) (b)

Figure 5.9. (a) Finite 4 × 6 Array, After Feed Section Change, (b) Active S-Parameters of the Finite 4 × 6 Array, After Feed Section Change

For most of the finite array applications, interdigital capacitances are employed. After moving towards the 4 × 6 array, spiral capacitance using unit cell elements were considered. First, there was a unit cell element that satisfies -10 dB input active S-Parameters in the 0.5-2.0 GHz frequency band. In the previous chapter, that

element's performance behavior under 4 × 4 finite array was given. Here it is reproduced in Figure 5.10 along with the view of the finite 4 × 6 array. In Figure 5.10, the same unit cell performance in 4 × 6 array is also given.

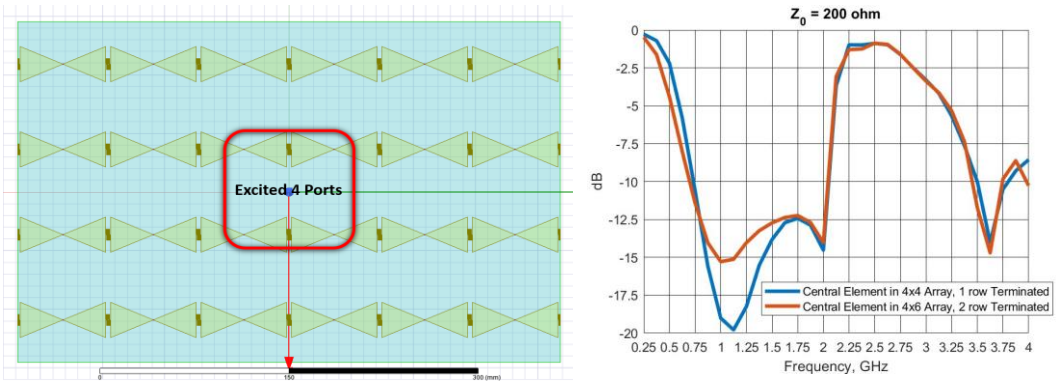

(a) (b)

Figure 5.10. (a) Finite 4 × 6 Array, Spiral Capacitance Element, (b) Active S-Parameters of the Finite 4 × 4 and 4 × 6 Array

Similar to the interdigital element, when inside finite 4 × 6 array, that unit cell has -4.2 dB active S-Parameter at 0.5 GHz. It has -2 dB active S-Parameters when in an 4 × 4 array. Some changes were also made in spiral capacitive element of 4 × 6 array. In Figure 5.11, the antenna shape and the resultant active S-Parameters are given. The capacitances that were obtained using spiral like shaped elements, in this final design; those capacitances are within the dipole arms. They are taken inside the dipole arms for further antenna miniaturization, as it can be seen in Figure 5.11. The length of the unit cell is 62 mm in this case, therefore allows to be grating lobe free operation at all frequencies and at all angles. The unit cell is smaller compared to the interdigital element's unit cell. This element provides -10 dB active S-Parameter for 0.5-2.0 GHz frequency as well, as indicated in Figure 5.11.

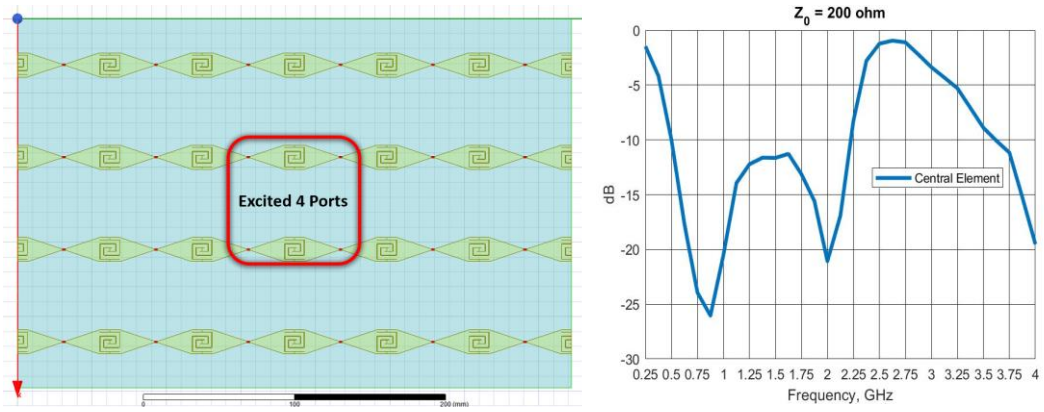

(a) (b)

Figure 5.11. (a) Finite 4 × 6 Array, Spiral Capacitance Element, After Finite Array Optimizations, (b) Active S-Parameter of the Finite 4 × 6 Array, After Finite Array Optimizations

CHAPTER 6

TCDA FEED METHODS

Tightly coupled dipole arrays are fed with lumped ports in the HFSS environment in the previous chapters. Lumped ports are the implementations of infinitely long transmission lines connected to the terminals, therefore lumped ports provide perfectly balanced outputs. One end of the lumped port has 180^{o} phase difference from the other end of the port. However, in reality, the antenna terminals must be fed from realistic feeds that provide balanced outputs in the end. Most RF systems work with 50 Ω impedance systems. The power that excites the antenna expected to be coming from a 50 Ω, coaxial feed; hence a transmission from the 50 Ω coaxial system, unbalanced, to a 200 Ω balanced system is required. Furthermore, since the antenna input impedance is 200 Ω, an impedance transformation of 1:4 shall be performed while a balanced to unbalanced connection is secured. Tapered baluns are devices that perform the mentioned operation. They perform unbalanced to balanced transformation, at the same time they change the impedance level gradually. The balun structure should be performing those operations in the frequency band of 0.5 GHz to 2.0 GHz, the antenna's desired frequency band of operation.

6.1 Tapered Baluns

As a first step, a microstrip line to parallel strip line transformer is implemented on a dielectric card that is available. As one end of the balun, parallel strip line end, needed to be 200 Ω, the thickness and the dielectric constant of the material needed to be determined carefully. The minimum allowed conductor trace width for the dielectric cards in the production facility were around 0.175 mm, hence for designs to be implemented, 0.2 mm of minimum trace width is chosen. Based on those facts,

the dielectric card chosen was RO4003 substrate having 3.55 relative dielectric constant. The thickness of the dielectric card is chosen as 0.813 mm.

For the implementation of tapered balun, where design guidelines given in [18] are taken. Four section Chebyshev impedance transformer of passband ripple Γ_m=0.05 is implemented on a tapered balun structure. The physical view of this structure is given in Figure 6.1. For the balun structure, the ground is implemented as an exponentially growing ground that starts with a large width and ends with a width that is equal to the width of the parallel strip line ending. Exponential growth constant is a controllable variable. The other conductor, that resides on the other end of the dielectric card is a trace that consists of four sections whoose widths are controlled at equally spaced distances along the balun. Together with the parallel strip line end and the microstrip end, the controlled impedance points make up a total number of 6.

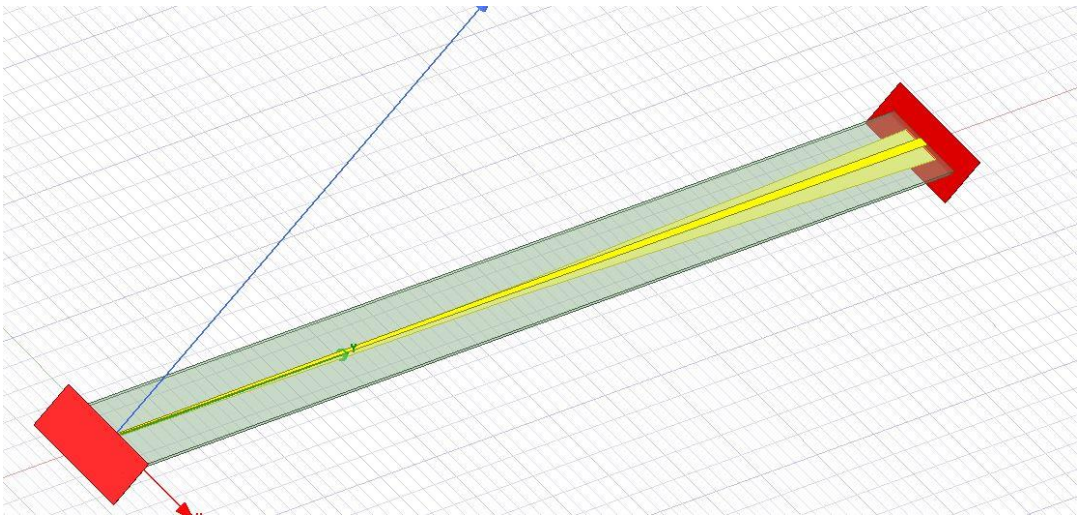

Figure 6.1. Physical view of the Tapered Balun

The balun structure starts with a microstrip line of 50 Ω characteristic impedance, ends with a parallel strip line of 200 Ω impedance. In between those two, the width

of the top conductor is controlled such that the impedance at the control points satisfies the Chebyshev transformer impedances. By this implementation, the top conductor becomes a linearly tapered trace whereas the bottom conductor is an exponentially tapered trace.

For the evaluation of the balun structure in the HFSS environment, 3 wave ports are assigned to the structure. First wave port is on the microstrip end of the balun, the other 2 are on the parallel strip line end of the structure, the unbalance between two output ports can be observed by such assignment. Port 1 is labeled as input port, it is a microstrip line of 50 Ω. Ports 2 and 3 are assigned at the end of the balun, they are output ports of the balun structure. A short segment of PEC sheet is placed in between parallel stripline outputs of the balun structure. In Figure 6.2, the assigned two outer ports, port 2 and 3, are given. Each port's integration line is from the center to the conductor, being opposite to each other as given in Figure 6.2. At the parallel strip line end of the balun structure, E field is perfectly divided between two ports. Placing such a short PEC sheet does not affect the actual field distribution of the parallel strip line fields, at the end of the balun structure. The actual E fields of the parallel strip line end of the balun are orthogonal to that PEC sheet's plane, provided that a perfect 180^0 phase difference is obtained between the voltages present at each parallel strip line. In Figure 5.2, the E field distribution of parallel strip line end of the balun are given for both of the cases. First case does not include such a PEC sheet, whereas second case includes that PEC sheet. As the field distributions are given in Figure 6.2 for both two cases, they are very similar. Calculated port impedances are equal to each other, being equal one half of the output port impedance of the balun structure. The calculated port impedances are 100 Ω each, one half of the 200 Ω. Therefore, by observing magnitude and phase differences between S_{21} and S_{31}, one can observe the unbalance between two ports. The main aim of the balun is to provide a perfectly balanced outputs; each strip has accompanying voltages of 180^0 phase difference and equal in amplitude.

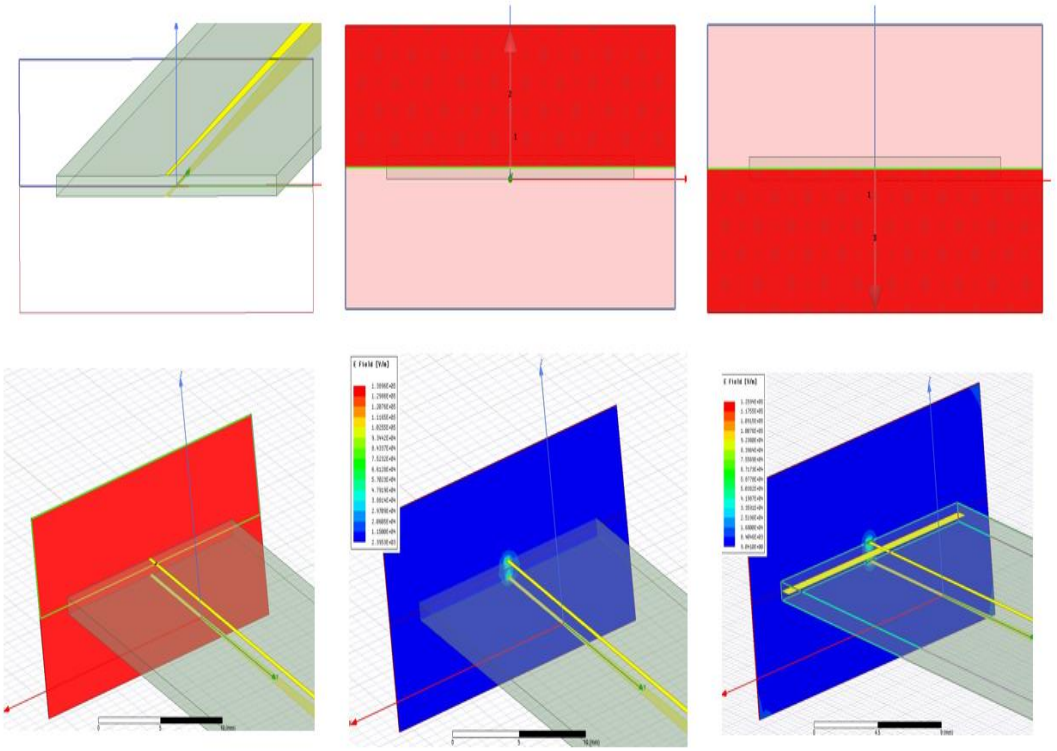

Figure 6.2. Port 2 and 3 Assignments and Their Integration Lines on the Parallel strip line End

For the microstrip ground plane width, 7.5 mm is chosen. That ground plane is tapered until to the parallel strip line end which has 0.24 mm trace width. The thickness of the dielectric card is chosen such that the parallel strip line end trace widths are not very thin for providing 200 Ω port impedance at the output. PCB production permitted specifications must be satisfied, therefore one cannot take arbitrary trace width for the parallel strip lines. The length of each section should be around λ/4 in the dielectric medium at the center frequency. The dielectric card material has 3.55 dielectric constant; each section would be approximately λ/4 at the center frequency, results in each section length is around 30 mm in length. Along the balun, 6 impedances are controlled which results in a 5 equal length sections.

Controlled impedance locations include the input and output ports. Total balun length makes 150 mm.

In Figure 6.3, the calculated port impedances, S-Parameters for those 3 balun ports, the magnitude and phase differences between ports 2 and 3, i.e. the output ports, are given. In an idealized situation, the magnitude differences between the balun ports should be zero dB and the phase difference between them should be 180º. As it can be seen in Figure 6.3, the magnitude difference is nonzero and phase difference fluctuates around 180º. The magnitudes' variations are large, as compared to the phase variations; hence they gather more attention. The maximum magnitude variation between output ports are 1.2 dB, where each port should ideally receive -3 dB relative power. However, when the phase curve is investigated, the phase variation from the ideal situation is just 12.5º. This is not as crucial as the magnitude variation; if the S-parameters are viewed as a complex excitations on complex plane, the effect of 1.2 dB magnitude difference would be more important, as compared to the 12.5^0 phase difference from the ideal 180º.

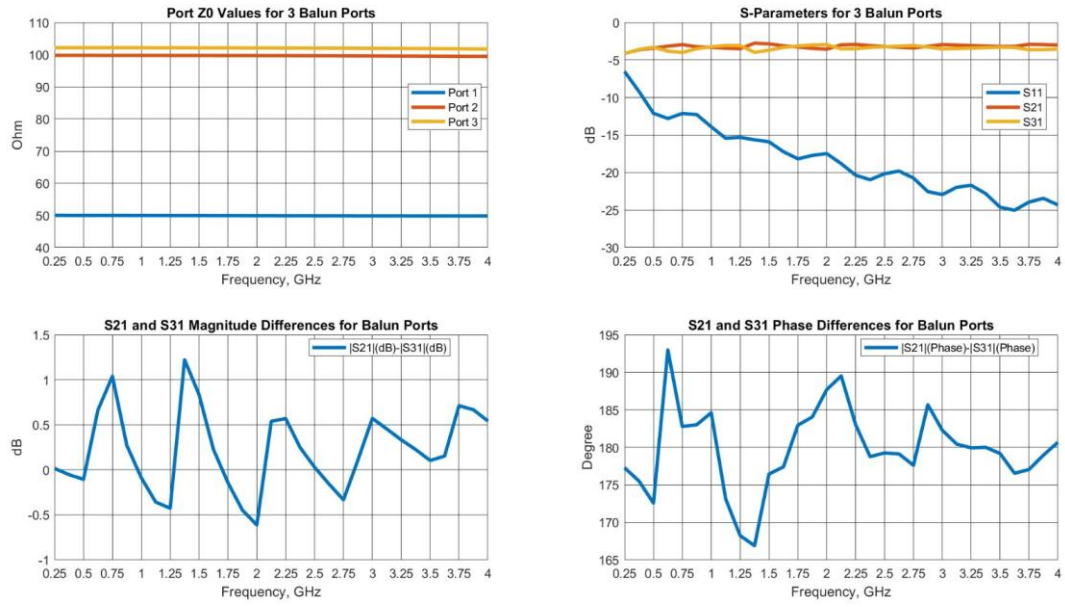

Figure 6.3. S-Parameters Results for the Tapered Balun

The balun structure is 150 mm long. However, the distance between the ground plane and the antenna radiator plane is 60 mm, shorter than the half of the balun length. To miniaturize the balun structure, the dielectric card is replaced with a card of RO6006 substrate material of 6.15 relative dielectric constant; the widths for the 6 control locations are recalculated. The thickness of the substrate made 1.27 mm to be able obtain 200 Ω at the parallel strip line end. The new balun's S-Parameters results are given in Figure 6.4. In Figure 6.4, the results are given for various balun lengths, simple scaling the balun length does the job for the miniaturization of the balun, no extra calculations for the trace widths in the impedance control locations are needed. Only S_{11} values and magnitude differences between S_{21} and S_{31} are given for clarity.

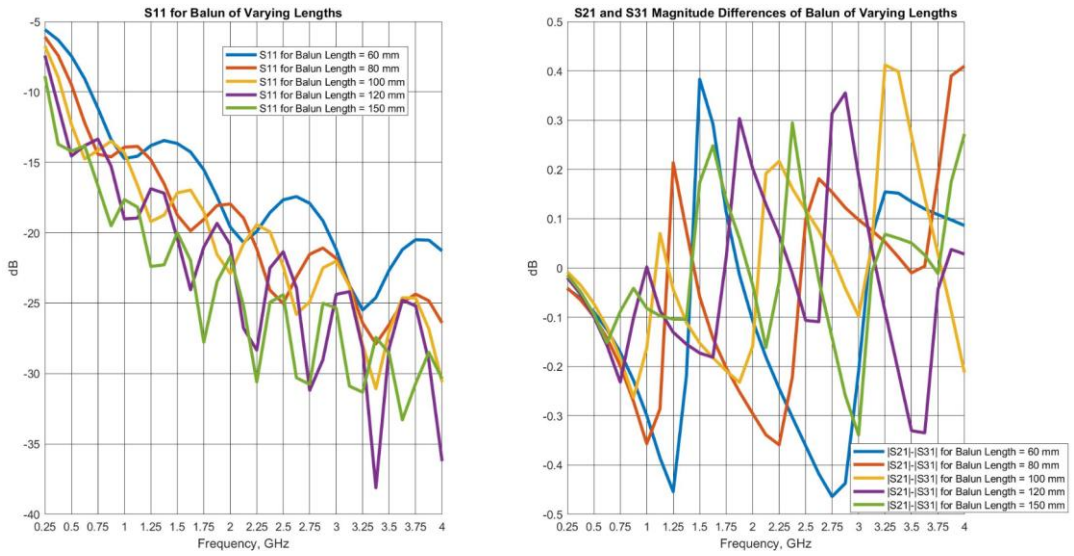

Figure 6.4. S-Parameters Results for Tapered Balun of RO6006 Subtrate for Various Lengths

As it can be seen in Figure 6.4, the balun cannot be simply scaled to 60 mm, which is ground plane spacing of the antenna, due to the fact that the S_{11} degrades and becomes worse than -10 dB for both 60 and 80 mm's in the desired frequency band. In terms of port unbalances in dB the best results are obtained for 150 mm balun

length. The worst unbalance is 0.25 dB, this balun structure is suitable for using as the antenna feed.

In order to test whether this kind of feeding scheme works for designed finite 4×6 TCDA, the central 4 elements, the elements that had the only excited ports, are connected to this balun structure. In Figure 6.5, the resultant electromagnetic structure is given. For the balun cards to fit in the foam that mechanically supports the radiator plane, a cavity of 4.2 mm radius is opened. The radius of this cavity should not be too large since the antenna's operation relies on the ground plane and this cavity structure perturbs the ground plane. For the balanced end connection, the parallel strip line ends are extended such that they touch to the dipole arms, dipole arms are extended as such as well. This kind of connection is not a realistic scenario but is appropriate for prototyping. More realistic feed modeling scenarios are required since the antenna's bandwidth heavily relies on the feed structure. 2 wires that are soldered to the dipole arms and balun's parallel strip line arms will be the real connection.

The results for the antenna fed with this balun structure are given in Figure 6.6. The results are good, active S-Parameters for the 4 ports are lower than -10 dB, except 0.5 GHz. Only 2 out of 4 ports is -8.5 dB while the other 2 is lower than -10 dB at 0.5 GHz. There are slight differences between the ports, it is believed that the reason behind this effect is the unbalance between balun's arms results in a clamping of groups of two active S-Parameters. Principal plane gains vs frequency are given in Figure 6.6 as well. In Figure 6.6, $\Phi = 0^o$ corresponds to the E-plane and $\Phi = 90^o$ corresponds to the H-plane. For those gains, impedance mismatch factor is not included.

As it can be seen in Figure 6.6, the patterns are not as qualified as they were in the lumped port excited antenna. Sidelobe levels are increased and the patterns are not perfectly symmetrical about the boresight for a fixed cut of E or H plane. In Figure 6.7, the patterns of lumped port fed antenna are given for reference. It is clear that in

terms of pattern quality, the antenna fed with this balun is worse than the lumped port counterpart.

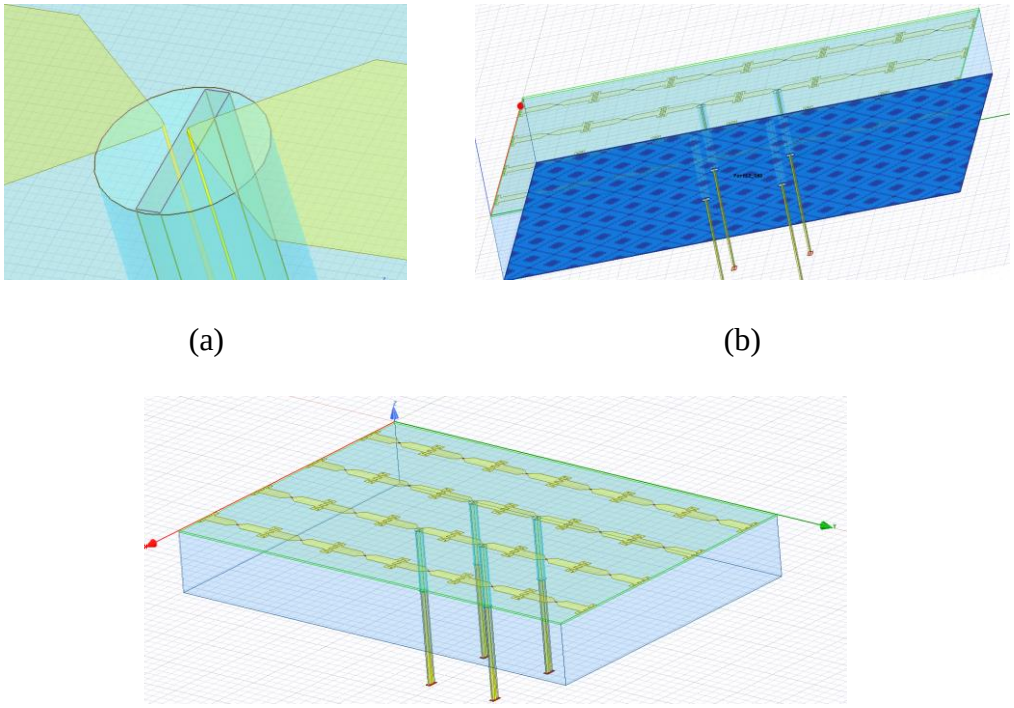

(a) (b)

(c)

Figure 6.5. The Antenna and the Feed; (a) Parallel strip line Connection to Antenna Terminals, (b) View Depicting the Perturbed Ground Plane, (c) The Entire Antenna and Feed Structure

The reason behind those low quality patterns may be due to the fact that the field lines are not protected or in more technical words, they are not electromagnetically shielded. Also a cavity of 4.2 mm radius that disrupts the ground plane, hence disrupts the antenna patterns resulting in unwanted beams that radiate towards direction other than broadside.

To be able to shield the feed lines, the following structure is constructed. For reducing the effect of unbalance, all the widths are taken as such that all impedances along the balun feed is 200 Ω. The width of the dielectric card is reduced to 2 mm, and a parallel strip line transmission line of 200 Ω is put on this card. The surroundings of this feed structure is covered with a metallic cylinder such that the field lines are protected from the reflections within the ground plane and radiating aperture. The trace width required for impedance of 200 Ω is calculated considering the shield structure and its radius. The reason of use of 1.2 mm radius shield lies on the fact that, smaller the feed lines; less disrupted reflection behavior from the ground plane. Total balun length is taken equal to the 60 mm, that is equal to the distance between ground plane and antenna radiator plane. Below the finite ground plane, at bottom, 4 wave ports of 200 Ω port impedances are assigned, one them can be seen in Figure 6.8. Furthermore, the connection to the antenna terminals were made more realistic situation, using finite width wires that extend from the dielectric card of balun to the dipole terminals. In reality, this connection will be performed by similar wires passing from a pair of holes in the dipole terminals and finalizing in the dipole arms.

For this new kind of testing feed scheme, the results obtained are better. The active S-Parameters are lower than -10 dB for all 4 ports and the patterns are of higher quality. Sidelobes are as low as lumped excitation case and the beams only pointing towards to the broadside. In Figure 6.9, those results are given.

For further investigation of the effect of shielding feed lines, the shield radius is swept across a few variables. The shield radius is taken 2.0 mm, 2.4 mm and 3.0 mm and the active S-parameters are given for those analysis’. In Figure 6.10, the results are shown. Only the patterns for the 3.0 mm radius shielded feed are provided due to the fact that the worst scenario is there according to the S-Parameters hence the worst pattern would likely to occur in that scenario.

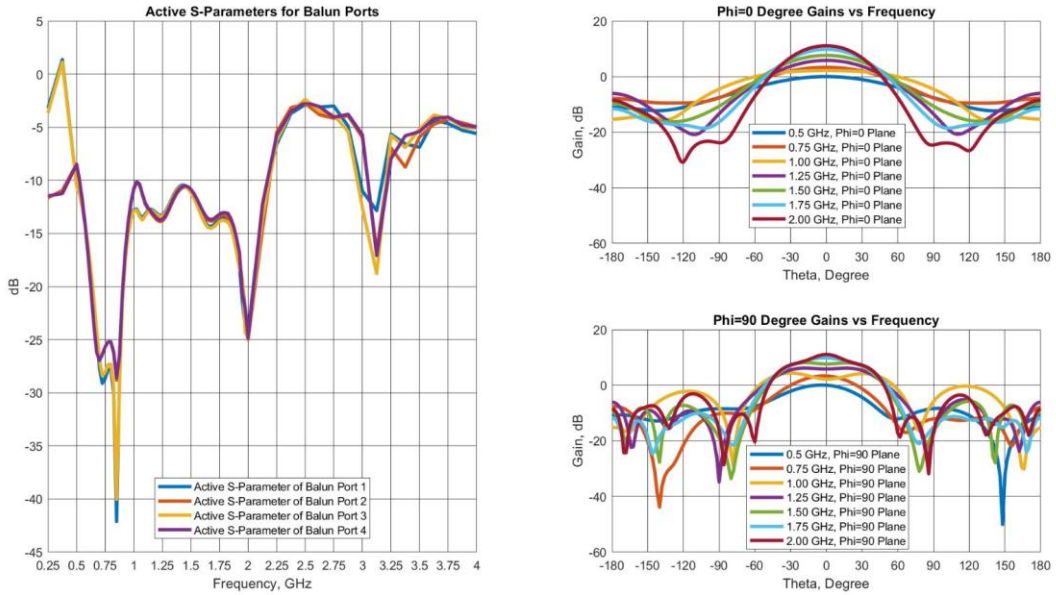

Figure 6.6. The Active S-Parameters of Balun Ports and The Gains in Principal Planes for the Antenna Fed with Balun

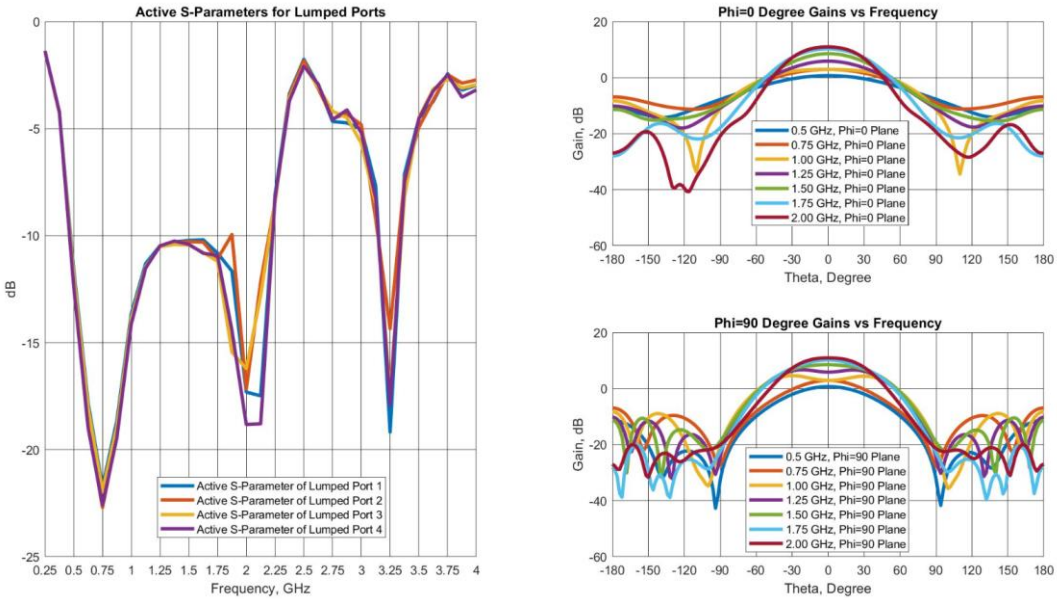

Figure 6.7. The Active S-Parameters of Lumped Ports and The Gains in Principal Planes for the Antenna Fed with Lumped Ports

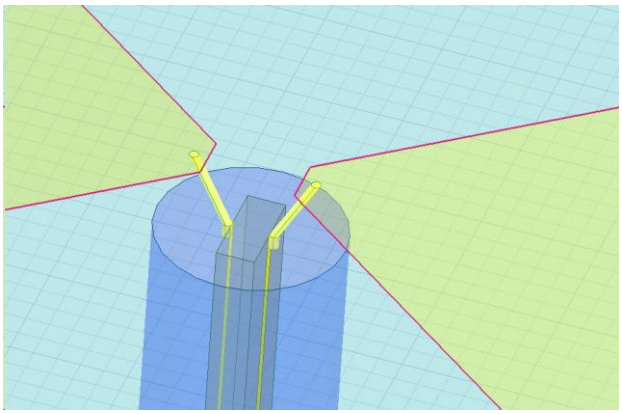

(a)

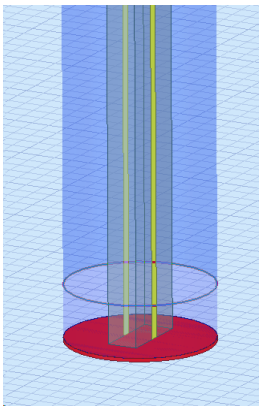

(b)

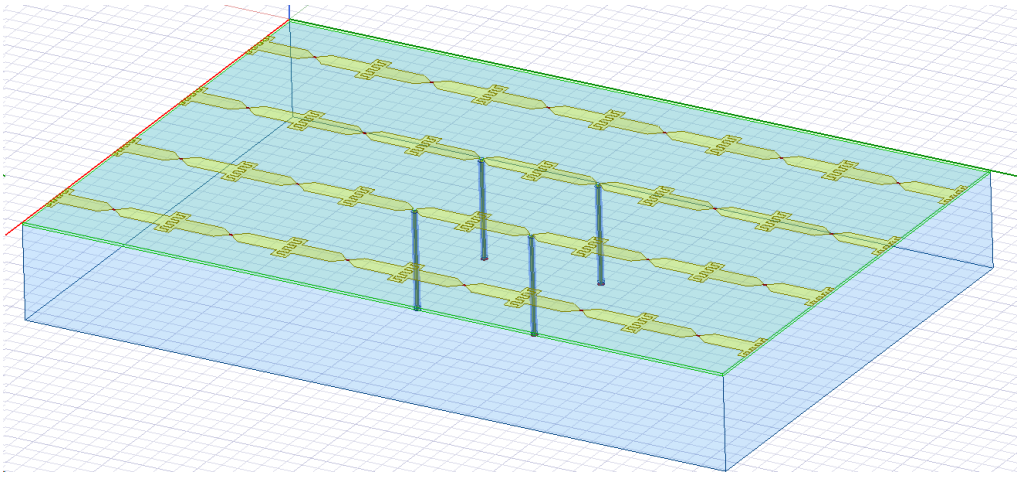

(c)

Figure 6.8. The Antenna and the Shielded 200 Ω Feed; (a) Parallel Strip Line Connection to Antenna Terminals, (b) Wave Port Excitation From a 200 Ω Impedance Port, (c) The Entire Antenna and Feed Structure

To be able to use tapered baluns in a shielded structure, the two conductors of the tapered balun must have the same trace widths inside the shielded structure. Note that the main goal of these feed topologies are to obtain a perfectly balanced two conductor output at the antenna plane. Different trace widths inside the shield structure will deteriorate the desired balanced output goals, conductors of different

widths would electromagnetically couple differently; hence their balances would be different than each other. Furthermore, even in the case that no shield structure is used, for those tapered baluns, there is a point along the tapered balun structure where the tapered balun is passing from the holes on the GND plane of the antenna. Even at that point, the balun's two conductors must have equal trace widths in order to couple equally to that GND plane of the antenna so that the outputs of the tapered balun would be balanced as desired. Otherwise, the unbalances observed at the end of the balun would be worse than the balun structure simulated independently residing in space, i.e. without any ground planes or other objects around.

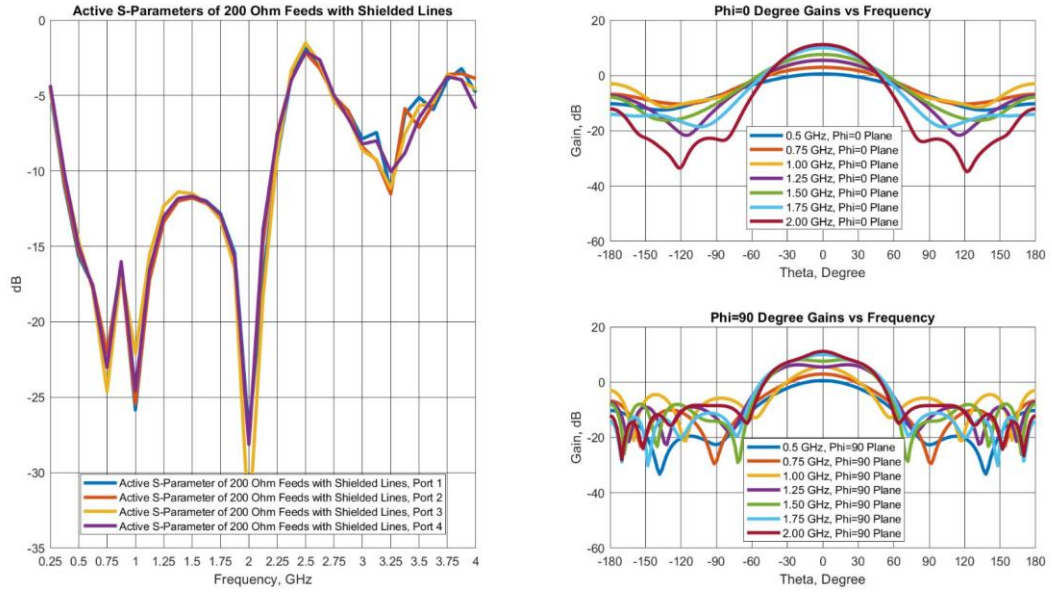

Figure 6.9. The Active S-Parameters of 200 Ω Feeds with Shielded Lines and The Gains in Principal Planes for the Antenna Fed with 200 Ω Feeds with Shielded Lines

In the light of those facts, the tapered balun structure present is revised accordingly. Rather than using exponential ground plane and on top of that linearly tapered accompanying conductor, the sections of each conductor were made of discrete

transmission line sections, just as original Chebyshev taper [19] describes. For the 0.813 mm of RO4003 cards that were used before, 2 last sections at the output of the balun settles into the shield, where they are always composed of twin lines. The remaining sections consist of microstrip transmission line. All sections together build up the shield tapered balun structure of Chebyshev transforming impedances.

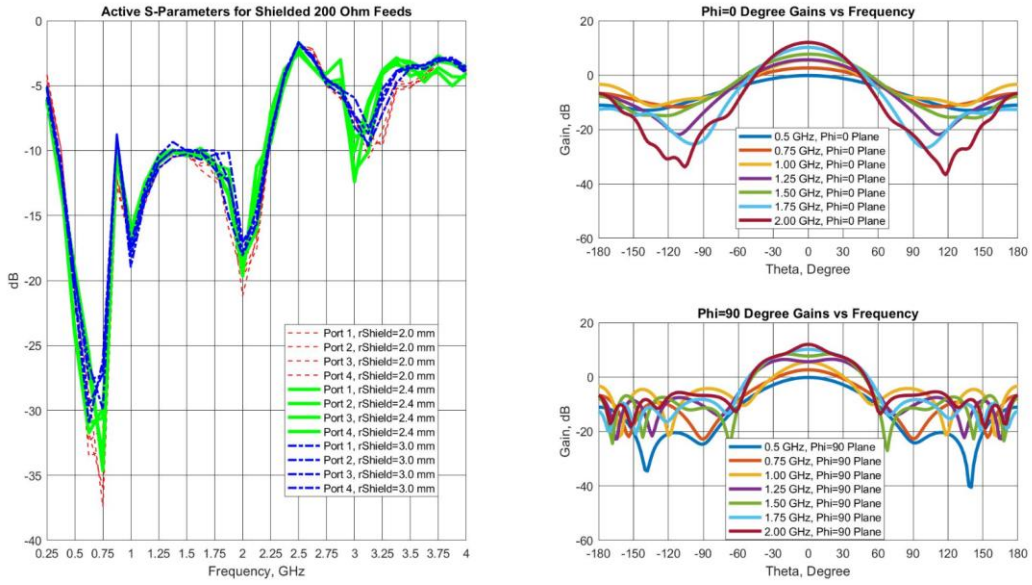

Figure 6.10. The Active S-Parameters of 200 Ω Feeds with Shielded Lines for Different Shield Radii and The Gains in Principal Planes for the Antenna Fed with 200 Ω Feeds with Shielded Lines of 3.0 mm Radius

The length of each section is taken to be 30 mm, where four sections of transforming impedances are used. The first three section were the impedances according to the three section, Γ_m=0.2 Chebyshev transformer impedances whereas the last section were the implementation of 200 Ω parallel strip line inside the shield. The last three sections out of all four sections were consisted of parallel strip line type transmission lines. The first section was the made using a microstrip line of 4 mm GND width for a 50 Ω SMA connector to be plugged in. In Figure 6.11, the balun structure is given.

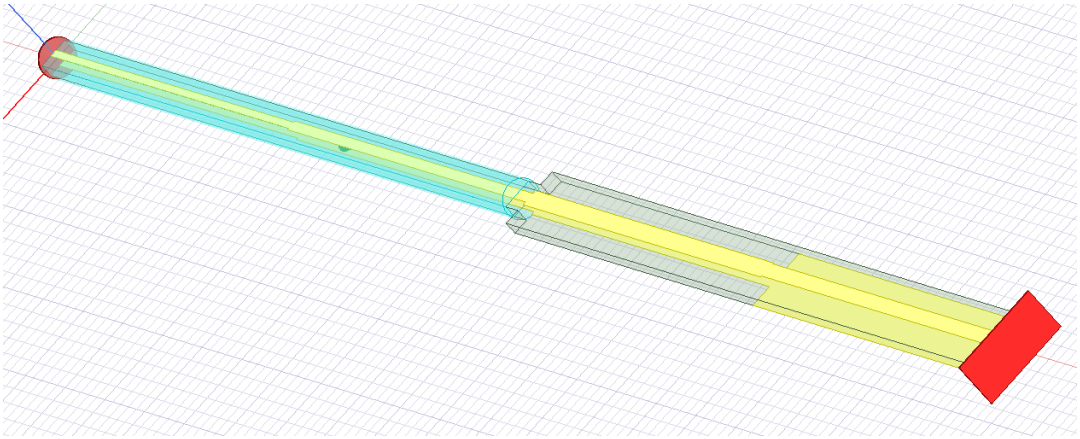

Figure 6.11. Physical view of the Shielded Balun Using Discrete Tranmission Line Sections

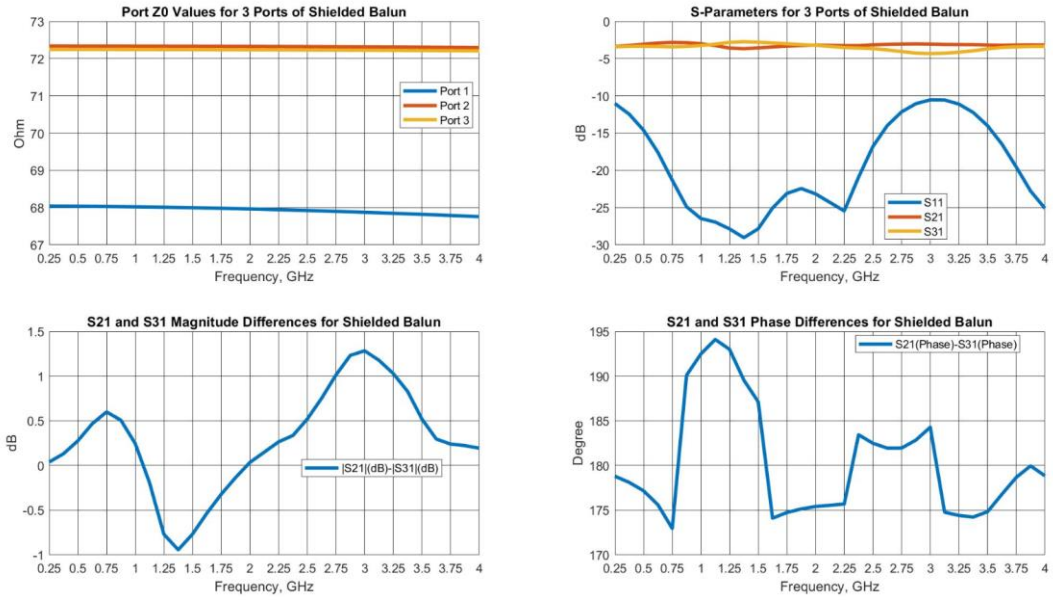

Figure 6.12. S-Parameters Results for Shielded Balun

In Figure 11, the red surfaces contain the input and output ports of the balun. The input port is a microstrip line whereas the output port is a parallel strip line

implemented on a dielectric substrate and the surrounding is shielded with a pipe like structure. The blue cylindrical object is the shielding structure for this balun. The shielded sections reside inside the antenna whereas the other parts extend below the antenna ground plane. Total balun length is 120 mm whereas the antenna has distance between its radiator plane and the ground plane is 60 mm.

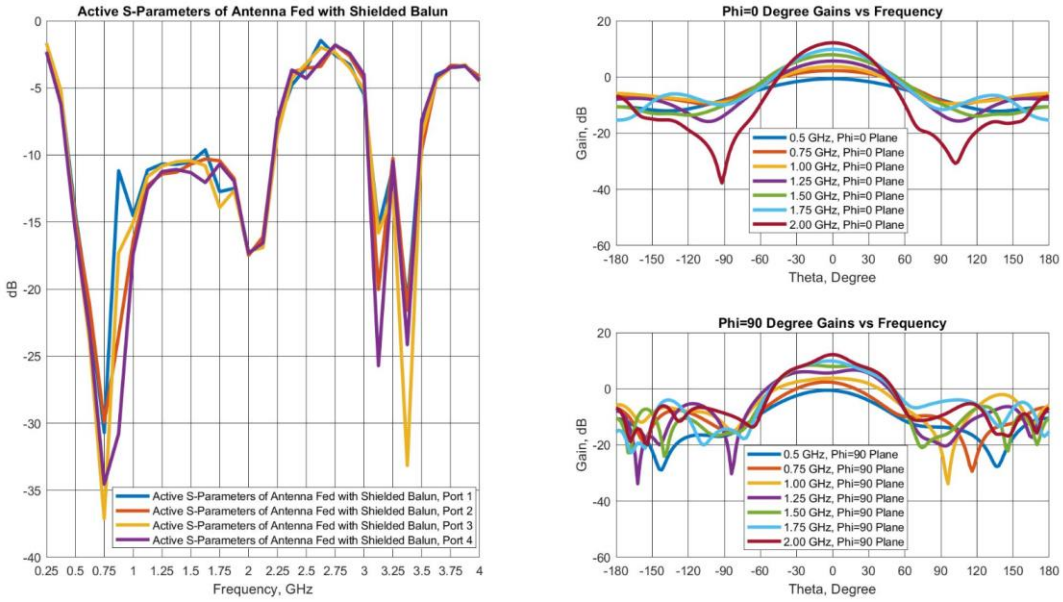

Figure 6.13. The Active S-Parameters for Antenna Fed with Shielded Balun and The Gains in Principal Planes for Antenna Fed with Shielded Balun

This balun structure's S-Parameters results are given in Figure 6.12. Note that this balun has maximum 1 dB amplitude unbalance between output ports whereas the 150 mm non-Shielded balun had similar maximum unbalance as well. However, in terms of real balun performance, the performance under feeding the antenna elements, the latter one is superior. The performance metrics of this new balun are given in Figure 6.13.

In Figure 6.13, it is seen that for all 4 ports' active S-parameters are lower than -10 dB and the patterns are of high quality. The sidelobes are as low as 200 Ω feeds with shields or the lumped port excitation of the antenna. In all these scenarios, the sidelobes were lower than -3 dB condition is satisfied. For all of those scenarios, the 4 ports active S-parameters are below -10 dB as well.

6.2 Tapered Baluns Using a Power Divider

Another feeding scheme that were incorporated was feeding two antenna unit cell's from one source via a power divider in order to reduce the impedance transformation ratio from 4:1 to 2:1. In addition, with the shielded ends used for this power divider balun composition structure, both feed miniaturization and high performance feed that allows patterns to be as good as if lumped excitation scheme applied. An impedance transformation of 100 Ω to 200 Ω is enough, hence feed structure can be miniaturized. In Figure 6.14, this feed structure is given. Two section Chebyshev transformer with an ending of a 180 Ω parallel strip line section is present in this structure. Total number of impedance control sections are three. Using only parallel stripline impedance sections inside the shield structure retained in this balun as well. The input port is a microstrip line of 50 Ω impedance. Each input port will feed two unit cells of the finite antenna. Out of three sections, the very first one is a microstrip line type of transmission line, the other two sections are parallel strip line type of transmission line sections. In Figure 6.14, the red surfaces indicate ports of the balun structure. The two outer ports at the two ends of the balun structure are again divided into half, their integration lines are arranged accordingly such that the balun structure can be evaluated from its S-parameters. For the corner present in the structure, no mitering is made. Only a triangle satisfying the continuity of the traces is placed. Prior to this balun, this cornering architecture were tried, it was compared with straight connections. In terms of electromagnetic field transmission, that kind of corner does not create any problem for design frequencies considered in this thesis.

Each transformer section is around 38 mm in length, λ/4 at the center frequency, as they needed to be for the Chebyshev transformer. This balun with its corresponding lengths, fits to the antenna structure well. No additional mechanical arrangements needed.

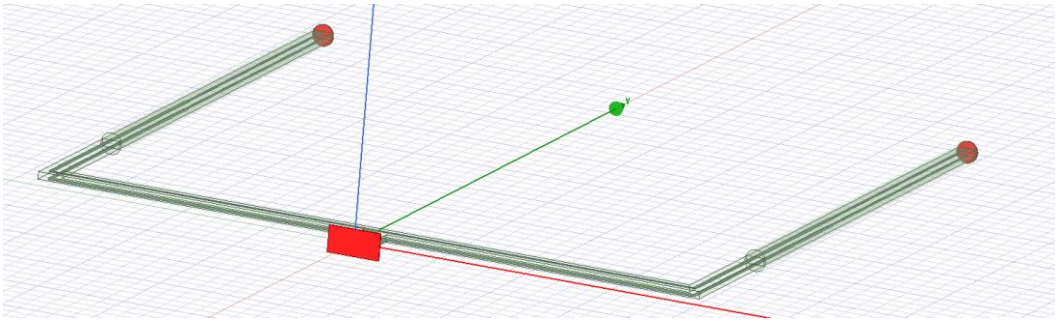

(a)

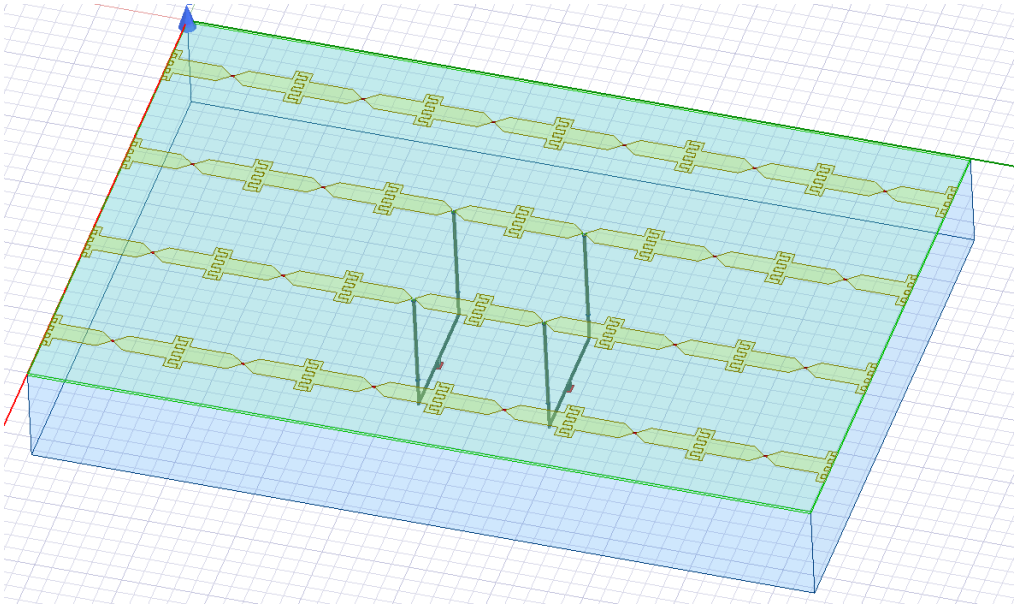

(b)

Figure 6.14. Balun Using PD ; (a) Balun Structure itself, (b) Balun Structure Connected to Antenna

In Figure 6.15, the S-parameters results for this balun are presented. The two outer ports are labeled as ports 2 and 3. Each of these outer ports consist of 2 ports hence the all outer ports are labeled as 2_1, 2_2, 3_1 an 3_2. The input port is simply labeled as 1. Amplitude unbalance between output ports are reduced to a value lower than 0.7 dB. Only half of the port impedance values of the outer ports are observed at ports 2_1, 2_2, 3_1 and 3_2.

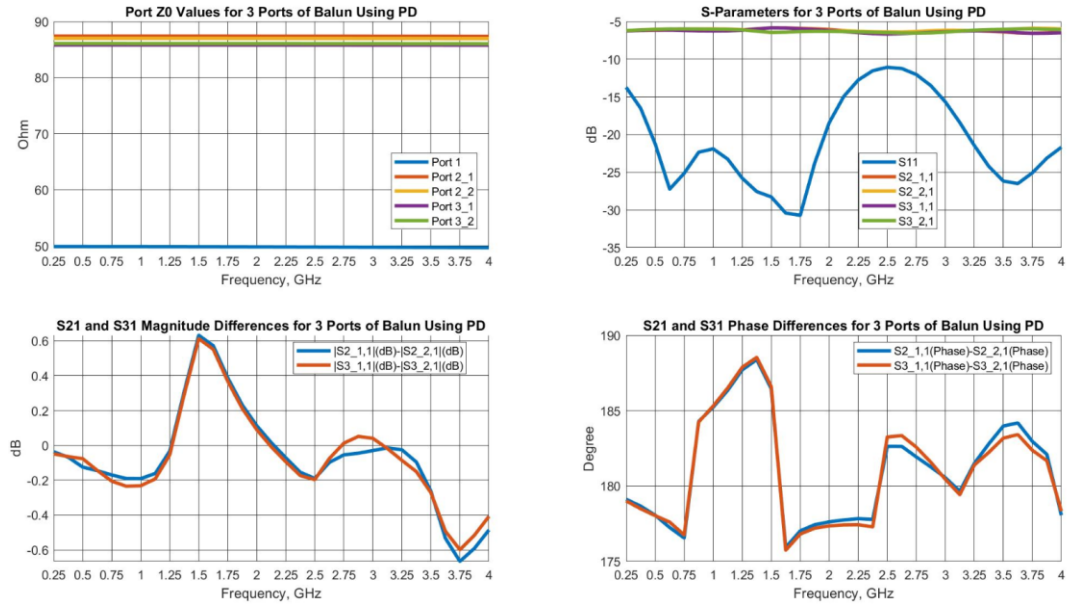

Figure 6.15. S-Parameters Results for Shielded Balun

After evaluating the balun structure without the antenna, the results seemed to be satisfactory enough to test the balun structure as an antenna feed. The length of the shield surrounding the balun's dielectric card was made equal to the foam present under the antenna. In Figure 6.16, the installment of this balun to the antenna structure is shown. For the installment of the balun to the antenna structure, the two feeds are placed such that they are not periodically distributed but one of the balun is the symmetrical of the other one. By doing such an arrangement, the patterns' qualities were made superior. However, while doing this symmetry operation, one

needs to be careful. Integration lines of two antenna feeds must have the same orientation, i.e. they must be pointing towards the same directions. In real life, this operation requires a 180^0 hybrid.

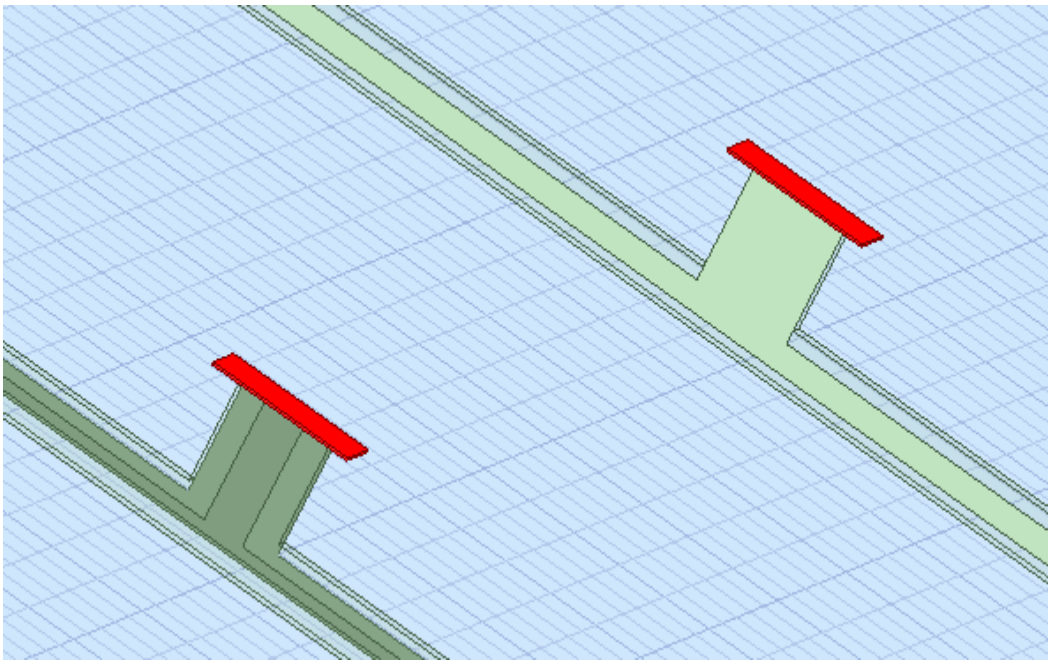

(a)

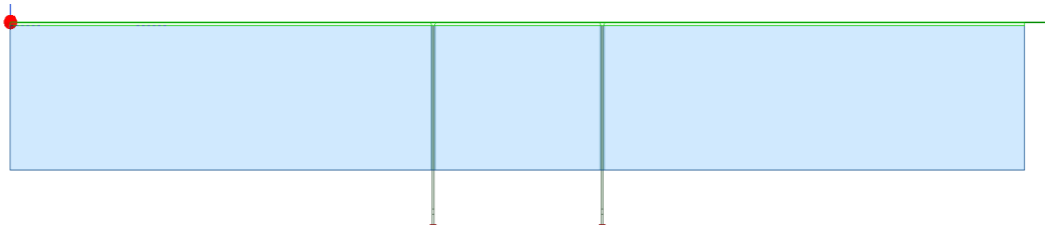

(b)

Figure 6.16. Installment of Balun Using PD on the Antenna; (a) View from the Top of the Antenna Depicting the Back to Back Installed Balun Feeds (b) View from the Side of the Antenna Depicting Miniaturized Feed and the Antenna

Finally, in Figure 6.17, the results of the antenna fed with this balun are presented. The active S-parameters are lower than -10 dB, except a frequency point around 1.5 GHz. Very little trade-offs were made to reduce that frequency point's active S-parameters below down to the -10 dB by changing the widths of the traces. The tradeoff was made between lower S_{11} and lower unbalance between the output ports. At the end, the worst active S-parameter at 1.5 GHz were made -8.85 dB, while the other frequencies in the desired band remaining lower than -10 dB. It is beneficial to note that, this feeding scheme retains the low profile behavior of the array, unlike other most TCDA papers present in the literature. The feeding extensions below the ground plane is only 21 mm, total antenna depth is therefore 81 mm; only 0.13λ at 0.5 GHz, the lowest operational frequency.

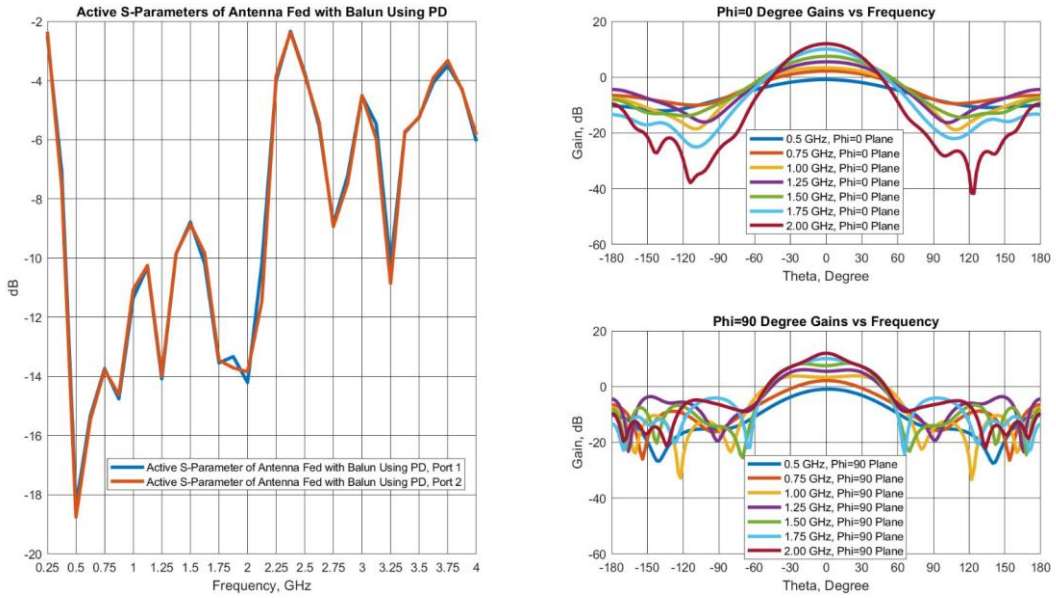

Figure 6.17. The Active S-Parameters for Antenna Fed with Balun Using PD and The Gains in Principal Planes for Antenna Fed with Balun Using PD

6.3 TCDA Feeding Using a Pair of 93 Ω Coaxial Cable

This kind of feeding scheme uses a pair of 93 Ω coaxial cable. The actual feeding scheme requires a pair of 100 Ω coaxial cables, but since 93 Ω coaxial cables were available at the facility; the feeding scheme was implemented using 93 Ω coaxial cables. UT-085-093 is the labeling of this coaxial cable. Consider a power divider of 50 Ω input and the two outputs of 93 Ω. Furthermore, consider this power divider as if it is realized using parallel strip line structure, i.e. the input port as well as two output ports are perfectly balanced ports realized using a pair of same width microstrip traces.

In Figure 6.18, the proposed feed structure is shown. The initial square region is miniaturized power divider section. This section implements the 50 Ω SMA coaxial connector modeled in the HFSS environment. After power divider section, two arms are tapered to microstrip line as one moves along the feed structure so that 93 Ω coaxial cables would connect to them. If those 93 Ω coaxial cables were to fed out of phase, i.e. 180^{o} phase difference between them, they can feed the antenna present. One of the cables will feed one arm of one unit cell of the antenna whereas the other one will the other arm. 93 Ω coaxial cables' outer conductors were electrically connected to each other, they act as a virtual ground. In Figure 6.19, connection of those cables to the antenna terminals are given. To improve the connection between the inner conductors and the dipole arms, a pair of half circles are added to the dipole arms such that the feed locations are similar to the lumped port excitations. The outer conductors behave like virtual ground, however they are connected to the antenna ground plane. As the inner conductors were fed differentially, they are able to feed the antenna unit cell.

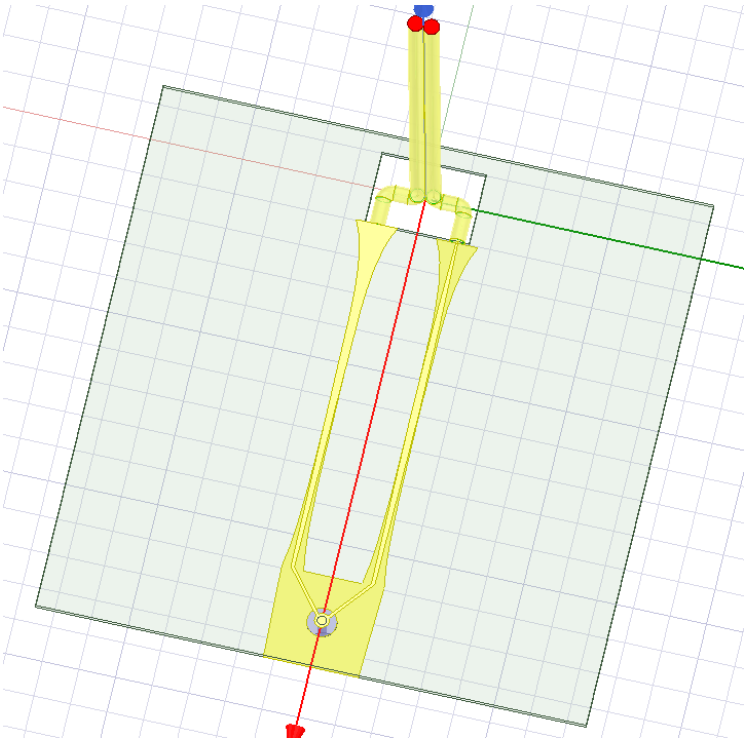

Figure 6.18. Feed Realization using a Pair of 93 Ω Coaxial Cables

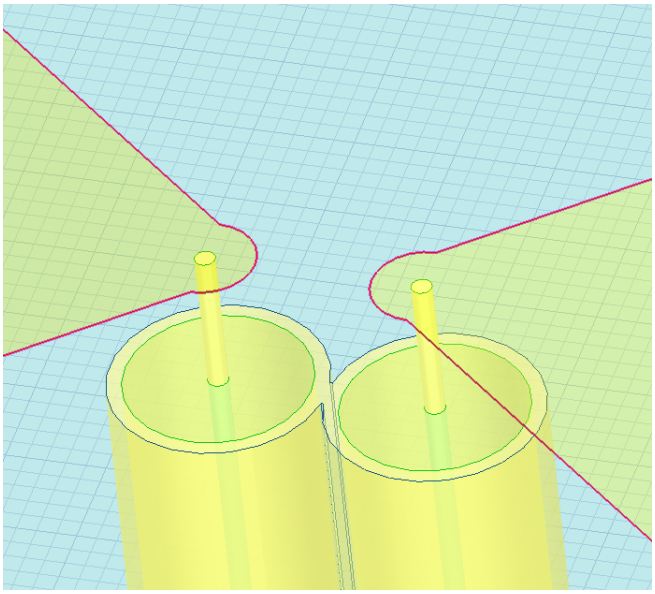

Figure 6.19. Connection of UT-085-093 Cables to the Antenna Terminals

In Figure 6.20, connection of coaxial cables to the arms of the power divider are given. A direct connection between parallel strip line type microstrip line and coaxial cable is not possible. As an engineering insight, the outer conductor of the coaxial cable should be connected to a microstrip line of larger ground plane than its diameter. Note that in Figure 6.20, one of the arms of the power divider has its ground plane below the dielectric card whereas the other one has its ground plane above the ground plane. The reason of this kind of action will be explained later.

The coaxial cables used in this structure are of different lengths. One of them is longer than the other one, the amount of difference in lengths is just as the width of the dielectric cards present, equal to 0.813 mm.

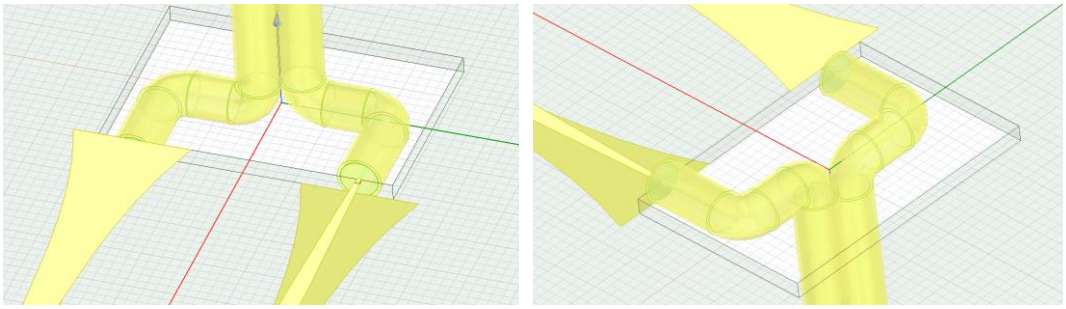

(a) (b)

Figure 6.20. Connection of UT-085-093 Cables to the Arms of the Power Divider, (a) Top View, (b) Bottom View

In Figure 6.21, the tapering of the arms of the power divider to a pair of microstrip lines are given. The power divider has its output ports in a microstrip line type transmission line. Gradually, as one moves along the feed structure, they are tapered to a pair of parallel striplines. Then, after achieving parallel striplines, they are retapared to microstrip again. However, the tapering is done in the following way: in one of the arms, the ground plane is implemented on top of the dielectric card whereas in the remaining arm; it is implemented on bottom of the dielectric card.

Along the taper, impedances of the feed structure are controlled at 5 points including the start and end of the taper. At all 5 points, the arms of the power divider has 93 Ω characteristic impedance. The first and second of those control points are responsible for providing 93 Ω characteristic impedance at their respective loactions. The third one is a parallel stripline type of transmission line, at the middle; it also provides a characteristic impedance of 93 Ω at its position. The fourth and fifth control points provide 93 Ω characteristic impedance as microstrip type transmission line; however they have their grounds on opposite sides of the dielectric card. By implementing ground planes at opposite sides of the dielectric card, theoretically a true 180^{o} phase difference is expected at the output ports. The length of the taper is 35 mm.

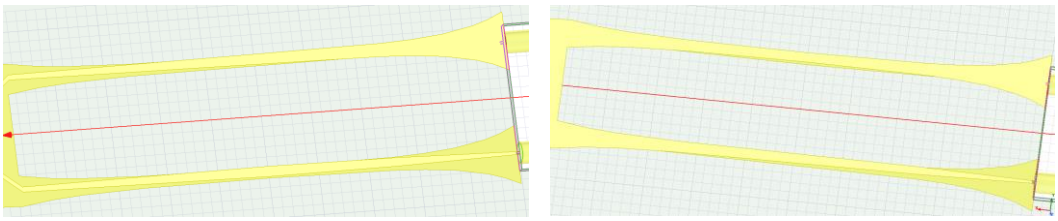

(a) (b)

Figure 6.21. Tapering of the Parallel Strip Line Outputs of the Power Divider to a Pair of Microstrip Lines, (a) Top View, (b) Bottom View

The power divider structure and the transition from the SMA connector to the microstrip type transmission line is implemented together. For the transition of the SMA connector to a microstrip line, a solder island is made on top of the dielectric card, where the inner conductor of the connector will be connected. For the square region of the connector which electrically touches to the outer conductor of the SMA connector will be connected to the square trace at the bottom of the dielectric card of the feed structure. This proposed structure is given in Figure 6.22.

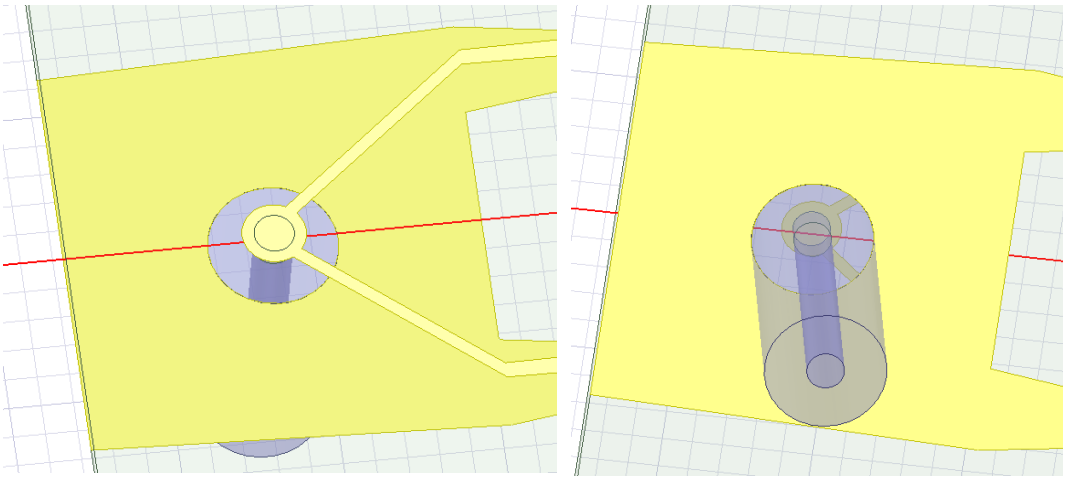

(a) (b)

Figure 6.22. Transition of SMA Connector to Feed, (a) Top View, (b) Bottom View

In Figure 6.23; the first half of the tapered section of this feed mechanism is given. From the input port, until parallel stripline ends presented in Figure 6.23, the two arms are of equal amplitude and equal phase. The two arms travel exactly same electromagnetic paths from the 50 Ω coaxial entry till parallel stripline sections.

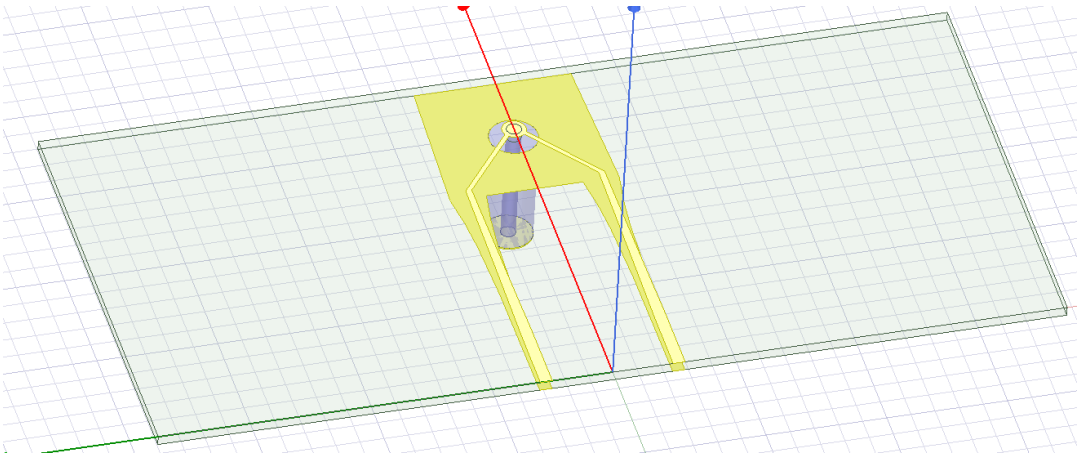

Figure 6.23. First Half of the Tapered Section of the Feed Mechanism

In Figure 6.24, the second half of the tapered section of this feed mechanism is given. Two signals of same amplitude and same phase that exist in two arms are input to the second half of the tapered section.

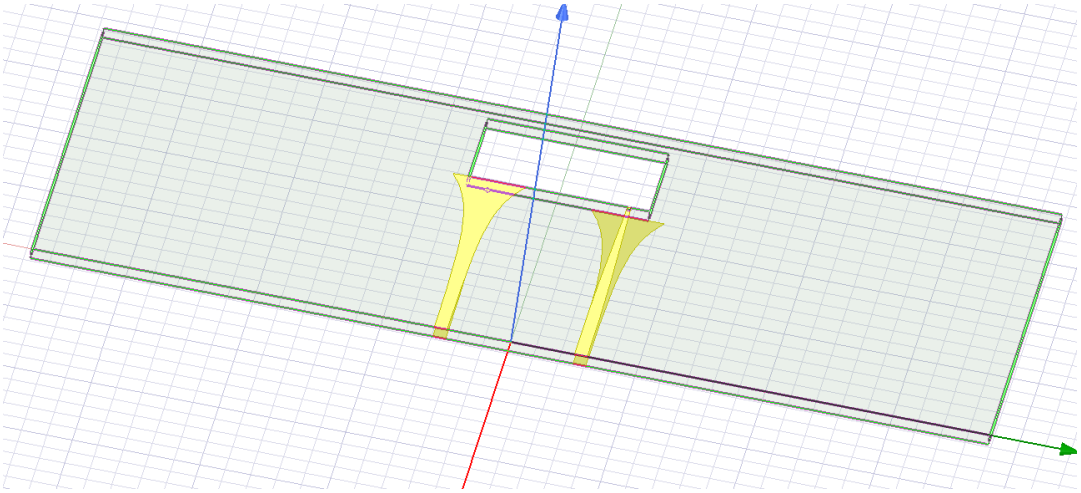

Figure 6.24. Second Half of the Tapered Section of the Feed Mechanism

As the second half is the section of the feed taper where 180^0 phase differences between each arm are given to the signals. This phase difference is given by natural shape of the taper given. One arm has tapered ground below the feed PCB whereas the other arm has tapered ground above the feed PCB. Therefore, at the end of the second half of the tapered section of this feed, actually there exist same signals at the two outputs. The author uses the word "same", because for the two signals, the electromagnetic path after the parallel stripline section is equal. Due to the fact that, one arm has its ground above and the other one has below; the two output signals are of opposite phase, that is 180^0 phase difference exists between each other.

.

Then, finally after obtaining two signals of same amplitude but opposite phases; the only need is to transfer those signals to the dipole terminals. This operation is done by coaxial RF cables of 93 Ω.

Finally, in Figure 6.25, the S-parameters results for this feed scheme are given. The input S-parameter is lower than -20 dB over the entire band. Also, the magnitude differences between the output ports are lower than 2 dB for the design frequencies. The phase differences between output ports are around 180^{o}, at the worst points the phase error retains lower than 15^{o}. The results are good enough for installment on the antenna as a realistic feed. This proposed feed structure is electromagnetically shielded and it is easier to manufacture compared to the previous feed structure. It also provides independent feeding of the antenna terminals and it is also small. The extension of feed networks below the ground plane is low. The first two feed mechanisms had longer extensions below the ground plane. The third one had shorter extensions as well, but it was not easy to manufacture, and it does not provide independent feeding of the antenna terminals. This latest version performs all those functions itself.

Before continuing to the antenna installment of this feed structure, some mechanical aspects of this feed structure will be given. This proposed feed structure's total length is little longer than the length of the area of the one unit cell of the antenna. In Figure 6.26, the top view of this complete feed structure is given. The dielectric card that contains all the feed structure prior to the 93 Ω coaxial cable connections were of 1 unit cell × 1 unit cell size of the antenna. However, the coaxial cables that feed each excited unit cell of the antenna are off centric in this dielectric card. While assembling this final proposed feed structure, the periodicity will be satisfied; unit cell approach could be used, however, feeding structure of one unit cell exceeds to the adjacent one.

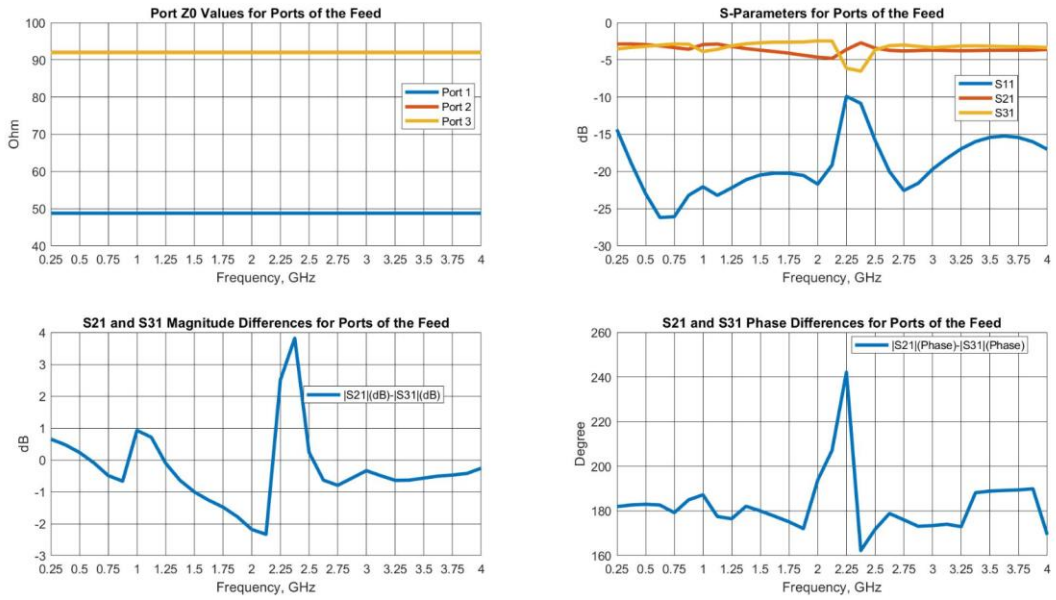

Figure 6.25. S-Parameters Results for Feed Implementation Using a Pair of 93 Ω Coaxial Cables

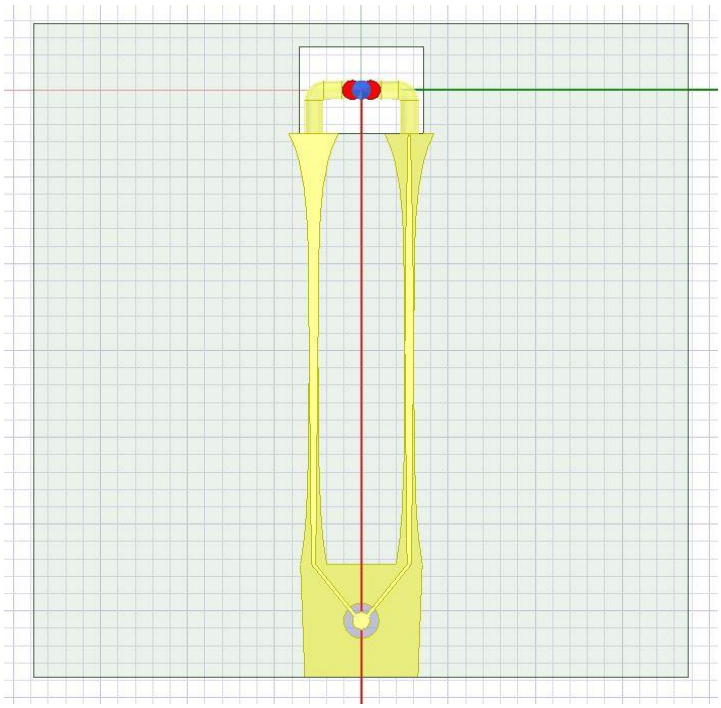

Figure 6.26. Top View Depicting the Area Occupied by the Feed Structure

In Figure 6.27, top view of the antenna installment of this feed structure is given. The periodicity of this feed structure is satisfied. Since this feed structure has no problem with periodicity, it can also be used in the infinite array unit cell analyses.

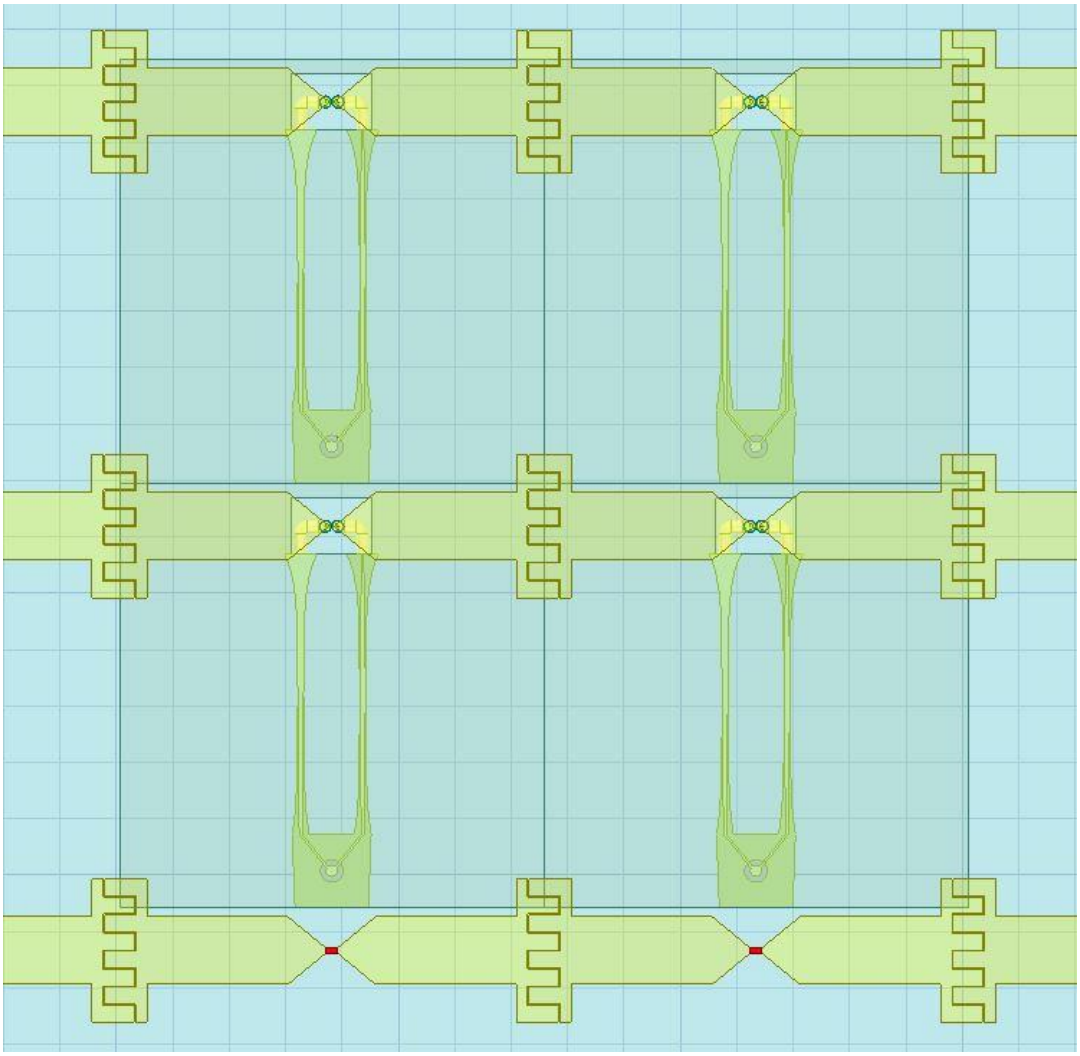

Figure 6.27. Antenna Installment of the Feed Using Coaxial Cables

Then, the antenna fed with this feed structure is evaluated. The results are given in Figure 6.28. The active S-parameters are good in the whole 0.5-2.0 GHz frequency band. They are all lower than -10 dB. Actually, the antenna integrated with this feed

structure provides 4.52:1 frequency bandwidth under all four active S-Parameters lower than -10 dB condition. This is the predicted theoretical bandwidth that agrees with the calculations provided in the previous chapters in this thesis.

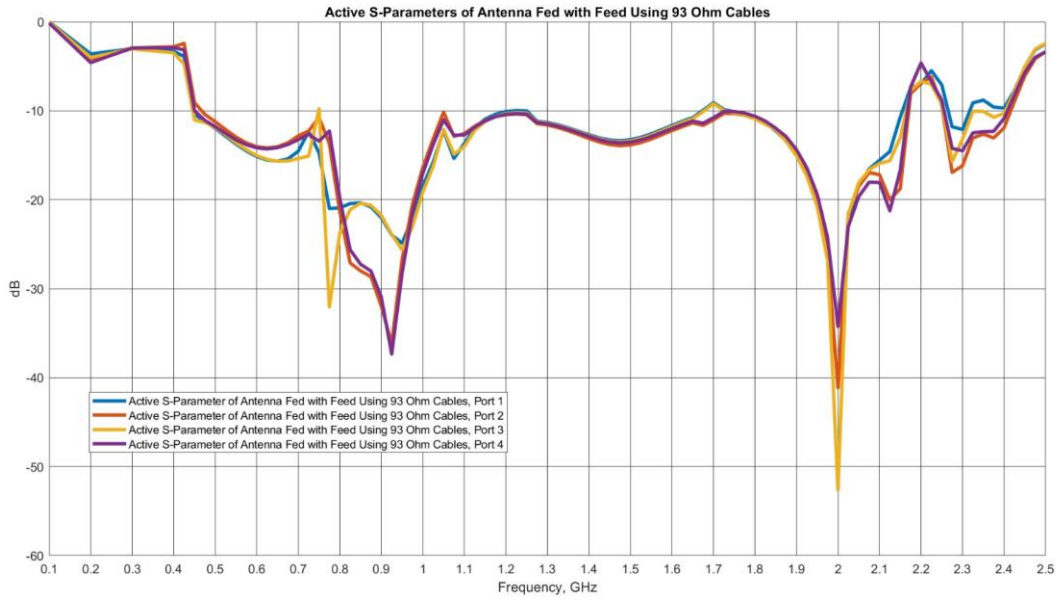

Figure 6.28. The Active S-Parameters for Antenna Fed with Feed Using 93 Ω Cables

In Figure 6.29, the gains of the antenna using this feed mechanism is provided. The patterns are of good quality; they are symmetrical around boresight axis. Sidelobe levels are low, for all frequencies they are lower than -2 dB; except 0.75 GHz which has sidelobe level of 0 dB. The worst sidelobe level of all frequencies was -6.9 dB in the lumped port excitation case. The only important difference from the lumped excitations is that the 0.5 GHz boresight gain is slightly lower. It is around -2.5 dB; whereas it was 0.69 dB in the lumped port excitation case. Gain pattern of 0.75 GHz is slightly deviated from the boresight axis. The reason for this deviation of approximately 15^0 is due to the unbalances between the outputs of the balun, i.e. feed mechanism applied.

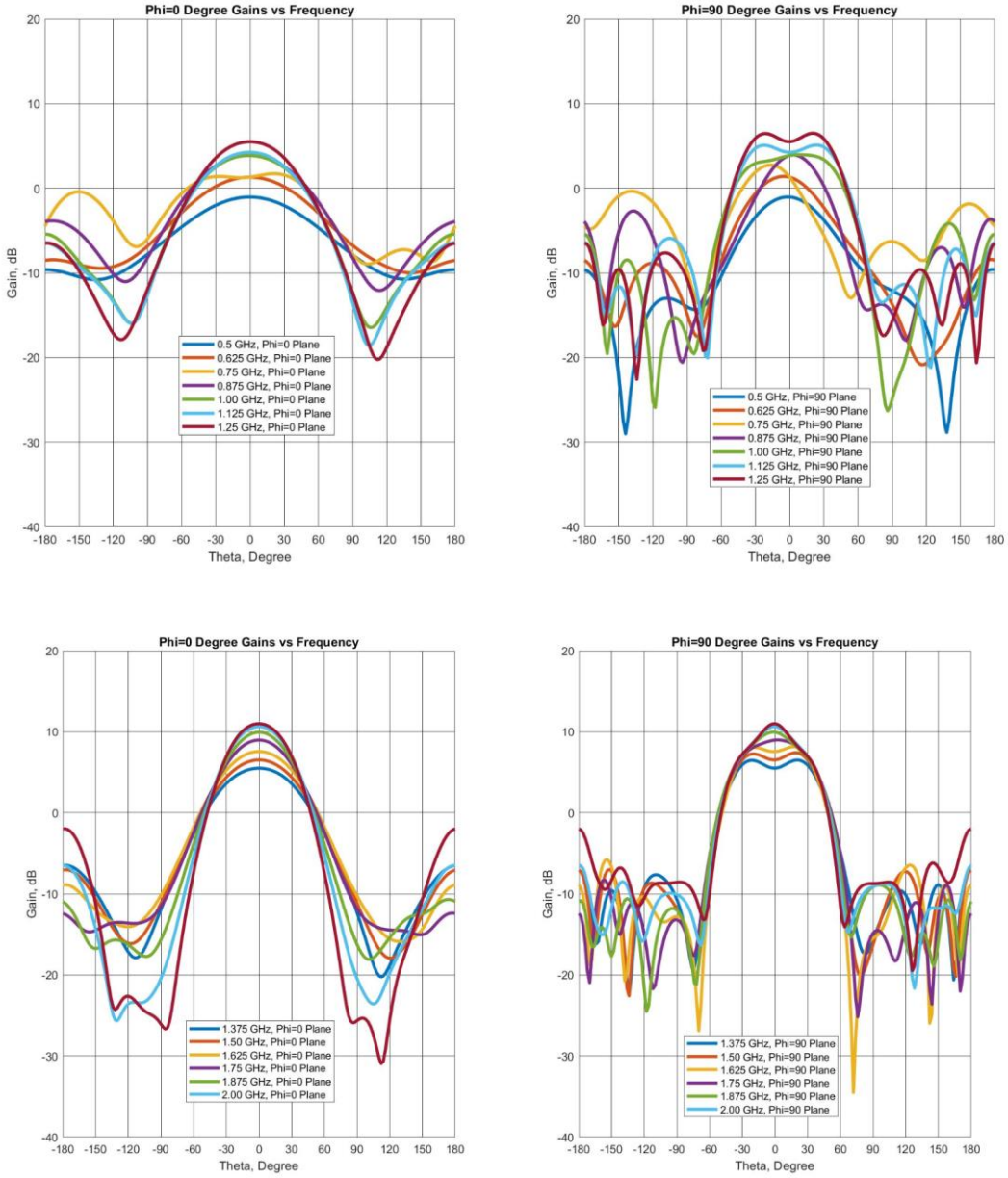

Figure 6.29. The Gains in Principal Planes for Antenna Fed with Feed Using 93 Ω Cables

This final given feed mechanism is used for antenna realization. This feed scheme also retains the low profile behavior of the antenna. The distance between the ground plane and feed PCB is 12 mm only, total antenna depth is 72 mm; only 0.12λ at 0.5 GHz. Therefore, the realized antenna is of low profile as well.

CHAPTER 7

REALIZATION OF THE TCDA

Antenna is built within the facility where the author is employed. First, the aperture is produced using PCB production technology. Second, the feed circuit is realized on a PCB. Then, with the help of some mechanical engineers; the finite thickness ground plane and the foam material between ground plane and antenna aperture are processed. In the simulations, the ground plane were implemented as infinitely thin PEC boundary condition. The necessary mechanical connection parts that holds feed PCB cards below the ground plane were manifactured by mechanical engineers as well. Finally, together with all the pieces; antenna is realized by the help of electronic technicians.

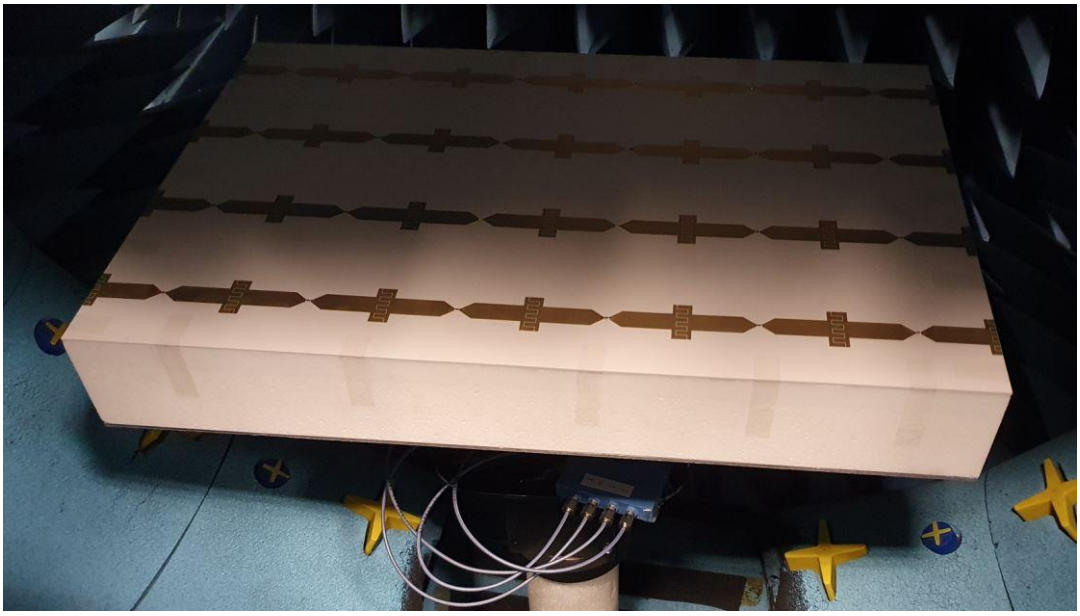

Figure 7.1. Top View of the Antenna Structure

For the realization of the antenna, initially balun cards are created via the PCB technology. Then UT-085-093 coaxial cables were arranged accordingly such that they fit well between the antenna radiation plane and balun cards. Then those two sets of pieces were unified. Then balun cards are assembled along with the other pieces of the realized antenna. In Figure 7.1, the completely assembled antenna structure, view from top, is given. A finite metallic GND plane is present. Above that, there is a foam and on top of the foam there exists the antenna PCB card. All the elements that are not excited are terminated with 200 Ω chip resistors.

In Figure 7.2, connectors of the antenna are given. 50 Ω SMA type connectors are used for energizing the active region of the array. Balun structures whose designs were given in the previous chapter are also visible in Figure 7.2. Black cylindical objects are present for mechanically supporting the antenna.

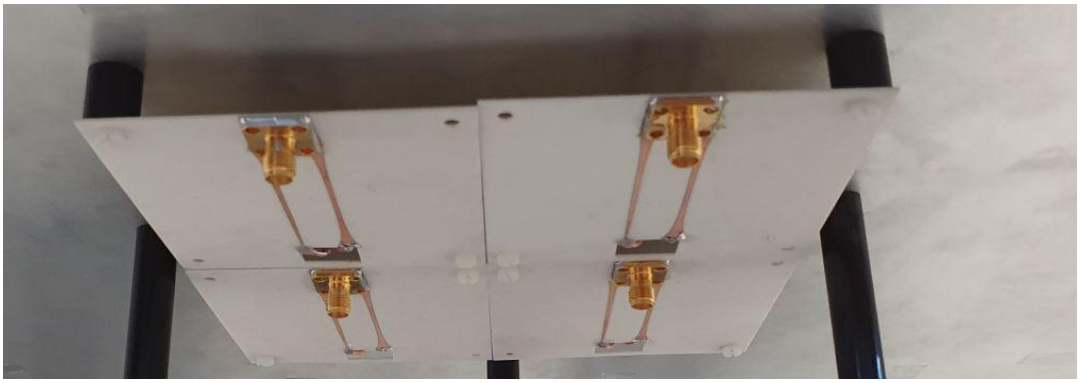

Figure 7.2. Back Side View of the Antenna Structure

7.1 S-Parameters Measurements

For energizing the antenna a four way power divider is used. It contains one port as input and four ports as outputs. The power divider has the following specifications: It has insertion loss of maximum 1 dB, amplitude unbalance of maximum 0.4 dB,

phase unbalance of maximum 6 degrees. Used power divider module specifications can be found in [20]. In Figure 7.3, view of the power divider and its connection to the antenna terminals are given. For connecting the power divider module to the antenna's input ports, 50 Ω RF cables are used.

Figure 7.3. Power Divider for Energizing the Antenna with its Connections

The author needs to state that, the power divider module is used solely for testing the antenna. The power divider module is not a part of the designed and manifactured antenna. An example application where power divider module is not used is as follows: one needs to scan the beam of this antenna. In that condition, four different

sources of variable magnitudes and variable phases will be directly connected to the antenna's input ports below the aperture.

Then, the the input port of the power divider, the corporate input, is connected to the network analyzer and its corporate S_{11} is measured. In Figure 7.4, measured corporate S_{11} and 4 port's simulated active S-Parameters are given. In previous chapters, the antenna together with its feed structure were simulated using four different sets of independent sources. Hence, in those simulations four way power divider network were used. The amplitudes and phases of those four different sources were equal, since broadside operation is considered only. Hence, in Figure 7.4; they are presented as four different port's active S-Parameters.

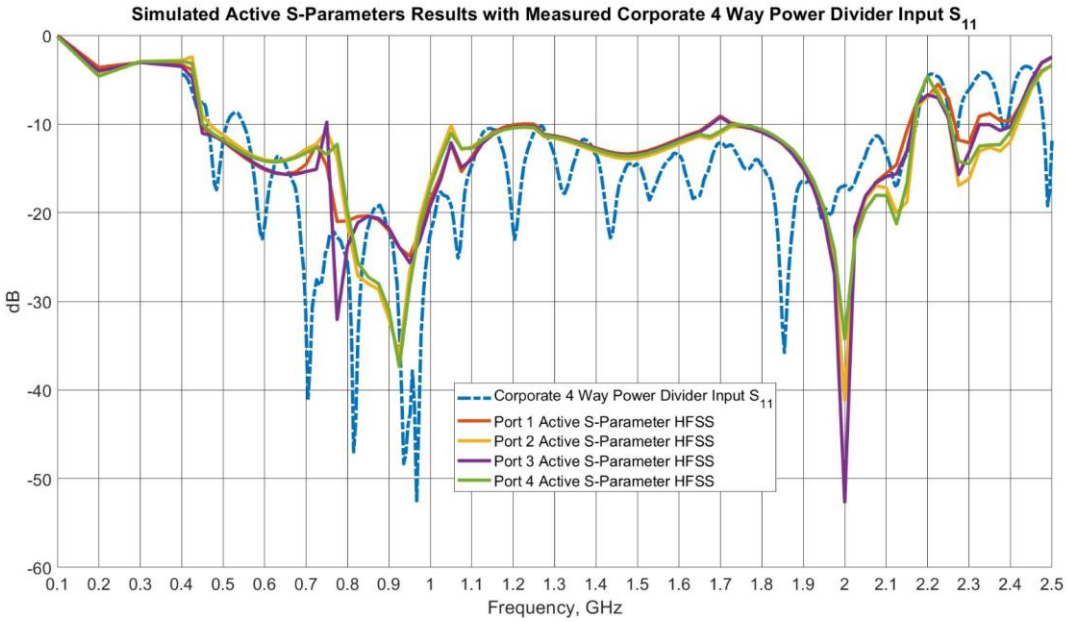

Figure 7.4. Simulated Active S-Parameters of the Antenna with Measured Corporate 4 Way Power Divider Input S_{11}

By examining Figure 7.4, a great agreement is observed with measurement results and simulation results. Corporate power input reflection coefficient is lower than -10 dB, except small portion 0.5 GHz and 0.6 GHz. The worst value of measured S_{11} is lower than -8.65 dB at that region. Similarly, by examining the corporate 4 way

power divider input, the return loss bandwidth is 4.63:1 under input S_{11} < -10 dB criterion.

Additionally, it should be noted that, the used power divider module operates in the band of 0.5 GHz to 2.0 GHz. The necessary amplitude unbalances and input return loss maximum specifications are given only for the band of 0.5 GHz to 2.0 GHz. Used power divider module specifications can be found in [20]. The measurement is conducted only in 0.4 GHz to 2.5 GHz due to this reason. Even though that is the case, at the frequencies lower than 0.5 GHz; the measurements and simulations agree. At the frequencies higher than 2 GHz, the measured S_{11} values are generally higher than simulations. The reason is due to the used power divider module operates between 0.5 GHz to 2.0 GHz. Furthermore, at a frequency higher than 2 GHz, the currents on the aperture and their image's generated by the finite GND plane cancel each other; resulting in a null in the broadside direction.

7.2 Antenna Pattern Measurements

Antenna pattern measurements were conducted using SATIMO Starlab measurement chamber. It is a chamber that fully enclosed with absorbers, it can measure 3D pattern of the antenna. In Figure 7.5, the antenna's front view in the measurement chamber is given. For measurements, initially an antenna whoose gain is tabulated for a set of frequency points is measured. That antenna used is SATIMO SH400 antenna. In [21], the datasheet for this antenna is given. That antenna's gain is tabulated from 400 MHz starting frequency. The reason for provided measurements start from 0.4 GHz is due to that fact. The author does not have access to a reference antenna that operates lower than 400 MHz for the SATIMO Starlab measurement chamber. Using that reference antenna, the actual measured gains are calibrated accordingly. The software inside the SATIMO Starlab measurement chamber does the necessary gain calibration.

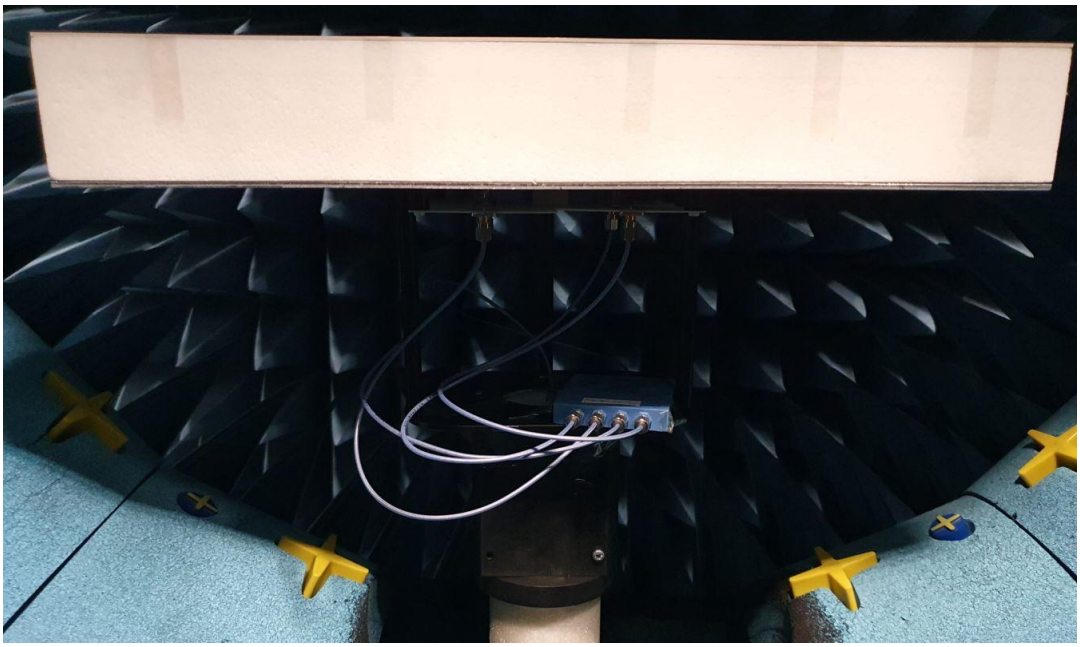

Figure 7.5. Antenna Front view inside the Chamber

In Figure 7.6 and Figure 7.7, the measured antenna realized gains together with the simulated realized gains are given. Investigating Figure 7.6, it is observed that the pattern deflection occured in the realized gain simulation results, around 750 MHz due to the non ideal structure of the balun structure is transferred to 500 MHz region in the measurements. For 750 MHz, $\Phi=90^0$ plane pattern has its peak gain approximately 15 degree shifted from the boresight in the simulations. However in the measurements, a similar affect is observed at 500 MHz pattern, while the 750 MHz pattern became more qualified, i.e. its peak gain is along the boresight.

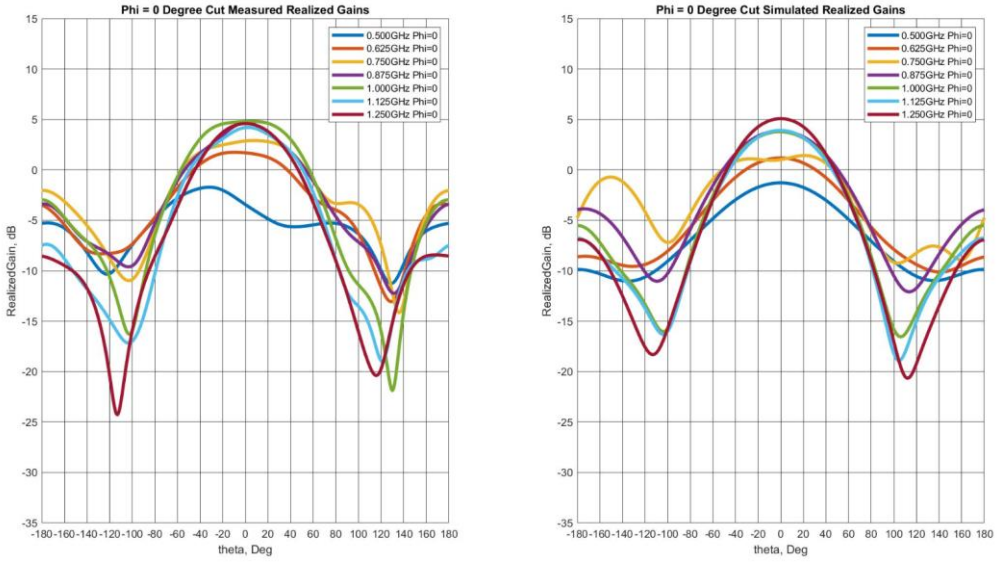

(a)

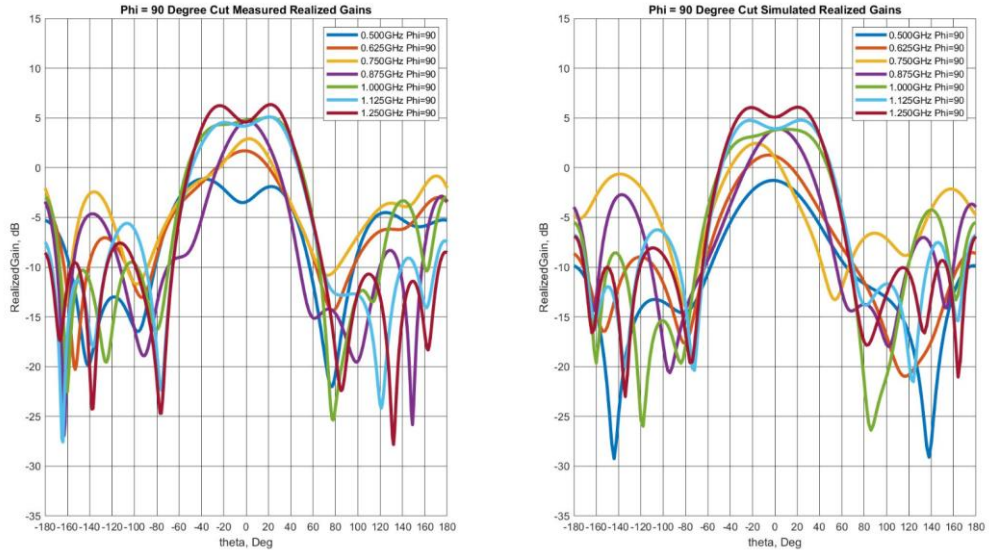

(b)

Figure 7.6. (a) Measured Realized Gains with Simulated Realized Gains, $\Phi=0^0$ Cut, (b) Measured Realized Gains with Simulated Realized Gains, $\Phi=90^0$ Cut, 0.5-1.25 GHz Frequency Band

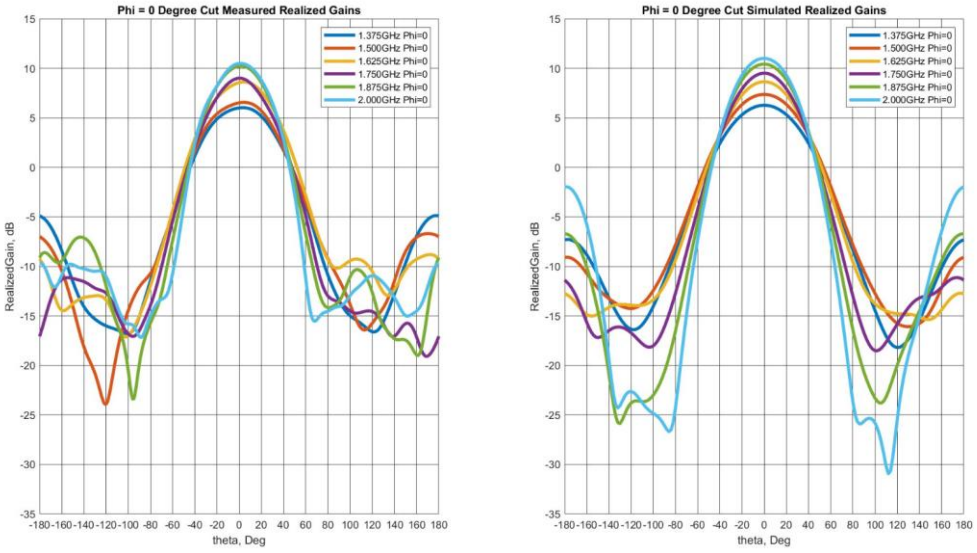

(a)

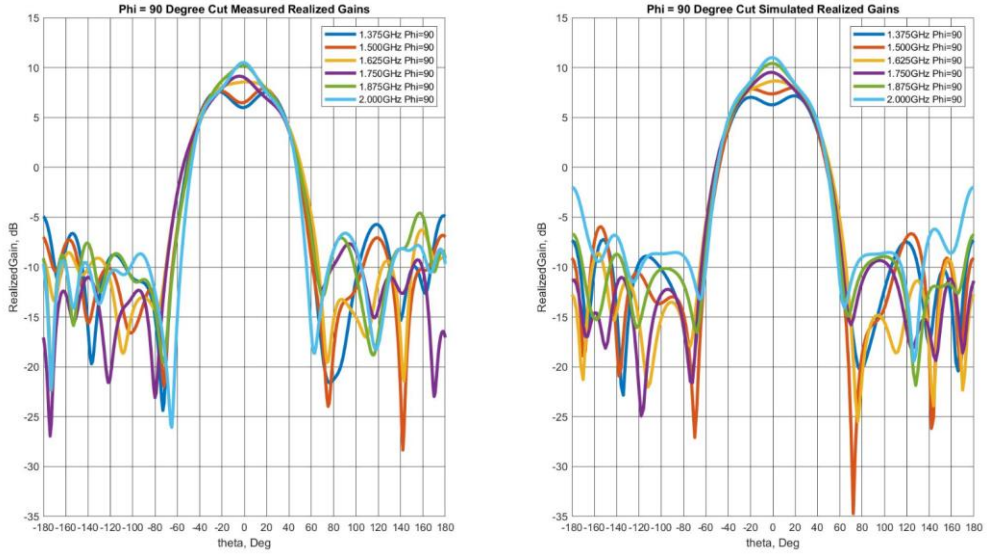

(b)

Figure 7.7. (a) Measured Realized Gains with Simulated Realized Gains, $\Phi=0^0$ Cut, (b) Measured Realized Gains with Simulated Realized Gains, $\Phi=90^0$ Cut, 1.375-2.000 GHz Frequency Band

Finally, in Figure 7.8 the boresight realized gains vs frequency together with the measured boresight realized gains are given with the formula that relates the effective aperture to the directivity. For the effective aperture calculations, only the exicted area of the aperture is taken into account, as it was done on the previous work about this subject. The used area is composed of 4 unit cells, at the center. Each unit cell is 75.1 mm by 75.1 mm in lenghts.

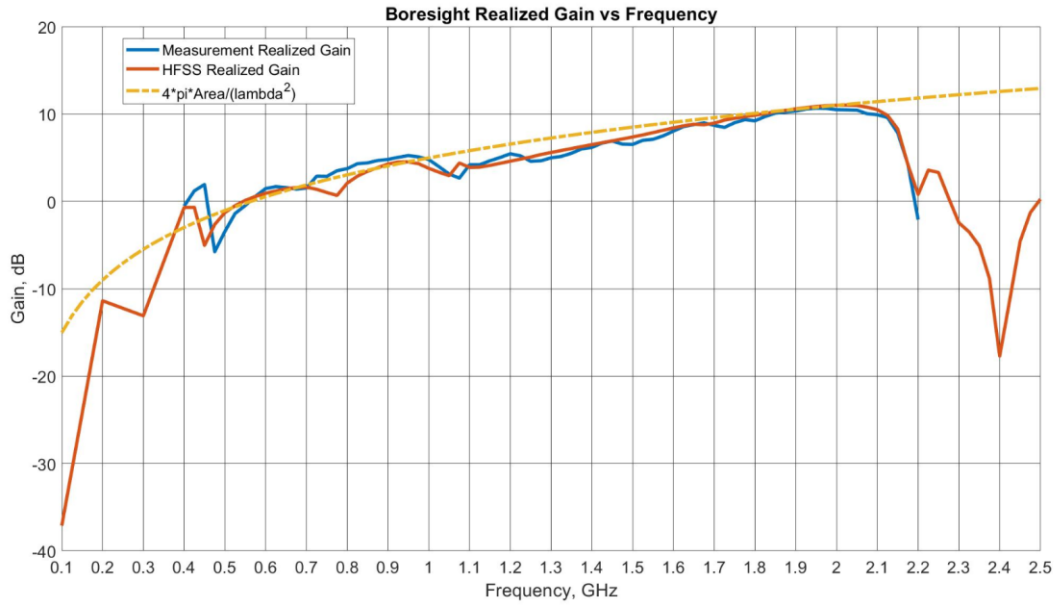

Figure 7.8. Boresight Realized Gain vs Frequency Results

By examining Figure 7.8, it is observed that both simulated HFSS realized gains and measured realized gains drop severely after 2.1 GHz frequency. The reason of this effect is due to the existence of ground plane. Due to ground plane presence, nulls occur in the patterns along the boresight directions. Hence boresight realized gains at those frequencies drop severely when compared to the effective area directivity formula both in the simulations and in the measurements. By referring to Figure 7.8, at some frequencies the measured and simulated gains are higher than effective area directivity formula and at some frequencies it is lower. The reason of this observation

is due to the the following fact: The excited region is two unit cell by two unit cell whereas the finite ground plane is four unit cell by six unit cell in size. Therefore for some frequencies the reflections from that ground plane resulted in constructive intereference with the direct waves from the aperture, along the boresight. At some frequencies they resulted in destructive interference along the boresight. Hence, whereas the interference was constructive, the gains were higher and they were lower at the destructive interference.

In Figure 7.9, the measured efficiency of the antenna is given. Note that efficiency takes into account both mismatch efficiency and radiation efficiency. Radiation efficiency does not take into account losses due to input impedance mismatch between source and antenna input impedance. Radiation efficiency takes into account the conductor and dielectric losses. It is the ratio of peak gain to peak directivity. However, efficiency is the ratio of peak realized gain to peak directivity. In other words, efficiency is the total radiated power over total input power. All those definitions are based on [22], where [22] uses IEEE Standard 145–1993. For calculating efficiency, peak realized gain over peak directivity is used.

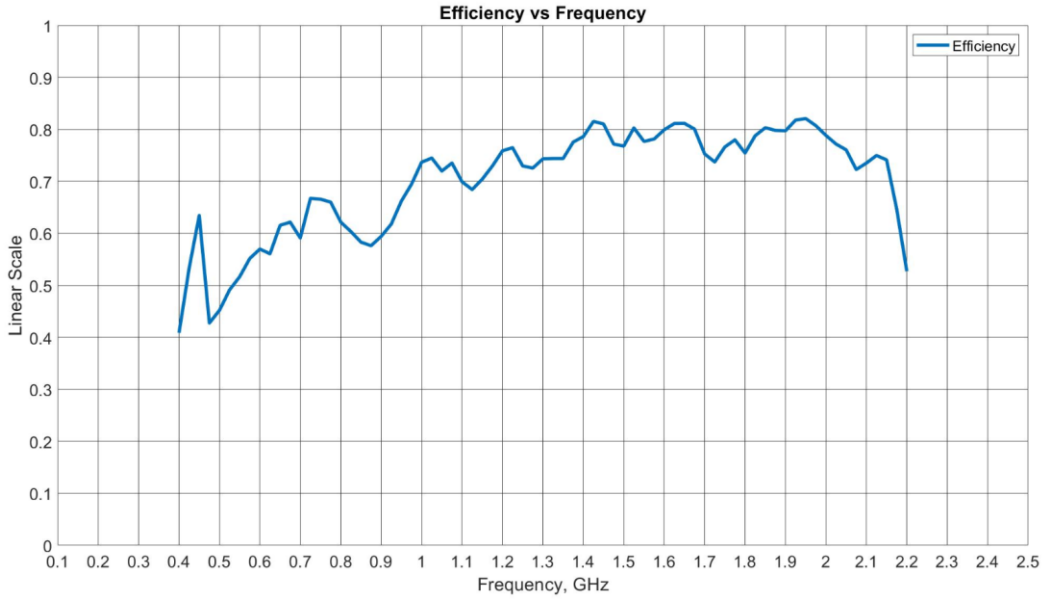

Figure 7.9. Antenna Efficiency from Measurements vs Frequency

The antenna efficiency is around 0.8 at higher frequency end of the antenna, however it drops below 0.6 values towards 0.5 GHz. The reason is most likely due to the resistively terminated ports that reside in the aperture. Note that, initial aperture that uses actual unit cell prior to the finite antenna aperture design had active S-Parameters close to zero dB at low frequency region of the desired frequency band. By optimizing the unit cells such that excited ports have active S-Parameters lower than -10 dB, at the same time that optimization process have reduced the efficiency of antenna. Infinite array unit cell analyses had efficiencies higher than 0.9 in the 0.5 to 2.0 GHz frequency band. Efficiency is considerably high at the high freqeuncy region of the desired frequency band even though aperture has lots resistively terminated elements.

Finally, the author wants to state that the previous realized gain measurements were compansated by the amount of loss dissipated in the 4 way power divider network, which is solely used for testing and energizing the antenna terminals. The maximum amount of compansated loss was 1.4 dB. That power divider has never been part of the designed antenna, was never modeled in the HFSS environment, the author had borrowed it from a neighboring department different than his own that he is working for. Realized gains provided from the HFSS never had those loss values in the figures. The uncompansated measurement results are given Figure 7.10, Figure 7.11, Figure 7.12 and Figure 7.13.

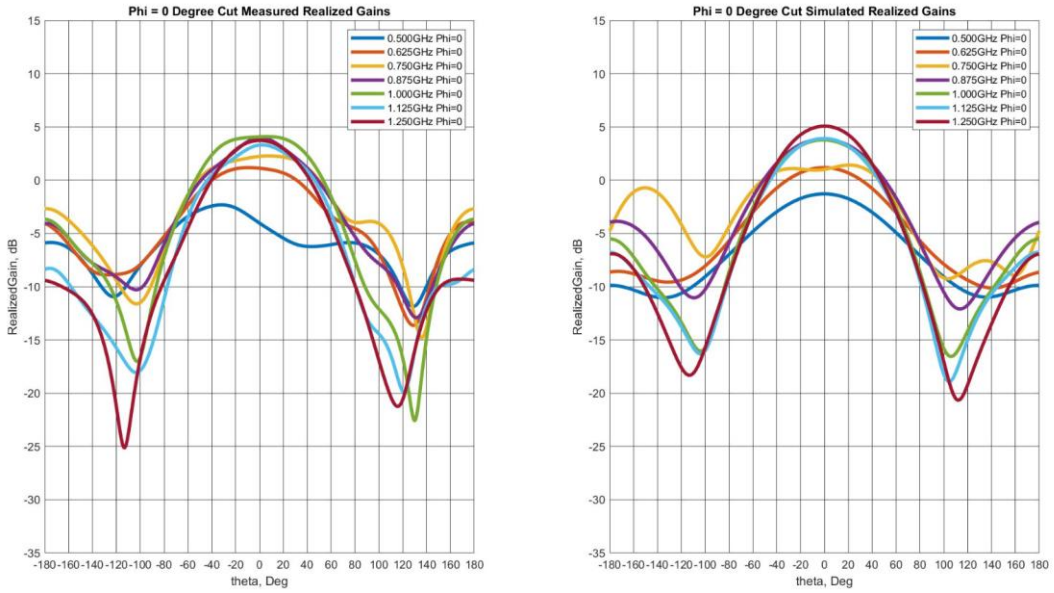

(a)

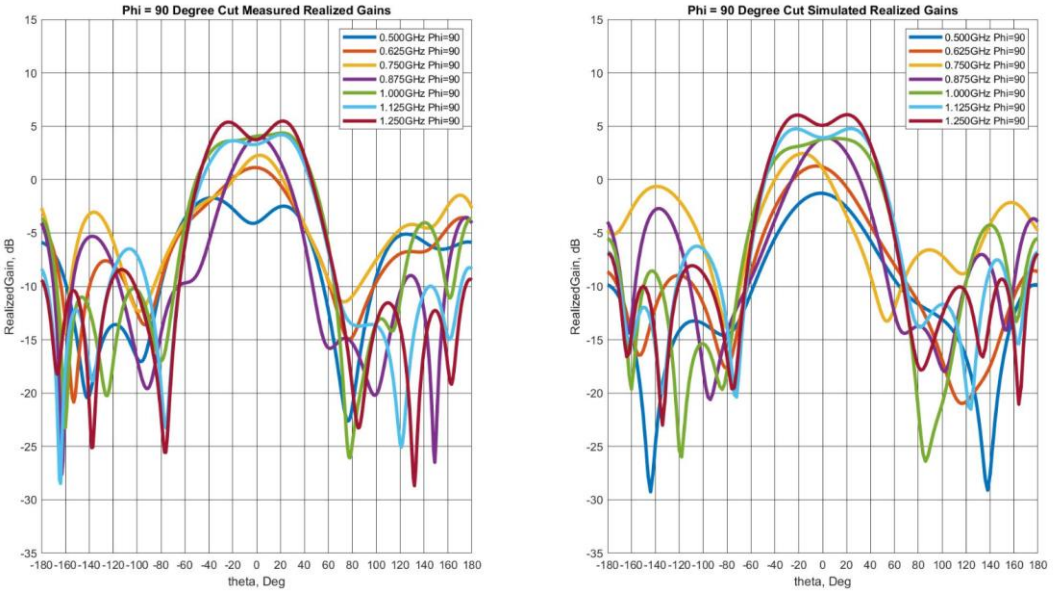

(b)

Figure 7.10. (a) Measured Realized Gains with Simulated Realized Gains, $\Phi=0^0$ Cut, (b) Measured Realized Gains with Simulated Realized Gains, $\Phi=90^0$ Cut, 0.5-1.25 GHz Frequency Band

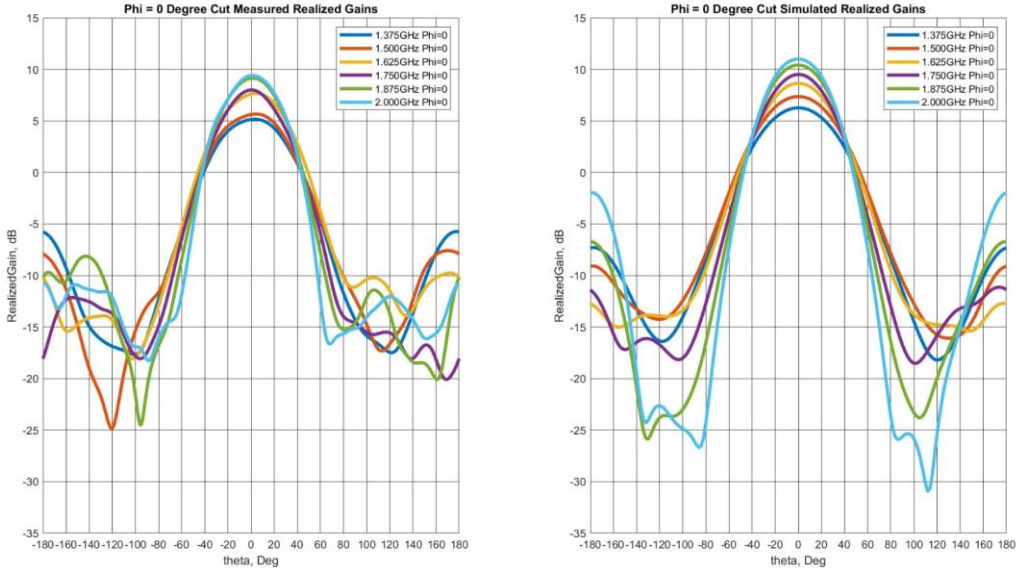

(a)

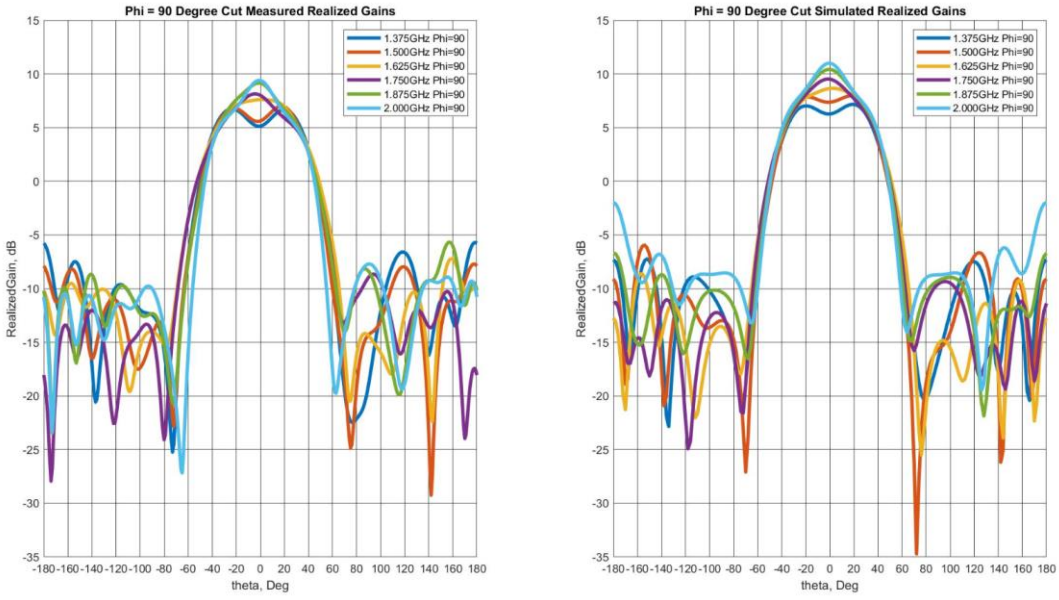

(b)

Figure 7.11. (a) Measured Realized Gains with Simulated Realized Gains, $\Phi=0^0$ Cut, (b) Measured Realized Gains with Simulated Realized Gains, $\Phi=90^0$ Cut, 1.375-2.000 GHz Frequency Band

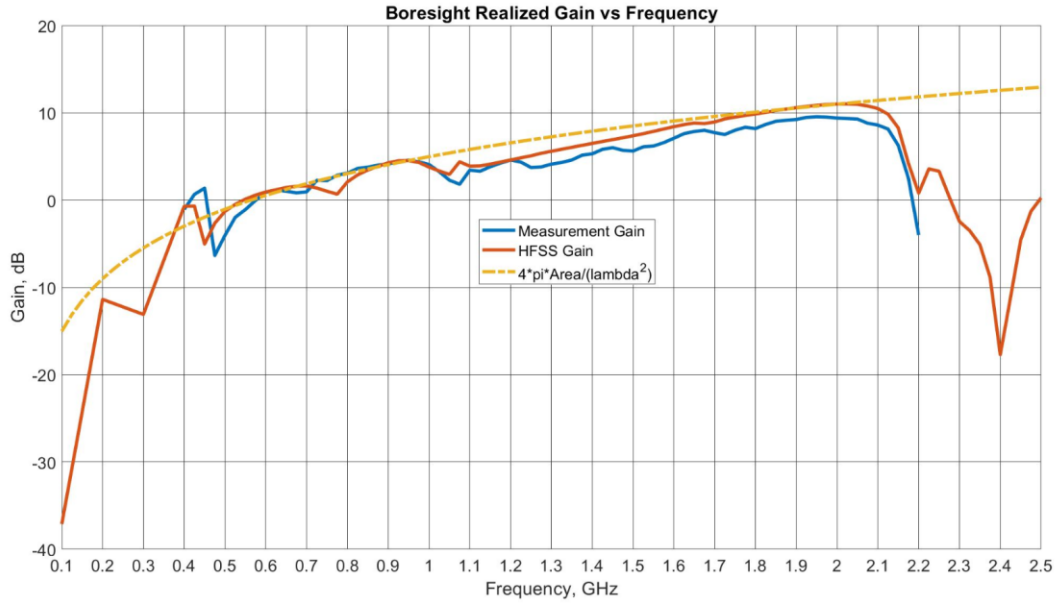

Figure 7.12. Boresight Realized Gain vs Frequency Results

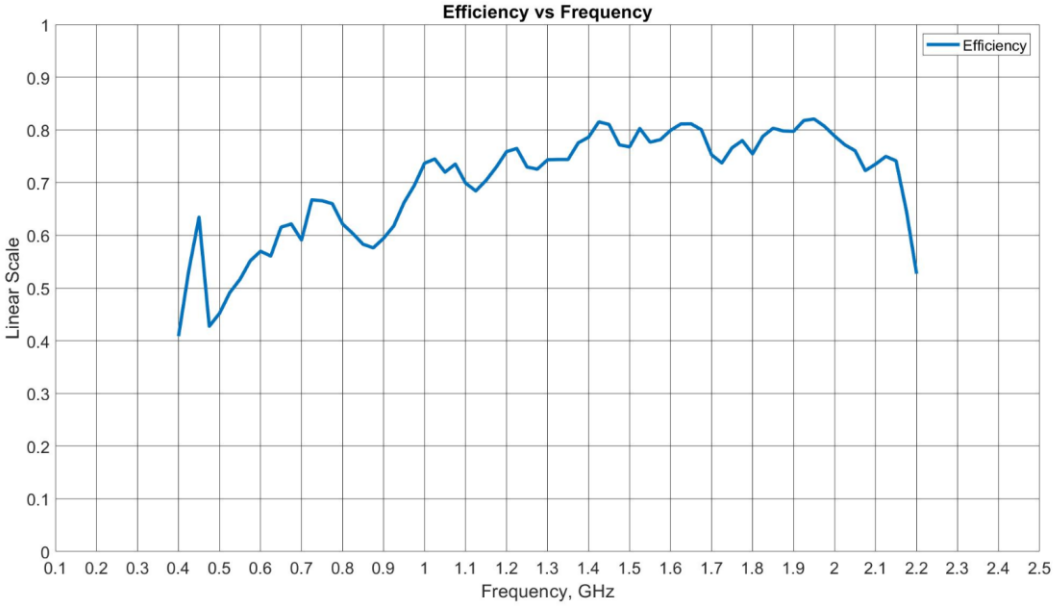

Figure 7.13. Antenna Efficiency from Measurements vs Frequency

CHAPTER 8

CONCLUSIONS AND FUTURE WORK

In this thesis, the work is focused on the wideband tightly coupled dipole arrays.

First, a literature survey on tightly coupled arrays is carried out. The similar array concepts operating at similar bandwidths usually have their physical size several wavelengths along boresight; however tightly coupled dipoles are important because of they have dimension along boresight very low; approximately 0.1λ at the lowest design frequency. Several TCDA's implementations are provided, most of them use superstrates, FSS's above the aperture of the array, unlike the designs given in this thesis. Then operation principles of tightly coupled dipole arrays on the unit cell level are investigated. A MATLAB code is written for modeling the unit cell of the tightly coupled dipole arrays by making some assumptions.

Then, tightly coupled dipole array concept is investigated on the HFSS environment using the concept of unit cell. Two different unit cell types are generated, one using interdigital type capacitance between dipole tips which is patented in the previous works while the other one using spiral shaped capacitive coupling between dipole arms, which is the main contribution of this thesis. These two unit cells are optimized in such a way that the active S-parameters in the bandwidth of operation of the antenna becomes -10 dB.

In Chapter 3, a unit cell that incorporates spiral shaped capacitance that is developed, and tested in finite antenna environment. Concept of stick array, which is explained in Chapter 4, is applied. Gradually increasing the number of elements while retaining some elements that are on the edges, a number of resistively terminated elements are suggested. A small MATLAB script is written and used for applying different excitation schemes to any finite sized array aperture.

Then, two finite tightly coupled dipole array apertures of 4×4 and 4×6 elements are designed. Only the central four elements are excited. The desired operational bandwidth was 0.5 GHz to 2.0 GHz, which is a theoretical statement that were given previously for input return loss of 10 dB. In addition, due to the fact that the unit cell size on those apertures are lower than $0.5\ \lambda$ at any frequency, only fundamental TEM mode operates for those apertures. No grating lobes occur at any frequency and any scan angle. Therefore they satisfy the ability to scan the antenna's beam in any desired direction in the upper hemisphere.

Next, different antenna feeding methods are investigated. Since the antenna has input impedance around 200 Ω values and it requires a balanced input, several types of balanced feed structures are designed and examined for use as a realistic feed. Only one of the feed methods were chosen to be used in the manufactured the antenna.

Finally, a prototype antenna was manufactured. First, balun cards were realized using PCB production technology. Then those cards were connected to the antenna terminals via coaxial cables. For measurements, a power divider was used for energizing the antenna. Measurements were conducted using a network analyzer and SATIMO measurement chamber. Those measurements were compared with the simulation results. A good agreement is observed between the measured and simulated results.

The key contributions of this thesis are given below:

- By working on this problem, the author has conducted literature survey on wideband arrays. The deficiencies of existing widebands arrays are provided, the reasons for using tightly coupled dipole elements in order to obtain ultrawideband operation is given.
- The author also has gained a deeper understanding on the operations principles of tightly coupled dipole arrays. Actually, in general, the author has gained deeper insight on the design of array antennas. The author understood that how the mutual coupling that exists along the E-planes of the dipoles increases the bandwidth of dipole elements, which have 10%-20%

bandwidths in an isolated fashion, to bandwidth ratios of 4:1 under VSWR<2 condition. A MATLAB code is developed, it provides input impedance and bandwidth of unit cell of tightly coupled dipole antenna. The code allows one to optimize unit cell ground plane distance, unit cell lengths, operational frequency band and the desired VSWR in the desired frequency band.

- The author has developed a novel TCDA unit cell based on spiral shaped capacitive elements. The motivation behind this attempt was due to the fact that previous unit cell implementations such as interdigital type capacitance based elements are patented. The developed unit cell shape, provides further miniaturization on the unit cell in the finite array environment.
- The author has designed two different finite sized apertures based on two kinds of unit cell types that satisfy the design requirements stated previously. Both apertures excited elements satisfy the requirement of active S-Parameters below -10 dB in the entire 0.5-2.0 GHz frequency range. First aperture is designed using interdigital type capacitance unit cells, its dimensions are 0.5λ by 0.75λ at the lowest operating frequency, that is 0.5 GHz. The second aperture is designed using spiral type capacitance based unit cells, its dimensions are 0.4λ by 0.6λ at the lowest operating frequency, that is 0.5 GHz. The spiral based unit cell element miniaturizes the finite sized array aperture. Both apertures have 0.1λ depth at the lowest frequency of operation that is 0.5 GHz. Distance between the aperture and ground plane is 0.1λ at 0.5 GHz.
- The author has investigated several feed architectures to be used for the exciting the TCDA elements. The reasons why conventional tapered balun feed architecture cannot be used is understood. It is determined that shielded feed lines are required, also the two conductors between the aperture and ground plane must be equivalent to each other. Designed two different feed networks that are shielded and mechanically fits to the antenna. Those two feed networks have very little extensions below the ground plane, therefore they retain the low profile property of the antenna; unlike most of the studies

conducted on this subject. By considering the feed architecture applied on the realized array, the total antenna depth is just 0.12λ, that depth includes the feed PCB card.

- The author has fabricated a TCDA of 4 by 6 elements using one of the apertures. The necessary measurements are conducted, excellent agreements between simulations and measurements are observed.

As a future work, tightly coupled dipole array design can be extended to higher frequencies. In this thesis, number of elements were restricted by the finite PCB size that the antenna aperture is realized. That restriction prevented the use of unit cells optimized for the frequencies of interest in this thesis. However, the available number of elements were too low for the finite array behavior to catch up the infinite array unit cell behavior.

Another future work is that implementation of tightly coupled antenna comprised of dual orthogonal dipoles. The necessary feed structure could be studied for that architecture as well.

By adding one or more superstrates above the antenna aperture can be studied in the future. Arrays capable of delivering 9:1 bandwidth ratios are obtainable using such superstrates above the aperture. However, it should be noted that addition of superstrates to increase the array thickness along the boresight axis.

REFERENCES

[1] H. Holter, "Dual-Polarized Broadband Array Antenna With BOR-Elements, Mechanical Design and Measurements," in IEEE Transactions on Antennas and Propagation, vol. 55, no. 2, pp. 305-312, Feb. 2007, doi: 10.1109/TAP.2006.886557.

[2] J. J. Lee, S. Livingston and R. Koenig, "A low-profile wide-band (5:1) dual-pol array," in IEEE Antennas and Wireless Propagation Letters, vol. 2, pp. 46-49, 2003, doi: 10.1109/LAWP.2003.812243.

[3] Joon Shin and D. H. Schaubert, "A parameter study of stripline-fed Vivaldi notch-antenna arrays," in IEEE Transactions on Antennas and Propagation, vol. 47, no. 5, pp. 879-886, May 1999, doi: 10.1109/8.774151.

[4] E. L. Holzman, "A wide band TEM horn array radiator with a novel microstrip feed," Proceedings 2000 IEEE International Conference on Phased Array Systems and Technology (Cat. No.00TH8510), Dana Point, CA, 2000, pp. 441-444, doi: 10.1109/PAST.2000.858992.

[5] H. Wheeler, "Simple relations derived from a phased-array antenna made of an infinite current sheet," in IEEE Transactions on Antennas and Propagation, vol. 13, no. 4, pp. 506-514, July 1965, doi: 10.1109/TAP.1965.1138456.

[6] H. A. Wheeler, "The Radiation Resistance of an Antenna in an Infinite Array or Waveguide," in Proceedings of the IRE, vol. 36, no. 4, pp. 478-487, April 1948, doi: 10.1109/JRPROC.1948.229650.

[7] MLA : Hansen, Robert C. Phased array antennas. Vol. 213. John Wiley & Sons, 2009.

[8] Munk, Ben A. Finite antenna arrays and FSS. John Wiley & Sons, 2003.

[9] Munk, Ben A. Frequency selective surfaces: theory and design. John Wiley & Sons, 2005.

[10] I. Tzanidis, K. Sertel and J. L. Volakis, "Interwoven Spiral Array (ISPA) With a 10:1 Bandwidth on a Ground Plane," in IEEE Antennas and Wireless Propagation Letters, vol. 10, pp. 115-118, 2011, doi: 10.1109/LAWP.2010.2070786.

[11] J. P. Doane, K. Sertel and J. L. Volakis, "A Wideband, Wide Scanning Tightly Coupled Dipole Array With Integrated Balun (TCDA-IB)," in IEEE Transactions on Antennas and Propagation, vol. 61, no. 9, pp. 4538-4548, Sept. 2013, doi: 10.1109/TAP.2013.2267199.

[12] I. Tzanidis, K. Sertel, and J. L. Volakis, “UWB low-profile tightly coupled dipole array with integrated balun and edge terminations,” IEEE Transactions on Antennas and Propagation, vol. 61, no. 6, pp. 3017–3025, 2013, doi: 10.1109/TAP.2013.2250232.

[13] J. A. Kasemodel, C. Chen and J. L. Volakis, "Wideband Planar Array With Integrated Feed and Matching Network for Wide-Angle Scanning," in IEEE Transactions on Antennas and Propagation, vol. 61, no. 9, pp. 4528-4537, Sept. 2013, doi: 10.1109/TAP.2013.2266090.

[14] Durham, Timothy E., et al. "Phased array antenna with discrete capacitive coupling and associated methods." U.S. Patent No. 6,856,297. 15 Feb. 2005.

[15] Durham, Timothy E., et al. "Multi-layer capacitive coupling in phased array antennas." U.S. Patent No. 6,822,616. 23 Nov. 2004.

[16] Rumsey, V. H. "Reaction concept in electromagnetic theory." Physical Review 94.6 (1954): 1483.

[17] H. Holter and H. Steyskal, "On the size requirement for finite phased-array models," in IEEE Transactions on Antennas and Propagation, vol. 50, no. 6, pp. 836-840, June 2002, doi: 10.1109/TAP.2002.1017665.

[18] Pozar, David M. Microwave engineering. John wiley & sons, 2009.

[19] R. Levy, "Explicit formulas for Chebyshev impedance-matching networks, filters and interstages," in Proceedings of the Institution of Electrical Engineers, vol. 111, no. 6, pp. 1099-1106, June 1964, doi: 10.1049/piee.1964.0170.

[20] SIGATEK SP50404 Power Divider 4 way 0.5-2.0 GHz, accessed 24 August 2020, https://www.sigatek.com/Power-Dividers/4-way-Dividers-0.5-40-Ghz/SP50404-Power-Divider-4-way-0.5-2.0-Ghz.html

[21] SATIMO SH400, accessed 29 August 2020, https://www.mvg-world.com/sites/default/files/2019-11/Datasheet_Antennas_Dual-Ridge%20Horns_08_19_BD2.pdf

[22] Balanis, Constantine A. Antenna theory: analysis and design. John wiley & sons, 2016.

[23] Holland, Steven S., and Marinos N. Vouvakis. "The planar ultrawideband modular antenna (PUMA) array." IEEE Transactions on Antennas and Propagation 60.1 (2011): 130-140.

[24] Holland, Steven S., Daniel H. Schaubert, and Marinos N. Vouvakis. "A 7–21 GHz dual-polarized planar ultrawideband modular antenna (PUMA) array." IEEE Transactions on Antennas and Propagation 60.10 (2012): 4589-4600.

[25] Bah, Alpha O., et al. "A wideband low-profile tightly coupled antenna array with a very high figure of merit." IEEE Transactions on Antennas and Propagation 67.4 (2019): 2332-2343.

[26] Johnson, Alexander D., et al. "Phased Array with Low Angle Scanning and 46: 1 Bandwidth." IEEE Transactions on Antennas and Propagation (2020).

[27] Zhou, Wenyang, Yikai Chen, and Shiwen Yang. "Efficient Design of Tightly Coupled Dipole Array Using an Equivalent Circuit-Based Approach." IEEE Access 8 (2020): 14013-14023.

[28] Cavallo, Daniele, et al. "A 3-to 5-GHz wideband array of connected dipoles with low cross polarization and wide-scan capability." IEEE transactions on antennas and propagation 61.3 (2012): 1148-1154.

[29] Neto, Andrea, and J. J. Lee. "Ultrawide-band properties of long slot arrays." IEEE transactions on antennas and propagation 54.2 (2006): 534-543.